Miscibility, Viscoelastic Reinforcement, and Transport Properties of Blend Membranes based on Sulfonated Poly(phenylene sulfone)s

Von der Fakultät Chemie der Universität Stuttgart
zur Erlangung der Würde eines Doktors der
Naturwissenschaften (Dr. rer. nat.) genehmigte Abhandlung

Vorgelegt von
Torben Saatkamp
aus Filderstadt

Hauptberichter	Prof. Dr. Joachim Maier
Mitberichter	Prof. Dr. Thomas Sottmann
Prüfungsvorsitzender	Prof. Dr. Bernhard Hauer

Tag der Einreichung	21.06.2021
Tag der mündlichen Prüfung	27.07.2021

Max-Planck-Institut für Festkörperforschung
2021

Die Neugier ist die mächtigste Antriebskraft im Universum, weil sie die beiden größten Bremskräfte im Universum überwinden kann: die Vernunft und die Angst.

Walter Moers, *Die Stadt der träumenden Bücher*, S. 313

Erklärung über die Eigenständigkeit der Dissertation

Ich versichere, dass ich die vorliegende Arbeit mit dem Titel *Miscibility, Viscoelastic Reinforcement, and Transport Properties of Blend Membranes based on Sulfonated Poly(phenylene sulfone)s* selbständig verfasst und keine anderen als die angegebenen Quellen und Hilfsmittel benutzt habe; aus fremden Quellen entnommene Passagen und Gedanken sind als solche kenntlich gemacht.

Declaration of Authorship

I hereby certify that the dissertation entitled *Viscoelastic Reinforcement, and Transport Properties of Blend Membranes based on Sulfonated Poly(phenylene sulfone)s* is entirely my own work except where otherwise indicated. Passages and ideas from other sources have been clearly indicated.

Name/Name: Torben Saatkamp

Unterschrift/Signed: _____

Datum/Date:

ACKNOWLEDGEMENTS

This work would not have been possible without the guidance, support, and contributions of numerous people. First, I would like to thank Professor Joachim Maier for welcoming me into his group and supporting me in making the best use of the unique opportunities that students are granted in the excellent environment at his department. I would also like to thank the members of my examining committee, Professor Thomas Sottmann as the co-examiner and Professor Bernhard Hauer as the committee chair for their involvement in this work. I am most grateful to my supervisor Klaus-Dieter Kreuer who took me under his wing early on and whose mentorship has been key in my scientific and personal development over the last years. I would like to particularly thank Giorgi Titvinidze who has been a mentor, a colleague, and a friend above all during these last years. I want to thank Madeleine Burkhardt and Sofia Weiglein for the indispensable "behind-the-scenes" work they tirelessly provide. Similarly, it is hard to overstate how grateful I am for the work of the entire supporting staff at the Institute. I thankfully acknowledge the financial support of the German Federal Ministry of Education and Research within PSUMEA-2 and PSUMEA-3 that allowed for an inspiring and fruitful collaboration with our colleagues at the HS in Freiburg as well as those at the ZSW in Ulm, whom I want to thank. I further thank the company partners within the project, namely FUMATECH BWT, BOSCH, and SIEMENS who have been great collaborators. It was great to be part of the Physical Chemistry of Solids department, which is due to the amazing people that I had the pleasure of working with during my time there. Among them, I am particularly thankful to Rotraut Merkle and the source of help that she was for me in all circumstances. Technical and personal support especially by Annette Fuchs is something I am very, very grateful for. I thank Udo Klock, as well as Florian Kaiser, Armin Sorg, Barbara Reichert, and Uwe Traub for their technical expertise and wholesome support throughout the years. I cherish and am grateful for the close personal bonds with many colleagues, fellow PhD students, and my office mates Simon, Kyungmi, Max, and especially Andreas that allowed me to navigate through ups and downs and that I hope will extend far beyond our shared time. On a personal level I want to sincerely thank my family and friends for their continued support in these last years. It goes without saying that I am forever and wholeheartedly grateful for everything my parents, my sister, and Patricia helped me with.

ABSTRACT

Chemical energy that hydrogen may generate during combustion and the corresponding electrical energy are interconvertible by means of a fuel cell (FC) and by the electrolysis of water (WE), which allows for the utilization of the complementary nature of these two key energy vectors towards energy sustainability. A proton exchange membrane (PEM) made from an ionomer is commonly employed as the electrolyte in mobile fuel cell applications and in water electrolyzers that require dynamic operability and pressurized product gases. New PEM materials are needed to increase performance, reduce environmental impact, and allow for a more targeted design of PEMFC and PEMWE systems, all of which is in some way limited by the use of the established perfluorosulfonic acid (PFSA) type ionomers.

This work's focus lies on sulfonated poly(phenylene sulfone)s (sPPS), a unique group of fluorine-free cation conducting ionomers. They are unique in terms of their chemical stability and transport properties, however, typical in terms of their salt-like brittleness in the dry state and extensive swelling at high humidity and in water. To make the unique properties of sPPS available in application, the goal of this work is to take a comprehensive approach to their viscoelastic reinforcement. Therefore, the structure of this thesis entails three related aspects along the process from pure materials to the optimization of robust PEMs for application.

The first chapter focuses on the optimization of the intrinsic viscoelastic properties of a particularly suited sPPS (termed S360, with IEC 2.78 meq g^{-1}, EW 360 g mol^{-1}) which lays the groundwork for reliable and systematic further development. To achieve this, relevant properties of S360 are first characterized and viscoelastic shortcomings as seen in water uptake measurements and tensile tests under dry conditions ($\leq$ 30% relative humidity, RH) discussed. The step-growth polymerization of S360 is optimized after finding significant inorganic contamination retained in the established purification process of the widely used monomer sulfonated difluorodiphenyl sulfone (sDFDPS), allowing for the preparation of the ionomer in reproducible high molecular weight. Relevant properties of high molecular weight S360 are characterized and an enhancement of mechanical properties at 30% RH as well as when submerged in water is found. Access to reproducible high quality of S360 enables its first-time use and study as a PEM in a completely fluorine-free WE cell. At 80 °C, record performance

amongst fluorine free electrolytes in PEMWEs of 3.48 A cm^{-2} at 1.8 V is achieved, showcasing the potential of sPPS for application.

The second chapter entails the identification and better understanding of a suitable and versatile reinforcement concept for creating robust membranes based on sPPS. To achieve this, the established homogeneously miscible acid-base polymer blends of sulfonated ionomers with poly(benzimidazole) (PBI, and its derivatives PBIO and PBIOO) are discussed in-depth and chosen for later systematic optimization in combination with sPPS. Since the origin of miscibility in PBI blends with sulfonated ionomers is insufficiently described in literature and could facilitate targeted design of new blend components, a model acid-base polymer blend system comprising pyridine-functionalized poly(sulfone) (PSU) is created. Pyridine groups of different basicity tethered to PSU in varying concentration are used to investigate the effect that interpolymer acid-base interaction strength and concentration have on miscibility in blends with 80 wt% S360, as derived from the blend membranes' cross-sectional SEMs. High mutual compatibility is achieved at high concentration of weak interpolymer interaction, which is interpreted with regards to the observed miscibility in PBI blends. Based on the derived role that hydrogen bonds may play in PBI blends, the difference of interpolymer interaction in solution (during membrane formation) and in the dry membrane is described. This could enable the development of new blend concepts in the future. An exemplary miscible blend that comprises interpolymer hydrogen bonds only in solution but not in the final membrane is shown.

The third chapter describes the optimization and balance of properties in the previously described polymer blends with PBIO, following the goal to prepare membranes which can be evaluated in fuel cells and fabricated on a wider scale in order to bring the attractive properties of sPPS into application. To achieve this, S360-blend membranes of varying PBIO content are characterized with regard to conductivity and mechanical properties in various conditions. High mechanical robustness is achieved in S360 blends with 30 wt% PBIO but is accompanied by dramatic reduction of conductivity, due to the charge-consuming acid-base interaction. The findings are translated into blends with fully sulfonated sPPS (termed S220, with IEC 4.54 meq g^{-1}, EW 220 g mol^{-1}) which allows for the creation of membranes that combine mechanical toughness with high conductivity at a ratio of 25 wt% PBIO in S220, making the material suited for production on a commercial casting line and fuel cell testing. Membranes based on S360

that comprise 15 wt% PBIO are designated for further studies in PEMWEs, where membrane requirements differ significantly from that in PEMFCs, highlighting the versatility of the reinforcement approach chosen in this work. Finally, first fuel cell tests of thin spray coated PBIO blend membranes are conducted, and initial durability testing of sPPS-based membranes in fuel cells is possible.

Overall, the results presented in this work are strongly interrelated which underlines the importance of comprehensiveness in the successful viscoelastic reinforcement of sulfonated poly(phenylene sulfone)s. Ultimately, the blend membranes resulting from this work can be used as a platform for further development of sPPS-based PEMs in the future.

ZUSAMMENFASSUNG

Chemische Energie, die Wasserstoff bei der Verbrennung einzubringen vermag, und die korrespondierende elektrische Energie sind mittels Brennstoffzellen (FC) und durch die Elektrolyse von Wasser (WE) ineinander umwandelbar, was die Nutzung der komplementären Natur dieser beiden wichtigen Energievektoren mit dem Ziel eines nachhaltigen Energiesystems ermöglicht. Eine Protonenaustauschmembran (PEM) besteht aus einem Ionomer und wird üblicherweise als Elektrolyt in mobilen Brennstoffzellenanwendungen und in Wasserelektrolyseuren eingesetzt, die eine dynamische Betriebsfähigkeit und unter Druck stehende Produktgase bereitstellen sollen. Neue PEM-Materialien werden benötigt, um höhere Zellleistungen erzielen zu können, die Umweltbelastung von PEMFC- und PEMWE-Systemen zu reduzieren und ein gezielteres Systemdesign zu ermöglichen. Momentan werden diese Entwicklungen teilweise durch den breiten Einsatz etablierter fluorierter Ionomere auf Perfluorosulfonsäurebasis (PFSA) gebremst.

Der Fokus dieser Arbeit liegt auf sulfonierten Poly(phenylensulfon)en (sPPS), einer einzigartigen Gruppe von flourfreien, kationenleitenden Ionomeren. Sie sind einzigartig in Bezug auf ihre chemische Stabilität und Transporteigenschaften, jedoch typisch in Bezug auf ihre salzartige Sprödigkeit im trockenen Zustand und ihre starke Quellung bei hoher Luftfeuchtigkeit sowie in Wasser. Um die einzigartigen Eigenschaften von sPPS für die Anwendung nutzbar zu machen, ist es das Ziel dieser Arbeit, einen umfassenden Ansatz für ihre mechanische Verstärkung zu wählen. Daher umfasst der Aufbau dieser Arbeit drei zusammenhängende Aspekte entlang des Prozesses vom reinen Material bis zur Optimierung von robusten PEMs für die Anwendung.

Das erste Kapitel konzentriert sich auf die Optimierung der intrinsischen viskoelastischen Eigenschaften eines besonders geeigneten sPPS (bezeichnet als S360, mit IEC 2,78 meq g^{-1}, EW 360 g mol^{-1}), was die Grundlage für eine zuverlässige und systematische Weiterentwicklung in späteren Kapiteln legt. Dazu werden zunächst relevante Eigenschaften von S360 charakterisiert und viskoelastische Unzulänglichkeiten, wie sie sich bei Wasseraufnahmemessungen und Zugversuchen unter trockenen Bedingungen (≤ 30 % relative Feuchte, RH) zeigen, diskutiert. Die Stufenwachstumspolymerisation von S360 wird optimiert, nachdem signifikante anorganische Verunreinigungen, die im etablierten

Aufreinigungsprozess des weit verbreiteten sulfonierten Monomers Difluordiphenylsulfon (sDFDPS) mitgeschleppt wurden, identifiziert werden, was die Herstellung des Ionomers in reproduzierbar hohem Molekulargewicht ermöglicht. Relevante Eigenschaften von hochmolekularem S360 werden charakterisiert und eine Verbesserung der mechanischen Eigenschaften bei 30 % RH sowie in Wasser gezeigt. Der Zugang zu reproduzierbarer hoher Qualität von S360 ermöglicht dessen erstmalige Verwendung und Untersuchung als PEM in einer fluorfreien WE-Zelle. Bei 80 °C wird die unter fluorfreien Elektrolyten in PEMWEs höchste Leistung von 3,48 A cm^{-2} bei 1,8 V erreicht, was das Potenzial von sPPS für die Anwendung zeigt.

Das zweite Kapitel beinhaltet die Identifizierung und das bessere Verständnis eines geeigneten und vielseitigen Verstärkungskonzepts zur Herstellung robuster Membranen auf Basis von sPPS. Dazu werden die etablierten, homogen mischbaren Säure-Base-Polymerblends aus sulfonierten Ionomeren mit Poly(benzimidazol) (PBI, und dessen Derivate PBIO und PBIOO) eingehend diskutiert und für eine spätere systematische Optimierung in Kombination mit sPPS ausgewählt. Da der Ursprung der Mischbarkeit in PBI-Blends mit sulfonierten Ionomeren in der Literatur nur unzureichend beschrieben ist, und es das gezielte Design neuer Blend-Komponenten ermöglichen könnte, wird ein modellhaftes Säure-Base-Polymerblendsystem auf Basis von Pyridin-funktionalisiertem Poly(sulfon) (PSU) erstellt. Hierzu werden Pyridingruppen unterschiedlicher Basizität, die in unterschiedlicher Konzentration an PSU gebunden sind, verwendet. Dies ermöglicht die Untersuchung des Effekts, den die Stärke der Säure-Base-Wechselwirkung zwischen den Polymeren und deren Konzentration auf die Mischbarkeit in Polymerblends mit 80 Gew.-% S360 haben, welcher aus Querschnitts-SEMs der Membranen abgeleitet wird. Eine hohe gegenseitige Kompatibilität wird bei hoher Konzentration schwacher Interpolymerwechselwirkung erreicht, was im Hinblick auf die beobachtete Mischbarkeit in PBI-Blends interpretiert wird. Basierend auf der abgeleiteten kompatibilisierenden Rolle, die Wasserstoffbrückenbindungen spielen könnten, wird der Unterschied der Interpolymerwechselwirkung in Lösung (während der Membranbildung) und in der trockenen Membran beschrieben, was die Entwicklung weiterer Blendkonzepte in der Zukunft ermöglichen könnte. Ein mischbares Polymerblend, das Wasserstoffbrücken nur in Lösung, nicht aber in der fertigen Membran aufweist, wird beispielhaft aufgeführt.

Das dritte Kapitel beschreibt die Optimierung der Eigenschaften der zuvor beschriebenen Polymerblends von sPPS mit PBIO, mit dem Ziel, Membranen herzustellen, die in einem größeren Maßstab hergestellt und in Brennstoffzellen evaluiert werden und die attraktiven Eigenschaften von sPPS in die Anwendung bringen können. Um dies zu erreichen, werden S360-Blend-membranen mit unterschiedlichem PBIO-Gehalt hinsichtlich ihrer Leitfähigkeit und mechanischen Eigenschaften unter verschiedenen Bedingungen charakterisiert. In S360-Membranen mit 30 Gew.-% PBIO wird eine hohe mechanische Robustheit erreicht, die jedoch mit einer dramatischen Verringerung der Leitfähigkeit einhergeht, bedingt durch die ladungsträgerverringernde Säure-Base-Wechselwirkung. Die gewonnenen Erkenntnisse werden auf Polymerblends mit vollständig sulfoniertem sPPS (bezeichnet als S220, mit IEC 4,54 meq g^{-1}, EW 220 g mol^{-1}) übertragen, was zu Membranen führt, die bei einem Verhältnis von 25 Gew.-% PBIO in S220 hohe mechanische Robustheit mit hoher Leitfähigkeit kombinieren, wodurch sich das Material dann für die Produktion auf einer kommerziellen Membrananlage und für Brennstoffzellentests eignet. Membranen auf Basis von S360, die 15 Gew.-% PBIO enthalten, sind für weitere Untersuchungen in PEMWEs vorgesehen, wo sich die Anforderungen an die Membran deutlich von denen in PEMFCs unterscheiden, was die Rolle der Vielseitigkeit des in dieser Arbeit gewählten Verstärkungsansatzes unterstreicht. Schließlich werden erste Brennstoffzellentests an sprühbeschichteten, dünnen Blendmembranen durchgeführt, und erste Haltbarkeitstests von sPPS-Membranen sind möglich.

Die in dieser Arbeit vorgestellten Ergebnisse sind stark miteinander verknüpft, was die Bedeutung der hier gewählten, umfassenden Herangehensweise für die erfolgreiche viskoelastische Verstärkung von sulfonierten Poly(phenylensulfon)en unterstreicht. Die aus dieser Arbeit resultierenden Blendmembranen können in Zukunft als Plattform für die weitere Entwicklung von sPPS-basierten PEMs dienen.

CONTENTS

LIST OF FIGURES

LIST OF TABLES

LIST OF ACRONYMS

CCM	Catalyst coated membrane
DMAc	Dimethylacetamid
DMD	Direct membrane depositioning
DMSO	Dimethylsulfoxid
EIS	Electrochemical impedance spectroscopy
EW	Equivalent weight
FC	Fuel cell
GDE	Gas diffusion electrode
GPC	Gel permeation chromatography
HT	High-temperature
IEC	Ion exchange capacity
NEP	N-ethyl pyrrolidone
NMP	N-methyl pyrrolidone
PBI	Poly(benzimidazole)
PDI	Polydispersity index
PEM	Proton exchange membrane
PFSA	Perfluorosulfonic acid
PSU	Poly(sulfone)
PTFE	Poly(tetrafluoroethylene)
RH	Relative humidity
SAXS	Small angle X-ray spectroscopy
SEM	Scanning electron miscroscopy
sPPS	Sulfonated poly(phenylene sulfone)
TGA	Thermogravimetric analysis
TPA	Tripropylamine
WE	Water electrolyzer
WU	Water uptake
XRD	X-ray diffraction

1 INTRODUCTION

Striving for a sustainable future in which global energy demand is decarbonized and anthropogenic greenhouse gas emissions arrive at net zero is a central task of current and future generations. In the last five decades global population doubled, total final energy consumption rose by more than 130% (from 49 PWh in 1971 to 116 PWh in 2018[1]), and demand for electricity increased fivefold[1]. Against this background, global efforts on a tremendous scale are underway to increase the amount of renewably sourced energy (mainly from solar, wind, and hydro) and to replace carbon-based. This is causing energy systems worldwide to change at an astonishing pace.

Along the road towards energy sustainability the inclusion of suitable energy vectors (carriers) that allow the transfer, in time and space, of a quantity of energy is essential[2]. Not only is this due to the transient nature of most renewable energy sources, it is also due to the requirement for continuous and instant satisfaction of energy demand and the fact that primary energy sources are often located at a place different from the site of energy demand[3]. Electrical energy and hydrogen are the two most important energy vectors on which such a sustainable energy system can be built in the future[2–6]. Both energy carriers should be put to best use and their complementary nature exploited: While electrical energy can be used in a multitude of applications for which hydrogen is not suitable, hydrogen provides means of energy storage (as intrinsic chemical energy) and can further be used as a reactant and feedstock in multiple industrial processes (most notably steel production and fertilizer manufacturing)[4]. The two energy vectors are also interconvertible – water electrolyzers (WE) allow for the generation of hydrogen from electrical energy and the chemical energy generated during combustion of hydrogen be converted to the corresponding electrical energy by means of a fuel cell (FC).

Both electrolyzers and fuel cells are types of electrochemical conversion devices in which the reactants/products (in the simplest case hydrogen and oxygen) are prevented from chemically reacting by separating them with an electrolyte. The electrolyte, which is in contact with the electro-catalytically active masses (electrodes), mediates the electrochemical reactions taking place at the anode and cathode by conducting a specific ion (proton, hydroxide, or oxide ion) at high rates during operation.

Electrolyzers and fuel cells are often classified based on the kind of electrolyte they employ. Proton conducting polymers (or proton exchange membranes, PEM) have been of particular interest as electrolytes. PEM-based water electrolyzers offer advantages over established alkaline systems (using caustic electrolyte solutions and a porous diaphragm) with regards to voltage efficiency, dynamic operability, and the ability to directly pressurize the product gases – but are significantly more expensive[7]. Low temperature (< 100 °C) fuel cells based on PEM electrolytes have already seen significant technological attention since they are well suited for transportation applications[8]: they offer high power density, fast start-up times, and the advantage of low weight and volume compared with other types of fuel cell systems[5,9].

PEMs are made from ionomers, i.e. a polymer in which a small but significant proportion of the constitutional units has ionic or ionizable groups[10]. The most prominent type of ionomers, originally discovered in the early 1960s[11], comprises a poly(tetrafluoroethylene) (PTFE) polymeric backbone to which a perfluorosulfonic acid (PFSA) moiety is covalently tethered. Their concentration within the ionomer is typically given as equivalent weight (EW) of material per mole of protogenic groups and varies for PFSA-type ionomers[12] (also: PFSAs) between 1500 g mol^{-1} to 600 g mol^{-1}. The inverse of the equivalent weight is the ion exchange capacity (IEC, in meq g^{-1}) of an ionomer. The super acidic PFSA moieties are extremely hygroscopic leading to hydration (solvation) and virtually complete dissociation of sulfonic acid anions and protons, even at low water activity (relative humidity, RH)[13]. The hydration water forms a percolating, tortuous, and locally flat aqueous domain network throughout the membrane[14], giving rise to long range water transport and enabling proton conductivity[13].

In PFSAs, the extremely dissimilar natures of the hygroscopic acid moieties and the strongly hydrophobic PTFE backbone lead to a strongly phase-separated membrane morphology and unique set of transport, chemical, and viscoelastic properties[12,13]. As a consequence, PFSAs are – after decades of research and a wealth of alternate PEM materials – still unrivaled with regard to their widespread commercial application in PEMWEs and PEMFCs[12]. This is true in spite of the fact that PFSA-type ionomers are costly, have severe ecological impact, suffer from softening at elevated temperature as well as considerable gas permeability, and allow only for very limited chemical variation which prohibits the tailoring of membrane chemistry and properties to specific requirements[13,15–17].

Among potential alternatives, fluorine-free (also: hydrocarbon) aromatic ionomers bearing sulfonic acid functional groups have been the most studied in the past years[15,18,19]. They span a variety of polymer architectures and are based on e.g. poly(arylene ether)s[20–24], poly(imide)s[25–28], poly(sulfone)s[29–32], or poly(phenylene)s[33–38] and their respective copolymers. Their versatile chemistry enables the tuning of specific properties and has facilitated the understanding of structure-property relationships in PEMs.

Hydrocarbon PEMs are fundamentally different from PFSAs, with typically significantly reduced acidity of the sulfonic acid moieties and a tortuous nano-morphology that exhibits less pronounced phase-separation[39–41]. As a result, at similar hydration levels (expressed as number of water molecules per functional group, λ), hydrocarbon PEMs typically exhibit significantly lower gas permeabilities, but also suffer from considerable loss of proton conductivity at low RH compared to PFSAs[13,39]. The finding that a local increase of concentration of ionic moieties in hydrocarbon PEMs provides a highly nonlinear contribution to their overall proton conductivity[35,42,43] – especially at low RH – was able to remedy this issue and lead to the creation of hydrocarbon PEMs with locally high IEC that significantly outperform PFSA-type PEMs[44].

At the same time, since hydration in these materials is a direct effect of the ion exchange capacity and itself affects virtually all other characteristics of an ionomer membrane[13], high IEC hydrocarbon PEMs often suffer from excessive water uptake at high RH (or water solubility) and brittleness under dry conditions (due to their highly ionic character) – problems whose significance can only truly be evaluated when testing the durability of prototype cells in conditions close to application.

While many studies have individually implied that fluorine-free aromatic PEMs have superior properties compared to PFSA-type PEMs with lower cost, few of them simultaneously possessed the required balance of properties spanning sufficient proton conductivity, high chemical as well as mechanical stability, and scalability of their approach[12,15,19]. This underlines that a comprehensive strategy is needed rather than a point-by-point perspective when high IEC hydrocarbon ionomers are developed for PEMWE and PEMFC application, starting with a promising material.

The central material in this work is the class of sulfonated poly(phenylene sulfone)s (sPPS), which offers high potential for application due to its attractive properties stemming from its unique chemistry: as well as high conductivity[32,42], sPPS offer extreme stability towards hydrolysis[32,43], very high thermooxidative stability[32,43], low electroosmotic water drag through strongly confined and finely dispersed aqueous domains[42], retained conductivity at low RH compared with less acidic hydrocarbon ionomers[39], and water insolubility even at high IECs. However, even though sPPS are unique in terms of their stability, transport properties, and morphology, they are typical in terms of their excessive swelling at high RH and brittleness under dry conditions. To make the unique transport and stability properties of sulfonated poly(phenylene sulfone)s available for application, a comprehensive approach to their viscoelastic reinforcement is to be taken. This is the goal of the present work. Therefore, the structure of this thesis involves three related aspects along the process from pure materials to cell optimization as shown in Figure 1.1.

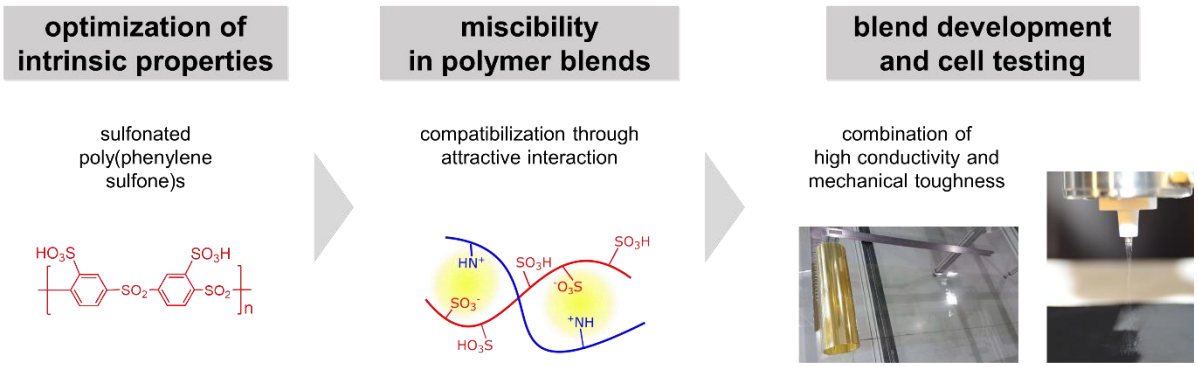

Figure 1.1 Thesis structure.

The first aspect (Chapter 3) is the optimization of the intrinsic viscoelastic properties of a particularly suited sPPS, which lays the groundwork for reliable and systematic further development. The second aspect (Chapter 4) entails the identification and in-depth understanding of a suitable acid-base blending reinforcement. The third aspect (Chapter 5) is the optimization and balance of properties in the previously identified versatile and scalable polymer blend, with the goal to prepare thin, robust, and highly conductive membranes that can be manufactured on a large scale and evaluated in cells and conditions close to application.

2 METHODOLOGY & EXPERIMENTAL TECHNIQUES

Where indicated, this work contains measurements and results which were obtained by project partners within the scope of PSUMEA-3, an integrated project funded by the German Federal Ministry of Education and Research (BMBF, grant code 03EK3045A). Project partners comprise the Hahn-Schickard Institut für Mikrosystemtechnik (HS-IMTEK) in Freiburg, Germany, the Zentrum für Sonnenenergie- und Wasserstoff-Forschung (ZSW) in Ulm, Germany, as well as FUMATECH BWT in Bietigheim-Bissingen, Germany.
CCM production, cell assembly and characterization of PEMWE cells (Chapter 3) as well as measurement of FC-performance and durability data (Chapter 5) was performed by Dr. Carolin Klose at HS-IMTEK. Blend membranes cast on a commercial pilot line (Chapter 5) as well as raw PBI-O was supplied by FUMATECH BWT.

This work further contains – where indicated – measurements and materials which were obtained in scope of a master thesis at the MPI für Festkörperforschung (MPI-FKF) in the group Physical Chemistry of Solids as well as data and materials which were obtained by partners at the Agricultural University of Georgia (AUG) in Tbilisi, Georgia.
Modification of PSU to yield PSU-Py(Me) (Chapter 4) was performed by Philipp Haizmann at MPI-FKF. Step-growth polymerization of sPPS materials, as well as GPC measurements (Chapter 3), and modification of PSU to yield PSU-Py(Keto) (Chapter 4) was performed by Prof. Dr. Giorgi Titvinidze at AUG.

2.1 ELECTROCHEMICAL IMPEDANCE SPECTROSCOPY (EIS)

Impedance spectroscopy is an essential electrochemical method for studying transport behavior of ion conducting polymers. In alternating current (AC) impedance spectroscopy ion-blocking electrodes (typically platinum) are used to measure the AC resistance (impedance Z) as a function of frequency ω (typically in the range of mHz to MHz) while the alternating current $I(\omega)$ is applied. The sample exhibits not only resistive but also capacitive properties which causes a phase shift of the induced voltage $U(\omega)$ vs. the applied current.

The impedance can be expressed as a frequency dependent complex impedance, given by

$$Z(\omega) = \frac{U(\omega)}{I(\omega)} = Z'(\omega) + iZ''(\omega) \tag{2.1}$$

with Z' being the dispersive real part and Z'' the absorptive imaginary part of the complex impedance.

In a Nyquist plot of $-Z''$ vs. Z' the phase angle can then be extracted and for its evaluation equivalent circuits are used. In case of pure ionic transport and transfer the equivalent circuit consists of an electrode circuit and an electrolyte circuit, which are in series. The electrode circuit consists of a resistor R_{CT} accounting for the impeded charge transfer in parallel with a capacitor accounting for the polarization of the electrode. The electrolyte circuit is a parallel connection of an ohmic resistor R_{el} for the transport and a capacitor representing the dielectric properties of the electrolyte. At low frequencies ($\omega \to 0$) the impedance approximates the sum of the electrolyte resistance R_{el} and charge transfer resistance R_{CT}. At high frequencies ($\omega \to \infty$) where the imaginary part of $Z(\omega)$ approaches zero, the measured resistance approximates R_{el}. With knowledge of the measured sample's geometry, its specific ionic conductivity σ can then be calculated according to

$$\sigma = \frac{l}{R_{el} \cdot A} \tag{2.2}$$

with sample length l and the sample's cross-section A.

The conductivity contribution of a single charge carrier type j is related to its drift mobility, which is related to the diffusion coefficient $D_{\sigma,j}$, whereby $D_{\sigma,j}$ can be related via the Nernst-Einstein equation to the measured conductivity, according to

$$D_{\sigma,j} = \frac{k_B}{c_j\left(z_j e\right)^2} \cdot \sigma_j \cdot T \tag{2.3}$$

with the number z_j of charges e per carrier, the concentration c_j, the Boltzmann constant k_B, and the temperature T.

2.1.1 Experimental

Membranes were dried under ambient conditions between paper towels and subsequently cut into rectangular samples of 1 cm width and 6 cm length. Sample stripes were clamped into a

commercial 4-electrode conductivity cell by FUMATECH BWT equipped with platinum wire electrodes of 1 cm distance and length and PTFE gasketing. The cell was connected to the frequency response analyzer Agilent 4192A LF by HEWLETT PACKARD to measure the impedance in the frequency range of 10^2 Hz to 10^7 Hz while applying a 100 mV sinusoidal AC potential. The heated open cell was further equipped with a liquid water inlet and exhaust through which deionized water was constantly fed to provide $p(H_2O) = 10^5$ Pa, while the measurement cell was temperature controlled in the range of 110 °C to 150 °C, taking at least 30 min to equilibrate in between 10 °C temperature steps.

2.2 THERMOGRAVIMETRIC ANALYSIS (TGA)

Water uptake behavior of membranes was measured in hydrated N_2 atmospheres via equilibrium thermogravimetric analysis in a modified humidifier system. The humidifier system consists of a double-walled glass container, in which demineralized water is temperature controlled by circulating water in the outer compartment. A constant nitrogen flow of 40 mL/min passed through the container ensures saturation of the humidifying gas, which is then led to the measurement chamber. Spatial separation of humidifier and measurement chamber in which the sample is suspended in a glass crucible is achieved by a heated transfer zone, allowing for independent temperature control. With the temperature (in °C) of water in the humidifier ϑ_W and of the sample chamber ϑ_S the saturation partial water pressure in the respective compartments e_W and e_S are calculated according to the empirical formulas

$$e_i(\vartheta_i) = 6.11\ hPa \cdot 10^{\frac{7.5\,\vartheta_i}{237.3\,°C+\vartheta_i}}\ ;\ \text{for}\ T < 70\ °C \tag{2.4}$$

$$e_i(\vartheta_i) = 5.94\ hPa \cdot 10^{\frac{7.29\,\vartheta_i}{226.53\,°C+\vartheta_i}}\ ;\ \text{for}\ T > 70\ °C \tag{2.5}$$

The relative humidity RH is then calculated from the ratio of saturation vapor pressure in both the humidifier and the measurement chamber, using

$$RH = \frac{e_W}{e_S} \tag{2.6}$$

The crucible in which the sample is suspended is magnetically coupled to a fine balance, which creates a closed sample chamber, enabling full humidity and temperature control, avoiding temperature inhomogeneities and water condensation.

2.2.1 Experimental

Dried membrane samples of at least 200 mg weight were inserted into the glass crucible which was cleaned and dried prior. The weight of the sample and crucible were recorded individually to ensure high accuracy of the resulting data. Specific T and RH conditions when recording hydration isotherms were held for 5 h to ensure full equilibration of the sample, both with increasing and decreasing humidity.

2.3 TENSILE TESTING

For evaluation of mechanical properties of polymer membranes, tensile strength tests are typically conducted. The sample is secured in between two clamps, one of which can be controllably moved outwards by either controlling the applied force or the rate of movement. In this way a material sample is elongated up to a desired extension percentage, or until fracture of the sample. The tensile strain, defined as the deformation δ a sample of length l undergoes during the measurement, plotted against the tensile stress, which results from the load P being applied to the sample's cross-section A, yields a stress-strain curve. A stress-strain curve typically contains a material's elastic deformation at low strain until the sample's proportionality limit (or yield point) is reached. Deformation in this regime is expected to be fully reversible. The Young's modulus E is defined as the constant of proportionality which describes the initial linear relationship between tensile stress and tensile strain. Strain exceeding a sample's yield point is irreversible and defined as plastic deformation. The point of fracture is also described as elongation at break. In the simplest case tensile strain and tensile stress are defined by

$$\text{strain} = \frac{\delta}{l} \tag{2.7}$$

$$\text{stress} = \frac{P}{A} \tag{2.8}$$

2.3.1 Experimental

Tensile tests were conducted using a DMA Q 800 by TA Instruments connected to a homebuilt humidifier with temperature and relative humidity control similar to the one described for TGA analyses. For each set of conditions, temperature and RH were kept constant for at least 5 h while continuously recording data in a dynamic mechanical analysis (DMA). The DMA was conducted by applying oscillatory sinusoidal tensile deformation with a frequency of 1 Hz, an amplitude of 20 μm and a preload force of 0.001 N on a dog-bone shaped sample in accordance with DIN EN ISO-527-1. The samples were equilibrated at target temperature and RH until a constant storage modulus was reached. Elongation-to-break measurements were consequently performed in either controlled force mode (increase of force by 1 N/min) or controlled strain mode (elongation of 1 mm/min). The corresponding stress was normalized to the cross-section of the membrane at ambient conditions and the equilibrated length of L_1 (12.0 mm length and 2 mm width at ambient conditions in accordance with DIN EN ISO 527-2).

2.4 GEL PERMEATION CHROMATOGRAPHY (GPC)

Gel permeation chromatography (GPC) is an established technique used in the determination of polymer molecular weights and their dispersity. Polymer samples dissolved in a liquid mobile phase are passed through the stationary phase at a defined flow rate and begin to separate based on their molecular size, or hydrodynamic volume R_h. Smaller macromolecules experience longer retention time on the porous support compared to larger ones, due to increased tortuosity of their pathway. Instruments are typically calibrated using a series of polymer samples (commonly polystyrene) of known molecular weights to establish a molecular weight vs. elution volume calibration curve. Polymer molecular weights are typically represented by their number-average molecular weight M_n which is calculated via

$$M_n = \frac{\sum M_i N_i}{\sum N_i} \tag{2.9}$$

with the total number of moles of all species N_i and their respective molar mass M_i.

Since larger macromolecules represent disproportionately more total sample mass than smaller ones of a given polymer batch, the weight-average molecular weight M_W – which typically is larger than M_n – is often given and calculated using

$$M_W = \frac{\sum M_i^2 N_i}{\sum M_i N_i} \tag{2.10}$$

The distribution of macromolecule weights is often characteristic of a specific type of synthesis or process and is represented by its polydispersity index (PDI). The PDI is calculated via

$$PDI = \frac{M_w}{M_n} \tag{2.11}$$

2.5 FURTHER EXPERIMENTAL TECHNIQUES

2.5.1 Scanning electron microscopy (SEM)

Samples were prepared for cross-sectional SEM by drying membranes in vacuum at elevated temperature. To generate high quality cross-sections, samples were split while submerging them in liquid nitrogen and fixing the cross-sections vertically on a sample holder. The equipped sample holder was introduced into a Merlin SEM by ZEISS, equipped with a Gemini column by ZEISS. For clear identification of different polymer phases, the internal InLens-, SE2-, and EsB-detectors were utilized and a voltage between 0.5 kV to 5 kV was applied. Backscattered electron images were recorded at 3 kV. Multiple sample pieces were analyzed to allow for imaging of representative cross-sections.

2.5.2 Membrane solution casting

Membranes of sPPS and sPPS-based blends were typically solution-cast from 5 wt% solutions of DMAc (or DMSO), by weighing the previously dried (> 7 d at 120 °C in vacuum) polymer powder and dissolving it in the respective solvent by stirring at approx. 100 °C overnight in a closed vessel. In the preparation of neutralized blend solutions, the previously dissolved sPPS was first neutralized (either by addition of equimolar amounts of tripropylamine (TPA) or by the addition of equimolar amounts of e.g., Li_2CO_3) before the desired dried blend component was added. In non-neutralized blends the dried blend component was directly added as powder to the dissolved sPPS solution. The overall blend mixture was kept stirring at approx. 100 °C

until all solids were fully dissolved. Afterwards the solution was cooled down to below 60 °C (to avoid fast evaporation in the oven) while stirring. The mixture was filtered, using Whatman GF/A disposable syringe filter of pore size 1.6 μm by GE and directly deposited onto leveled rectangular glass plates of 11x11 cm dimension in a heated vacuum oven. The polymer solution was allowed to homogeneously distribute on the entire glass substrate area for approx. 30 min at 60 °C. Subsequently vacuum was applied of typically 12 mbar, reaching 1 mbar by the end of the 2-day drying process. Mechanically robust membranes were additionally dried at 120 °C in vacuum for 1 d after the drying at 60 °C. Dry glass plates were previously conditioned by submerging them in a bath containing a mixture of KOH and isopropanol for approx. 5 d and subsequent washing with deionized water.

2.5.3 Membrane spray coating

DMD cells were fabricated by spray-coating a dilute sPPS-containing (1-3 wt%) solution of DMAc onto the catalyst layer of a heated GDE at 90-100 °C. Spray parameters were adjusted for different polymer solution as to ensure homogeneous and fine dispersion of solution droplets. An ExactaCoat spray-coater by SONOTEK was used for spray-coating, in combination with an AccuMist nozzle (180 kHz). For the spray-coating of brittle membranes, an area of approx. 25 cm^2 was sprayed in multiple layers (typical layer thickness of approx. 0.7 µm) with variable pauses in between layers as to ensure drying of the previous layer without full solvent removal (that resulted in brittle cracking). DMD half cells were removed from the hot bed and conditioned as described below.

2.5.4 Membrane conditioning

Cast membranes were submerged in an acidic aqueous solution containing 10 wt% sulfuric acid at typically 60 °C and stirred. The acidic solution was exchanged multiple times and the membrane subsequently washed neutral in stirred deionized water. This process was monitored by intermittently checking the washing water's residual conductivity. Conditioned membranes were either stored in water at room temperature or dried and pressed between paper towels.

2.5.5 Titration of ion exchange capacity (IEC)

Titration of IEC to determine the amount of sulfonic acid moieties in an ionomer membrane is a widely used technique[45]. For titration, a membrane (in its H^+-form) of approx. 50 mg was submerged into a room temperature solution of 1 M NaCl for at least 24 h or until ion exchange is complete. The resulting acidic solution was then titrated using a 0.01 M NaOH solution and a Titrino Plus 848 by METROHM. The IEC was calculated according to

$$IEC = \frac{V_{NaOH} \cdot c_{NaOH}}{m_{dry}} \tag{2.12}$$

with the membrane's dry weight m_{dry} titrant's volume $V_{:NaOH}$ and concentration c_{NaOH}.

2.5.6 Gravimetric determination of water uptake (WU)

Water uptake was measured by immersing a membrane of typically approx. 50 mg in water at different temperatures for at least 24h. The membrane's dry weight m_{dry} was recorded after the measurement by drying the sample in vacuum at 120 °C for at least 3 days and subsequent weighing. Water uptake (WU) and number of water molecules per sulfonic acid moiety (λ) were calculated by comparing membrane weights in their fully hydrated (m_{wet}) vs. fully dried state (m_{dry}), by including their prior titrated IEC, according to

$$WU = \frac{m_{wet} - m_{dry}}{m_{dry}} \tag{2.13}$$

$$\lambda = 10 \cdot \frac{WU}{18\frac{g}{mol} \cdot IEC} \tag{2.14}$$

3 OPTIMIZATION OF THE INTRINSIC PROPERTIES OF S360

In this chapter (see Figure 3.1), mechanical properties of S360 are characterized and their enhancement as a consequence of an optimized synthesis is studied. PEMWE cells based purely on improved S360 are prepared and examined for the first time.

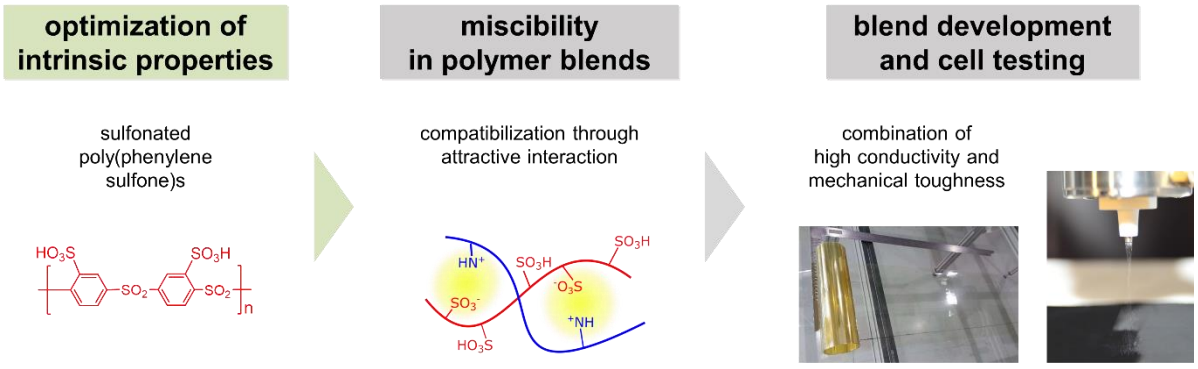

Figure 3.1 Thesis structure, first chapter.

Results in this chapter are in part and where indicated contained in publications by Katcharava et al.[46] and Klose et al.[47]

3.1 BACKGROUND

3.1.1 Sulfonated poly(phenylene sulfone)s (sPPS)

The polymer backbone comprising only para-substituted phenylene units connected exclusively by sulfone linkers, shown in Figure 3.2, is the origin of highly attractive properties in sulfonated poly(phenylene sulfone)s (sPPS, also: $sPSO_2$) and the reason why they are uniquely suited for further development as an alternative PEM, especially for application in fuel cells and electrolyzers.

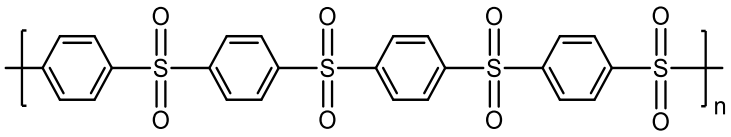

Figure 3.2 Chemical structure of poly(p-phenylene sulfone).

In contrast to the structurally related poly(arylene ether sulfone)s – high performance thermoplastic polymers – pure poly(p-phenylene sulfone) is poorly characterized[48–52] due to its complete insolubility.

The inclusion of a pure poly(phenylene sulfone) backbone in an ionomer with variable and defined ion exchange capacity was made possible synthetically in 2007 by the use of sulfonated monomers (as opposed to prior typical statistical post-sulfonation[53,54]) in a step-growth polycondensation reaction followed by the oxidation of the intermediate mixed sulfonated poly(phenylene sulfide sulfone) (sPSS) with hydrogen peroxide[32] (without cleavage of the polymeric backbone[32,42,55]). In the oxidized sPPS the para-positioned sulfone (-SO_2-) linkages and their strong electron withdrawing character (by means of negative inductive and mesomeric effect) reduce the aromaticity of the phenylene rings greatly[32] and significantly enhance the acidity of the protogenic groups. Combined with the insoluble backbone's tendency to aggregate in a linear and highly ordered "open book" morphology[50], this leads to a number of highly attractive properties in sPPS: extreme stability towards hydrolysis[32,43], very high thermooxidative stability[32,43], low electroosmotic water drag through strongly confined and finely dispersed aqueous domains[42], retained conductivity at low RH compared with less acidic hydrocarbon ionomers[39], and water insolubility even at high IECs (e.g. sPPS with 2.78 meq g^{-1}, equivalent weight (EW) of 360 g meq-1, termed sPPS-360 or S360, shown in Figure 3.3)[42]. When all phenylene units bear one sulfonic acid moiety, a water-soluble ionomer with IEC of 4.54 meq g^{-1} (EW of 220 g meq-1) termed sPPS-220 or S220, shown in Figure 3.3, can be prepared[53].

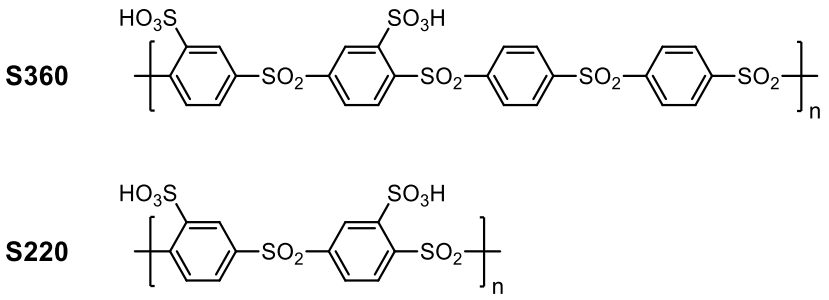

Figure 3.3 Chemical structure of S360 (also: sPPS-360) and S220 (also: sPPS-220).

Since the synthesis is straightforward and can yield a variety of materials with variable high IECs[32,43,56], the family of sulfonated poly(phenylene sulfone)s provides a scalable and adjustable plattform for a new type of PEMs.

However, even though sPPS are unique in terms of their stability, transport properties, and morphology, they are typical in terms of their excessive swelling at high RH and brittleness under dry conditions.

3.1.2 Excessive swelling and brittleness

The excessive swelling that sPPS membranes with high degree of sulfonation exhibit in water is typical for hydrocarbon PEMs[57]. While water uptake in the hydration regime of exothermal Langmuir adsorption (up to λ = 5-6 for PFSA-type materials[58,59], corresponding to approx. 70% RH) scales mostly linearly with IEC, water uptake in the region of mostly entropy driven osmosis is affected stronger by IEC. When a PEM is submerged in water (also: Schroeder's paradox[60]), this effect is most pronounced: in water, swelling of the membrane is ultimately limited by the internal pressure the polymer matrix may provide to counteract the osmotic pressure caused by continued dilution of charges[61,62]. Due to the higher water volume fraction at same λ (due to typically higher IEC) compared to PFSAs and weaker phase separation in hydrocarbons, the ability to counteract the swelling pressure is reduced and excessive swelling of high IEC hydrocarbon PEMs a common issue[36,63]. In water uptake measurements this tendency is expressed by an increased λ (number of water molecules per sulfonic acid moiety) in water with increasing IEC, e.g. from λ = 20 for an IEC of 2.49 meq g^{-1} to λ = 50 for an IEC of 3.50 meq g^{-1} with identical polymer architectures and under identical conditions[17].

Excessive swelling is not only detrimental due to higher gas permeability and loss of mechanical strength of the PEM, but also due to the dilutional effect it has on the material's protonic charge carriers. The introduction of more and more ionic, strongly hygroscopic functional groups leads to water solubility of any (non-crosslinked) high-IEC ionomer, as is the case for S220.

The brittleness under dry conditions (< 20% RH) that sPPS of different IEC exhibit is also commonly observed in highly sulfonated polyarylene ionomers[15,35,42,64–66]. As with virtually all properties of PEMs, the origin of brittleness lies within the interplay of the ionomer's molecular structure and its membrane's morphology: especially at high IEC and when sulfonic acid moieties are directly attached to the semi-rigid polyarylene backbone, the polymer backbone's tendency for self-aggregation is perturbed and the formation of morphology is dominated by strong electrostatic interactions. Under dry conditions this salt-like inter-polymer interaction thwarts the material's deformation (as opposed to hydrated conditions when ions are sufficiently shielded from one another, and the aqueous domain is "softer"). As a result, deformation under dry conditions commonly requires considerable strength (i.e., the material is stiff) but readily leads to the material's fracture (i.e., the material is not tough). In tensile tests (as described in Chapter 2.3) this is expressed by a high Young's modulus, short and random elongation at break and lack of yielding behavior. It is important to note that in tensile tests brittleness is not directly measured. Brittle PEMs further tend to fracture during membrane fabrication, e.g. during final solvent evaporation while solution-casting, as is indicated when membrane forming properties are discussed (affected among other factors by e.g. molecular weight).

3.1.3 Step-growth polymerizations

Step-growth polymerizations have played a key role in the creation of modern engineering plastics and high performance polymeric materials for nearly a century[67], making use of a tremendous variety of monomers for the deliberate design of material properties[68]. The reaction mechanism commonly involves the condensation of either two differently functionalized bifunctional monomers or the reaction of a single monomer containing both types of functional groups involved in the condensation reaction[69]. In case of the step-growth polymerization of

S360 the former is the case, where a sulfonated bisphenolic monomer bearing fluoride functional groups condenses with a non-sulfonated bisphenolic monomer bearing thiol functional groups[32] (see Chapter 3.3). During the polymerization, monomers first react to form dimers which subsequently combine to form tetramers, giving rise to a sequence of addition in which monomers are rapidly consumed during initial stages. As a consequence the reactive species in solution change quickly from high monomer and end group concentration to oligomers and low end group concentration[69]. High conversions are thus often marked by significant increase in viscosity, which in return limits polymer mobility and probability of further reactions[68,69]. Prediction of molecular weight evolution in step-growth polymerizations helps to better understand the criticality of monomer ratios in such reactions and was first described by Carothers in the 1930s and later expanded[67,70,71]. It describes the relationship between degree of polymerization $\bar{X}_n$ and degree of conversion p in different types of step-growth polymerizations. As in the synthesis of S360, in case of two bifunctional monomers that can only react with each other, the stoichiometric balance r of the two monomers needs to be included in the description, according to

$$\bar{X}_n = \frac{N_0}{N_t} \tag{3.1}$$

$$p = \frac{N_0 - N_t}{N_0} \tag{3.2}$$

$$r = \frac{N_a}{N_b} \tag{3.3}$$

$$\bar{X}_n = \frac{N_b + rN_b}{N_b + rN_b - 2rpN_b} = \frac{1 + r}{1 + r - 2rp} \tag{3.4}$$

with the number average degree of polymerization $\bar{X}_n$, the number of molecules at the beginning of the reaction N_0 and during reaction N_t, the number of monomers A and B at start, N_a and N_b, the stoichiometric ratio r (monomer B being defined as the majority monomer, thus $r \leq 1$), and the extent of the reaction p (reaching 1 at full conversion).

Two limits of the relationship can be described as in case the two monomers are present in equimolar amounts (r = 1) and in case that the conversion p is 100% according to

$$\bar{X}_n = \frac{1}{1-p};\ (r = 1) \tag{3.5}$$

$$\bar{X}_n = \frac{1+r}{1-r};(p = 1) \tag{3.6}$$

In case of r = 1, the polydispersity index is

$$PDI = 1 + p \tag{3.7}$$

The most important implication of Carothers' Equation is that polymers of high molecular weight prepared via step-growth polymerizations only form at high degrees of conversion[72]. To make it tangible: a conversion degree of 90% limits the degree of polymerization to only 10 – severely limiting the achievable mechanical properties of the product polymer.

3.1.4 Hydrocarbon-based PEMWEs

Similar to fuel cell application, Nafion and PFSA-type ionomer membranes are the prevalent polymer electrolyte in commercial PEMWE systems. They usually employ thick membranes of commonly between 100 µm and 175 µm thickness, thereby compromising between high performance and high durability paired with good gas separation properties[7,73,74]. As a consequence, the fluorinated ionomer membrane contributes considerably to overall system cost[75,76]. Environmental impact due to the leeching out of fluorine-containing degradation products is another worrisome aspect of widespread application of PFSAs in PEMWE[77–79]. Properties that many hydrocarbon ionomers could offer in terms of reduced cost, higher conductivity at full hydration, and increased thermomechanical strength are thus highly sought after advantages[73,80,81] over PFSAs in PEMWE application. Additionally, the nano-morphology of hydrocarbon ionomers, which typically is characterized by less pronounced phase-separation and reduced water drag through the membrane[39,82] also contributes to reduced gas permeability at same water content[25,83], thus potentially enabling the use of much thinner membranes.

Even though aforementioned excessive swelling of high IEC hydrocarbon ionomers when submerged in water is a typical mechanical issue they face, the overall viscoelastic requirements towards the use of alternate membrane materials in PEMWE cells are less

extensive compared to their use in PEMFCs. This stems from the constant conditions during operation of a water electrolyzer regarding temperature and hydration state, as opposed to strongly varying conditions in fuel cells, where repeat hydration and drying cycles lead to early mechanical failure of most hydrocarbon materials[84,85].

3.2 PROPERTIES OF S360

A strictly alternating structure of two sulfonated and two non-sulfonated phenylene units in a pure polysulfone backbone, shown in Figure 3.4, yields an ion exchange capacity of 2.78 meq g^{-1} (EW of 360 g mol^{-1}) and is termed sPPS-360 or S360. Due to strong insolubility of the pure poly(phenylene sulfone) backbone, low-IEC sPPS remain insoluble[32], while S360 with its considerably high IEC can be dissolved in several common polar organic solvents (NMP, NEP, DMAc, DMSO).

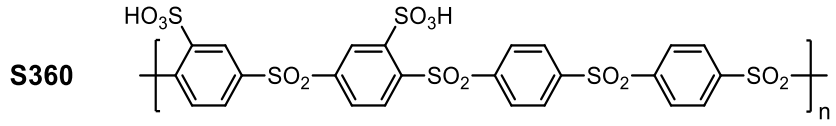

Figure 3.4 Chemical structure of S360 (also: sPPS-360).

Among sulfonated poly(phenylene sulfone)s S360 currently is the homopolymer with the highest ion exchange capacity while still being water insoluble and able to be cast and handled as a free-standing pure membrane. Out of the family of sPPS, S360 is therefore the best candidate for exploring reinforcement concepts and to identify critical issues that sPPS-based PEMs face when brought to fuel cell application, which will be explored in Chapter 4 and Chapter 5.

Virtually all properties of S360 are strongly correlated with the water content in the material under any given condition. While PEMWEs operate under constant conditions of full hydration at high temperature, the processing that starts with the membrane fabrication and includes careful cell assembly requires balanced mechanical properties to withstand storage and handling.

Isothermal water uptake measurements (via TGA, described in Chapter 2.2) of S360 conducted at 90 °C are shown in Figure 3.5 below. Depicted is the reversible water uptake behavior of S360 in terms of λ (water molecules per functional group) in the range of 10% - 90% RH.

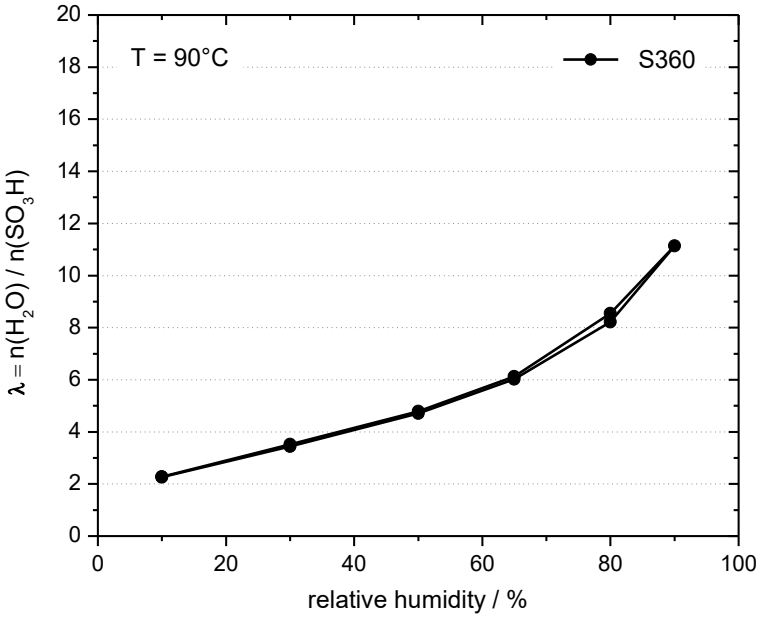

Figure 3.5 Hydration isotherm of S360 at T = 90 °C.

The hydration behavior of S360 is quite similar to that of Nafion up to a relative humidity of around 80%[12], underlining that hydration in this region is mainly determined by the thermodynamics of hydration of the sulfonic acid moieties. Compared to other hydrocarbon ionomers[86], at low RH the higher acidity results in a higher λ value. For better understanding of the significance of water content for mechanical properties, the following example is particularly helpful: a λ value of around 4 in typical ambient conditions corresponds in S360 – due to its high IEC (each bearing the same λ) – to a water volume content in of around 25 vol% (based on its density of approx. 1.6 g mL^{-1}).

High water contents also facilitate high mobility of hydrated proton species. When submerged in water at 30 °C, proton conductivity of up to 169 mS cm^{-1} was achieved in pure S360 membranes[32], which is the result of the material's high IEC. The specific proton conductivity of S360, as well as extruded (N117) and solution-cast Nafion (N212) measured under FC-typical relative humidity (as described in Chapter 2) are shown in Figure 3.6. With an IEC of

2.78 meq g^{-1}, S360 exceeds the conductivity of Nafion N117 (0.91 meq g^{-1} IEC) at 50% RH by a factor of approx. 2 and is similar to that of solution-cast Nafion N212 (0.91 meq g^{-1} IEC).

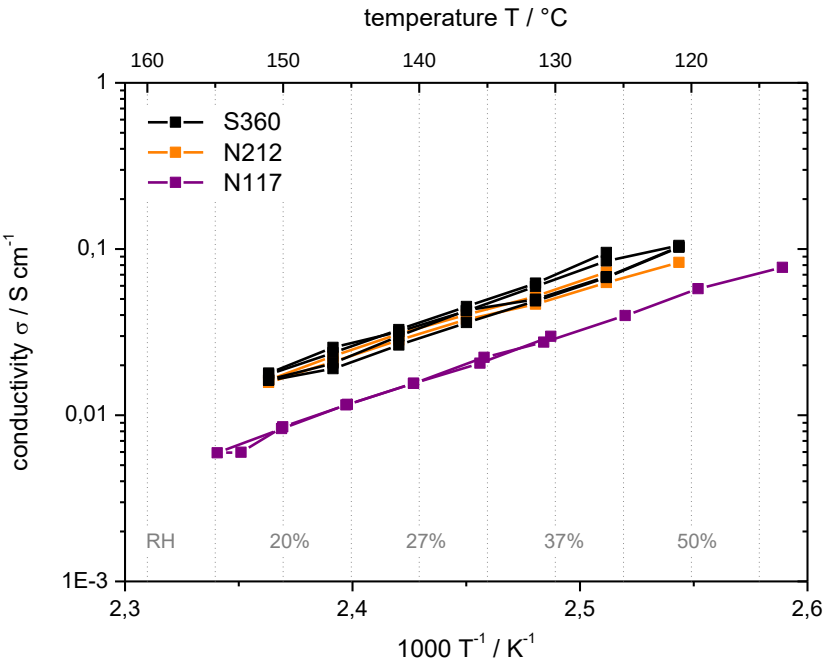

Figure 3.6 Proton conductivity of S360, N117, and N212 at $p(H_2O)=10^5$ Pa as a function of temperature.

The high acidity of sPPS is the reason that conductivity at low RH does not drop off in comparison to superacidic PFSAs, as is observed in less acidic hydrocarbon ionomers[63]. It should be noted that for constant λ, proton conductivity in sPPS has a higher activation enthalpy and higher pre-exponential factor than in Nafion[42] as a consequence of higher migration entropies (characteristic for vehicle type transport)[87]. The higher activation enthalpy of proton conductivity and the fact that S360 does not undergo softening at high temperature (no T_g below its decomposition temperature of about 280 °C as typical for sPPS[32]) make sPPS typical high-temperature materials and suited for higher operating temperatures in fuel cell applications (currently ≤ 90 °C).

This also means that different form PFSAs[12], viscoelastic properties of S360 are not significantly affected by temperature. Instead, the viscoelastic behavior is – in contrast to conductivity and water uptake at to a certain RH – expected to be dependent on the molecular weight of the ionomer. The most important parameter affecting mechanical properties is,

however, the relative humidity of the membrane's environment to which it is equilibrated: the aqueous-ionic domain that percolates S360's polymer matrix leads at high RH – due to significant water uptake seen above – to extreme softening of the material and in dry conditions gives rise to the formation of an "organic salt" due to low water content, thus causing brittleness. These shortcomings of viscoelastic nature have kept sPPS in general and S360 specifically from being applied in and further developed for PEMFC and PEMWE application. To evaluate which mechanical shortcomings originate from the ionomer's low molecular weight and which are intrinsic to the chemical structure of sPPS, high quality sPPS is needed. The need for consistent high molecular weight of sPPS is highlighted particularly well by the excessive and non-reproducible swelling behavior of low molecular weight S360 membranes in water: for low molecular weight batches of S360 (M_n < 15 kDa), samples tend to continuously swell in hot (80 °C) water and ultimately disintegrate – preventing any further tests. With increasing molecular weight accessed in the step-growth polymerization of S360, membranes of S360 become significantly more dimensionally stable and water uptake measurements and membrane behavior is more reliable. However, variation of dispersity for batches of intermediate molecular weight S360 (M_n of 15-30 kDa) leads to considerable sensitivity of the samples towards the conditions under which they are fabricated. This causes a vast spread of mechanical properties and especially water uptake behavior in water as is shown in Figure 3.7. The tested membranes were fabricated from batches of different intermediate-M_n S360 and cast from either DMSO or DMAc and dried under different conditions. Data from the initial publication of S360 is included for reference[32].

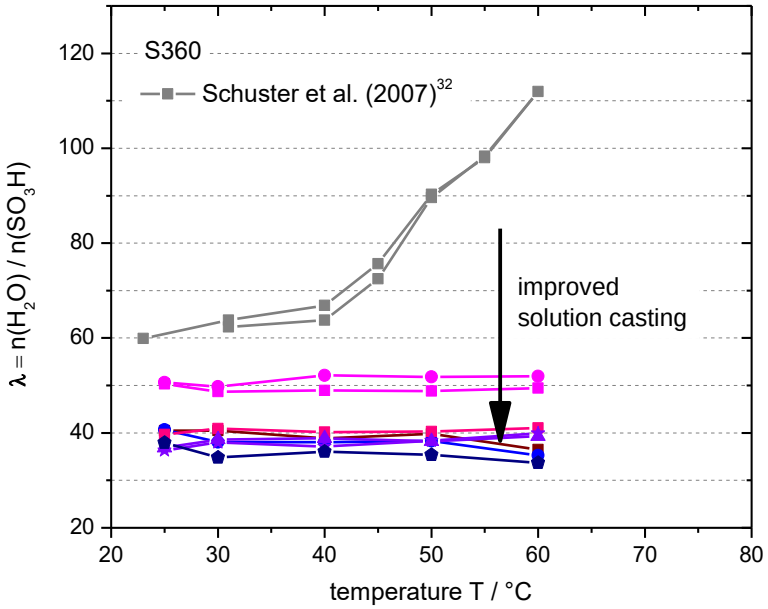

Figure 3.7 Water uptake of several S360 membranes in water as a function of temperature.

While the molecular weight of S360 was considerably high in its initial publication, (M_n of 62.5 kDa and M_W of 141.6 kDa), the membrane fabrication process (cast from NMP onto a hot plate) was not yet optimized. Vacuum-cast S360 membranes of lower molecular weight do not exhibit the tendency of drastically increased water uptake beyond approx. 45 °C but vary strongly in their uptake of around λ = 35-50, up to a temperature of 60 °C.

The amount of water in an S360 membrane is considerable not only in water, but also at high RH, and makes up around 47 vol% at 90% RH (as shown in Figure 3.5), which leads to extreme softening of the material. For the investigation of viscoelastic behavior of intermediate-M_n S360, tensile tests under high (90% RH), intermediate (50% RH) and low (≤30% RH) relative humidity were conducted on S360 with M_n= 42 kDa[46] and are shown in Figure 3.8.

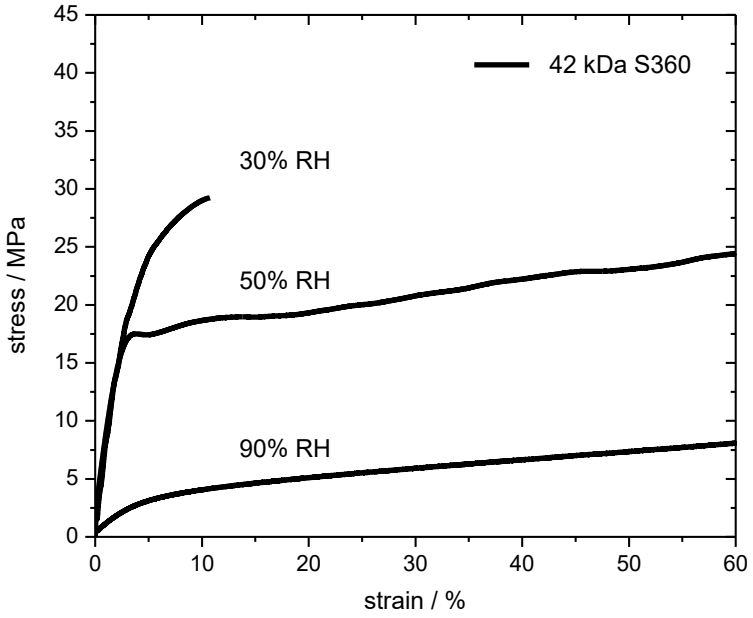

Figure 3.8 Tensile tests of 42 kDa M_n S360 at 90% RH (50 °C), 50% RH (90 °C), and 30% RH (90 °C)[46].

The results with regard to Young's modulus, yield strength, and elongation at break are summarized in Table 1. Numbers for water uptake (in λ) and approximate water volume content during testing are given for orientation.

Table 1 Tensile test results for 42 kDa M_n S360 at 90% RH (50 °C), 50% RH (90 °C), and 30% RH (90 °C).

	90% RH (50 °C)	**50% RH** (90 °C)	**30% RH** (90 °C)
Water uptake (λ)	11.1	3.5	2.2
Water content (vol%)	47	27	22
Young's modulus (MPa)	69	579	627
Yield strength (MPa)	3	17	25
Elongation at break (%)	>60	>60	11

It should be noted that a clear extraction of yield strength is not possible for very soft and for brittle behavior. At high RH, a low Young's modulus combined with low yield strength and early onset of plastic deformation that allows for more than 60% elongation is recorded. This

behavior is typical for high IEC materials and a clear consequence of the softening effect water has on S360. At 50% RH, the water content is reduced to 27 vol%, and the material exhibits significantly higher stiffness and yield strength. In such conditions, the material is flexible and can be easily handled. At 30% RH S360 with 42 kDa M_n exhibits first signs of brittle behavior, with a high modulus (comparable to other high IEC materials under similar conditions[17,22]) and considerable yield strength, but significant reduction of elongation at break to 11 % strain.

To explain why the tensile behavior of S360 changes so dramatically with RH, it needs to be considered that only the first couple hydration water molecules (in terms of λ) correspond to the exothermal hydration of sulfonic acid moieties[65]. Water adsorbed beyond that level is only loosely bound, and ionic moieties are electrostatically shielded from one another, which is why additional hydration water exerts a strong softening effect on the material.

As described in Chapter 2.3, brittleness is not directly quantified in tensile tests. However, the behavior of brittle samples is very characteristic: at very low RH, of between 0-20% RH, recording stress-strain data of pure S360 membranes is not reliable. Samples of pure S360 typically undergo random fracture either during preparation or during equilibration which takes place during a dynamic mechanical measurement (see Chapter 2). This behavior was recorded in tensile tests of S360 at 20% RH (90 °C) and 5% RH (90 °C), which are shown in Figure 3.9.

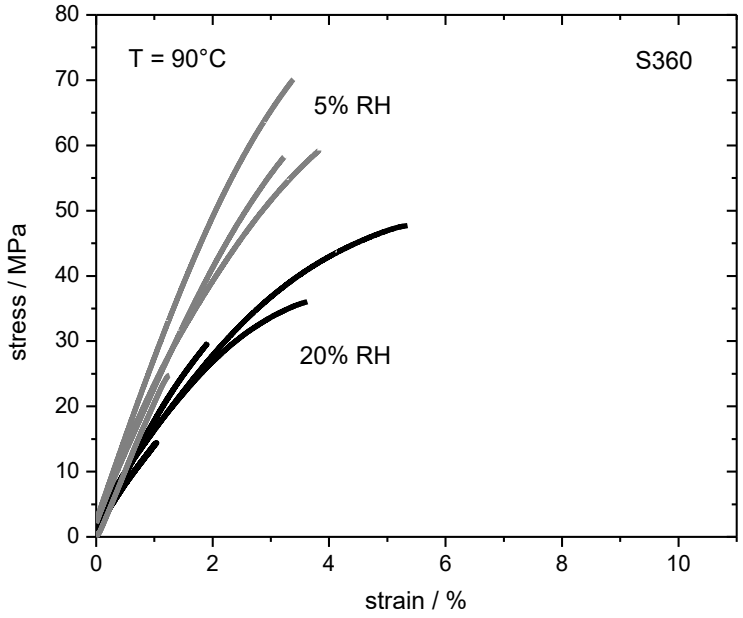

Figure 3.9 Tensile tests of S360 at 20% RH (90 °C) and 5% RH (90 °C).

Such erratic behavior does not allow for the analysis of any of the parameters in Table 1, but instead leads to the qualitative finding of brittleness under the applied conditions. Similar qualitative assessment of membrane behavior can be conducted by fully drying membrane samples in a heated vacuum oven at 90 °C. Membranes of several square centimeter area dried in such manner can then be bent and folded onto themselves resulting in fracturing if brittle – as is the case for S360.

The above discussed issues of excessive water uptake, especially when submerged in liquid water, as well as at high water activity (e.g. 90% RH) and brittleness under dry conditions (0-20%RH) combined with the sensitivity towards the membrane fabrication process are expected to be in some way affected by the ionomer's molecular weight. Therefore, the observed behavior underlines the necessity for reproducible high molecular weight of S360. Reproducible behavior also is a requirement for the investigation and systematic optimization of properties of polymer blends based on S360 or sPPS in general, as will be subject of Chapter 4 and Chapter 5.

3.3 OPTIMIZED STEP-GROWTH POLYMERIZATION OF S360

As is described above, the step-growth polymerization involved in the preparation of S360, shown in Figure 3.10, requires high conversion to achieve high molecular weights.

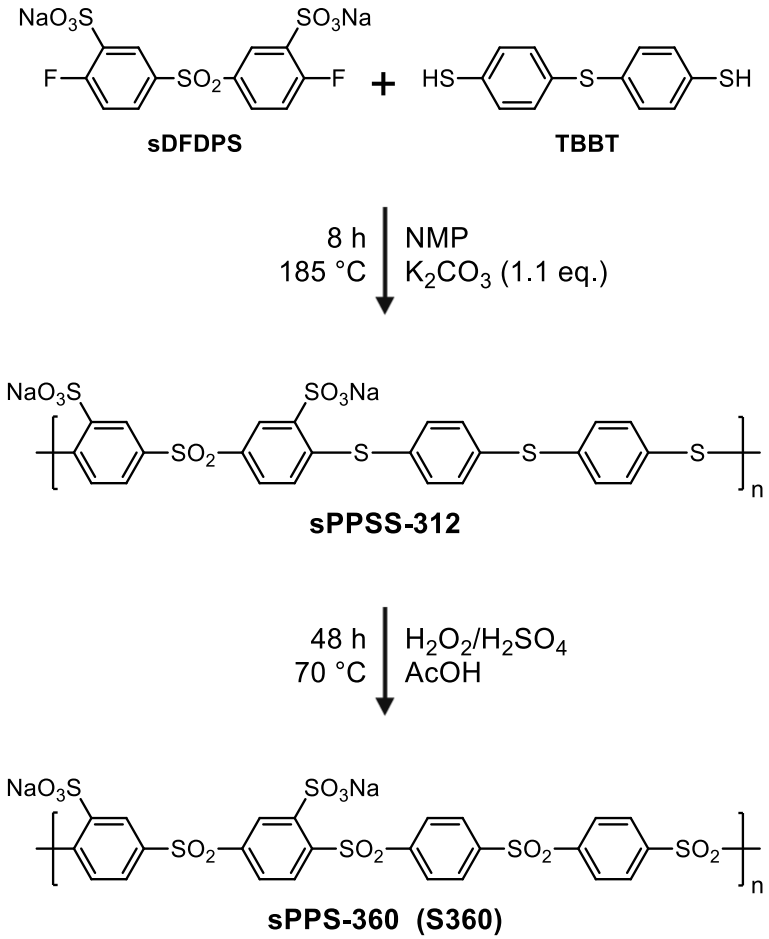

Figure 3.10 Preparation route of S360 via step-growth polymerization of sDFDPS and TBBT[46].

Repeated syntheses of S360 that followed the initial synthesis[32], reported in 2007, via the above shown scheme often were not able to reach the initially reported molecular weight: after oxidation, molecular weight values typically were in the range of 15-30 kDa M_n and 30-45 kDa M_W, with varying PDIs. It was consequently assumed that the required precise balance of monomers was rarely achieved. Subsequent study of the purity of thiobisbenzenethiol (TBBT) revealed no contamination via NMR and X-ray spectroscopy[46]. Next, a closer look was taken

at the typical preparation of the – in syntheses of hydrocarbon PEMs widely applied[88–92] – sDFDPS monomer, shown in Figure 3.11.

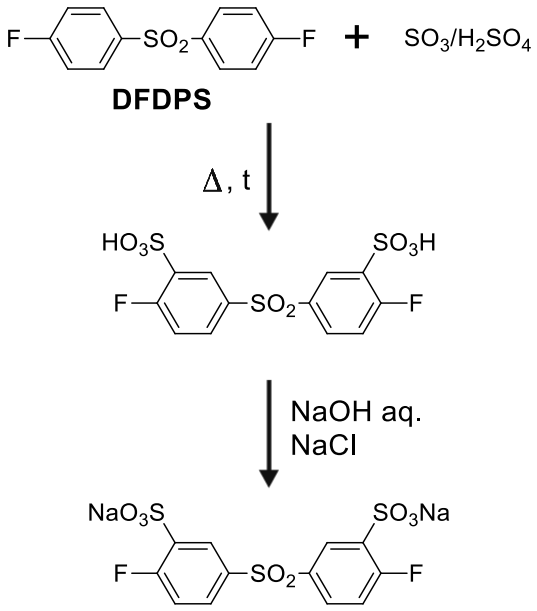

Figure 3.11 Preparation route of sDFDPS[46].

In its preparation, commercially available difluorodiphenylsulfone is typically first sulfonated by treating it with oleum followed by its neutralization with an alkali hydroxide – commonly sodium hydroxide (NaOH) – and then salted out from solution (e.g. by sodium chloride, NaCl)[46]. In a final step, the salted out sDFDPS is purified by recrystallizing it from an alcohol/water mixture. Monomer purity is commonly checked solely by NMR[89–91] and deviations of expected values in elemental analyses[29,88,90] are not further investigated.

It was found that the commonly applied purification step is not only not quantitative (as assumed) but also unreliable due to the similar limited water solubility of sDFDPS and Na_2SO_4. A thorough analysis found sodium sulfate contents up to around 10 wt% in sDFDPS[46], which has a detrimental effect on the stoichiometric balance of monomers. The monomer ratios were then corrected and conditions in the step-growth polymerization of S360 were subsequently optimized. As a result of corrected monomer ratios and improved synthetic conditions the molecular weight of S360 achieved number average molecular weights of M_n > 150 kDa[46]. The high molecular weight of S360 which can now be achieved in a highly reproducible

manner allowed for the increase of preparational scale (in the 100s of grams range) thereby meeting the requirements for the studies conducted in Chapter 4 and in Chapter 5. To quantify the effect that the improved high molecular weight of S360 has on the material, viscoelastic properties in terms of water uptake and stress strain behavior were studied and compared to the ones previously recorded. Results from tensile tests of high-M_n (154 kDa) S360 in comparison to intermediate-M_n (42 kDa) S360 are shown in Figure 3.12.

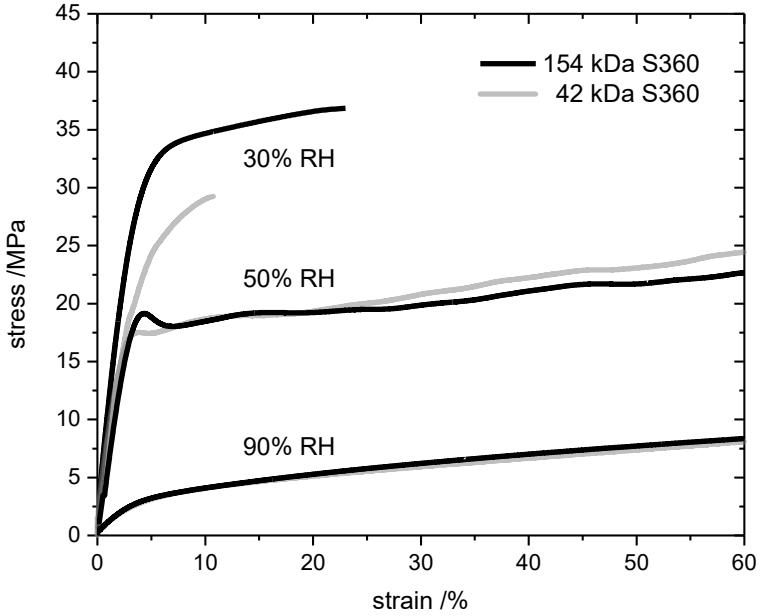

Figure 3.12 Tensile tests of 154 kDa M_n and 42 kDa M_n S360 at 90% RH (50 °C), 50% RH (90 °C), and 30% RH (90 °C)[46].

The results with regard to Young's modulus, yield strength, and elongation at break are summarized in
Table 2. Numbers for approximate water content under testing conditions (from TGA) are again given, and are not expected to be affected by S360's molecular weight.

Table 2 Tensile test results for 154 kDa M_n S360 at 90% RH (50 °C), 50% RH (90 °C), and 30% RH (90 °C).

	90% RH *(50 °C)*	**50% RH** *(90 °C)*	**30% RH** *(90 °C)*
Water content (vol%)	47	27	22
Young's modulus	69	661	938
Yield strength (MPa)	3	19	31
Elongation at break (%)	>60	>60	23

The biggest difference between intermediate and high molecular weight S360 (M_n of 154 kDa) in tensile tests can be seen at low RH of 30%: a more than 30% increase in Young's modulus is seen combined with a much more pronounced yielding behavior, which marks the transition from elastic to plastic deformation, and a more than twice as high elongation at break compared to S360 with M_n of 42 kDa. While it does not lead to reduced qualitative brittleness, evaluated as described in Chapter 3.2, it leads to more reliable membrane formation (not prone to fracture) and much facilitated handling, allowing for processing of the membrane in careful fabrication steps to prepare catalyst coated membranes (CCM) for PEMWE cells as described below.

However, at intermediate relative humidity, the improved molecular weight has insignificant effect on tensile behavior, which is reduced to a more pronounced yielding behavior compared to previously found in low M_n S360. As can be seen, tensile behavior at high humidity is identical for S360 independent of molecular weight. This underlines the dominating role that water plays at high hydration levels due to its loosely bound state and consequent strong softening effect on the material. Different to tensile behavior at 90% RH, water uptake measurements revealed significant effects in high-M_n S360 membranes, which reproducibly exhibit reversible water uptake of λ = 28 at room temperature with a significant temperature dependent increase beyond 60 °C up to λ = 51 at 95 °C, as is shown in Figure 3.13.

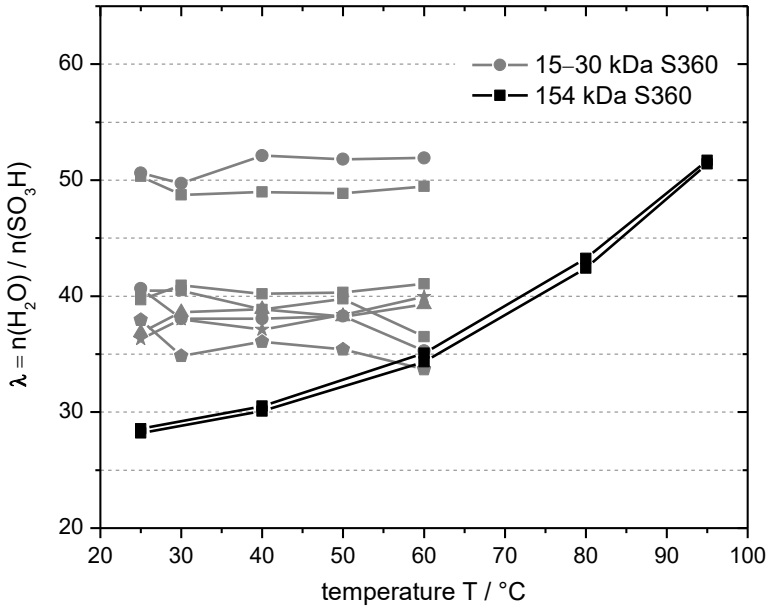

Figure 3.13 Water uptake of a 154 kDa M_n S360 membrane in water as a function of temperature.

This reversible water uptake behavior of high-M_n S360 vacuum-cast from DMAc (as described in Chapter 2) is well reproducible, including the increase of λ at elevated temperature. The significant decrease of λ in the range of 20-65 °C may be well explained by the continuation of swelling that is driven by osmotic pressure through the dilution of charges until it is equal to the counter pressure generated by the polymeric matrix, as described above. This reduction in λ therefore stems from the increased polymer chain lengths and resulting improved entanglement which strengthens the polymer matrix. Since water uptake measurements of low-M_n S360 cast in non-optimized processes could not be reproduced, the apparent change in temperature dependent water uptake of S360 is not evaluated further.

3.4 FLUORINE-FREE CELLS FOR PEMWE BASED ON S360

High molecular weight S360 allows for the fabrication of membranes for testing in electrolyzers, since operating conditions in PEMWE are less harsh than those of PEMFC in terms of mechanical degradation of the PEM as a result from varying operating conditions. PEMWE further makes use of much thicker membranes, which facilitates handling and reduces

the danger of pinholes and defects associated when fabricating membranes on a lab scale. Consequently, the preparation of S360-based cells for PEMWE was chosen in a feasibility study[47] (within the project described in Chapter 2) to showcase the attractive properties that sPPS-type membranes can bring to application.

Not only was it possible to include pure solution-cast S360 membranes of high M_n in PEMWE-typical CCM fabrication process, but a catalyst ink comprising only S360 as proton conducting ionomer was also created and applied for the first time[47]. A cross-sectional SEM of the spray-coated S360-based CCM (Anode loading: 1.5 mg cm^{-2} IrO2, cathode loading: 0.5 mg cm^{-2} Pt), depicted in Figure 3.14, shows the consistent quality of both membrane and catalyst layers.

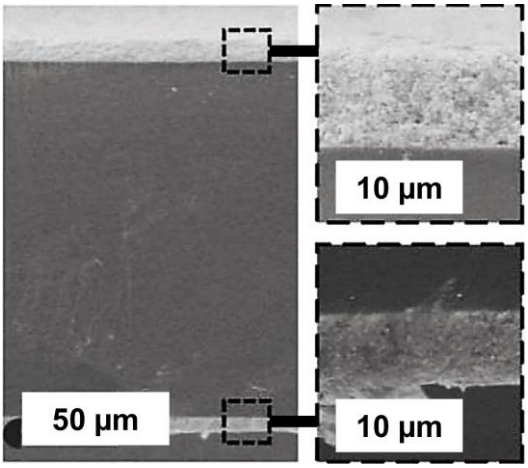

Figure 3.14 Cross-sectional SEM of the S360-based PEMWE MEA[47].

An identical cell based on Nafion N115 of comparable thickness was also fabricated and the two cells fully characterized[47]. The performance recorded for two identical pure S360 MEAs at 80 °C exceeded that of the previously reported highest performance with a hydrocarbon membrane in a PEMWE cell (utilizing PFSA in the CL) of 1.6 A cm^{-2} at 1.8 V[93] by far, as is shown in the polarization curves of both studied cells in Figure 3.15 below.

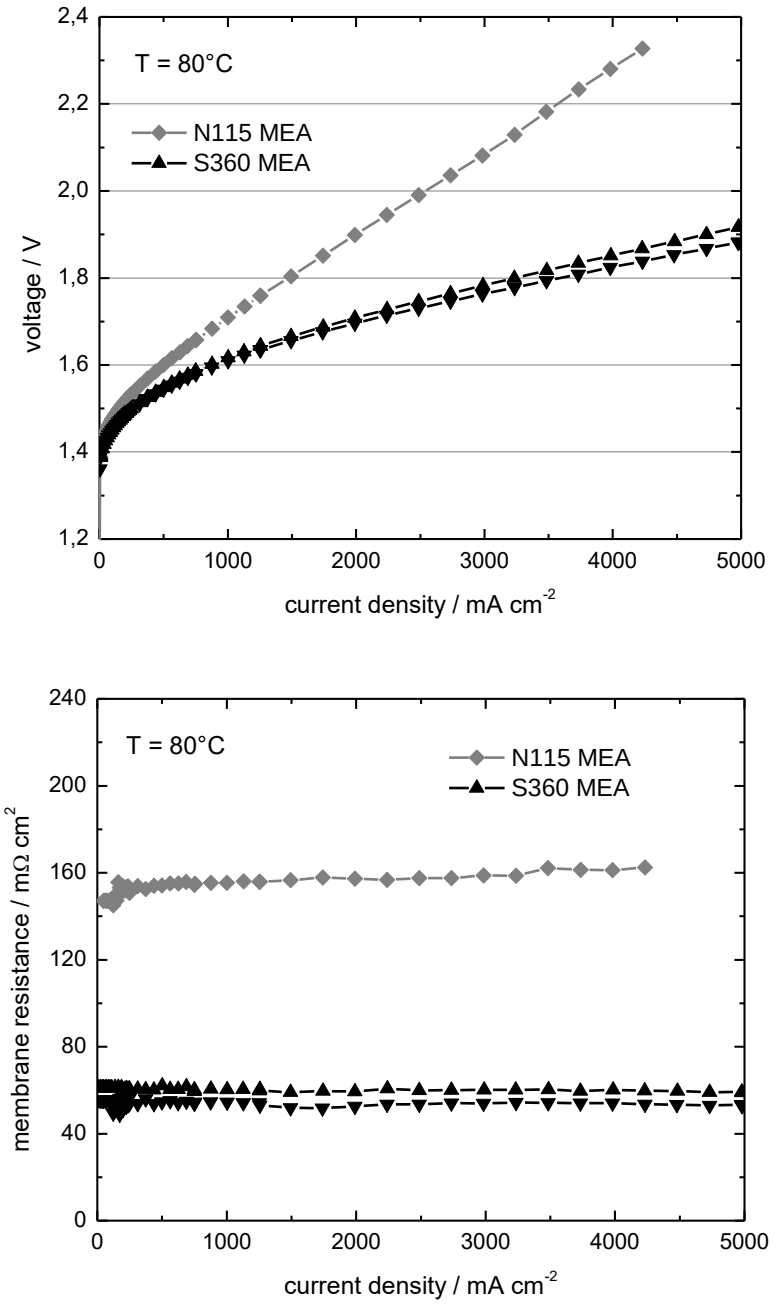

Figure 3.15 Cell polarization and membrane resistance for two Nafion and two S360 MEAs at 80 °C as a function of current density[47].

Record performance was achieved in the sPPS-MEA of 3.48 A cm^{-2} at 1.8 V[47]. The remarkable difference to the performance achieved in the N115-MEA could be mostly explained by the

more than 60% lower ohmic area resistance of S360 compared to N115[47] of 57 mΩ cm^2 vs 161 mΩ cm^2 and matches the conductivity expected from ex-situ measurements of S360. The successful implementation of a catalyst layer that is based on S360 helped avoid issues at the membrane-electrode interface that previous studies reported when applying PFSA-CLs[93,94]. The limitations of applying pure S360 in PEMWEs was shown by conducting a soft durability test of constant 1 A cm^{-2} current hold for 100 h[47]. The results of durability testing two sPPS-MEAs in this manner are shown in Figure 3.16.

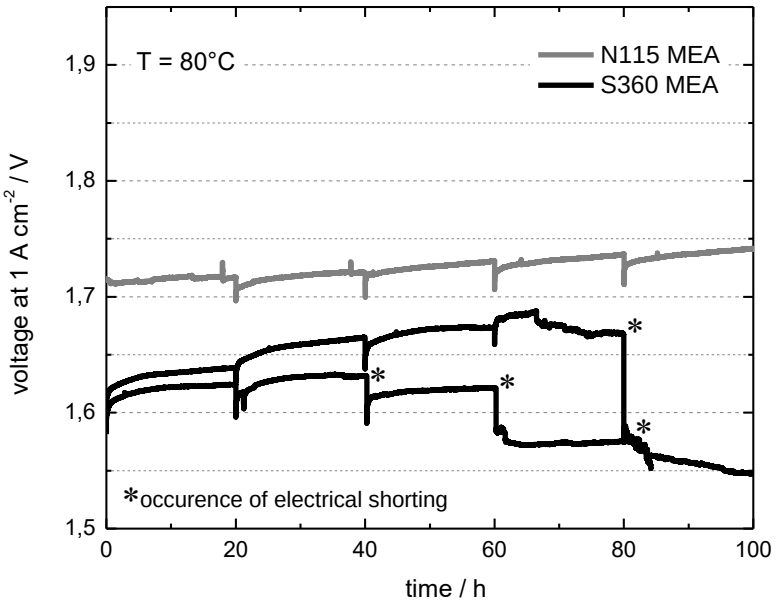

Figure 3.16 Voltage evolution during constant current hold at 1 A cm^{-2}in two S360-MEAs and a N115-MEA[47].

The occurrence of a number of electrical shorts in the S360-based MEAs conceals other degradation mechanism that would otherwise lead to a voltage increase over time[47,95]. Their formation is expected to arise from the previously characterized strong water uptake and thus softening of the membrane at high water temperature. An increase in durability and better gas separation properties could potentially both be achieved by suppressing the high water uptake of pure S360[47] through viscoelastic reinforcement, as studied in Chapter 5.

3.5 CHAPTER SUMMARY

In this chapter, mechanical properties of S360 were characterized and their enhancement as a consequence of an optimized synthesis studied. PEMWE cells based purely on improved S360 were prepared and examined for the first time.

- Water uptake of low molecular weight S360 in water was found to be particularly sensitive to the conditions during membrane fabrication, underlining the need for reproducible high molecular weight of S360.
- The step-growth polymerization of S360 was optimized after large amounts of inorganic salt contaminants originating from the monomer's established purification method were identified[46].
- Increased molecular weight of S360 was found to have significant effect on mechanical properties under dry (30% RH) conditions (50% increase in Young's modulus, 25% increase in yield strength up to 31 MPa and twofold increase in elongation at break) and when submerged in water (reduction of $\lambda \sim 50$ to $\lambda = 28$ at room temperature).
- A CCM based on high molecular weight S360 was created and tested in a PEMWE, achieving record performance of a hydrocarbon PEM of 3.48 A cm^{-2} at 1.8 V[47]. The sPPS-MEA suffered from poor durability most likely as a consequence of the severe softening in water that pure S360 exhibits.

As a result of the work reported in this chapter, polymer blending as a reinforcement strategy could be explored (Chapter 4) and optimized (Chapter 5).

4 MISCIBILITY IN POLYMER BLENDS BASED ON S360

In this chapter (see Figure 4.1), acid-base polymer blends as reinforcement strategy for sPPS are explored and blends of sPPS and PBIO are chosen for further optimization. A model acid-base polymer blend system is studied in regards to the effect that interpolymer interaction strength and concentration have on S360-blend morphology.

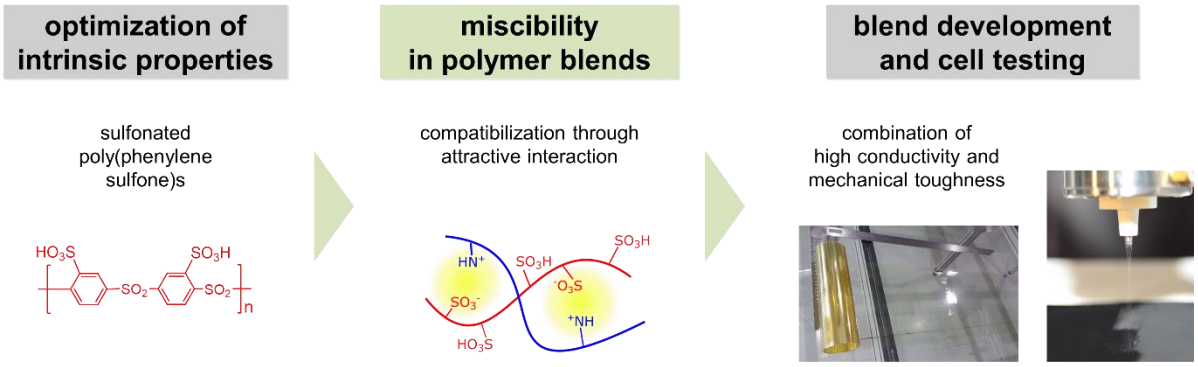

Figure 4.1 Thesis structure, second chapter.

As described in Chapter 2, syntheses in this chapter were performed by Prof. Dr. Giorgi Titvinidze (AUG) and Philipp Haizmann (MPI-FKF).

4.1 BACKGROUND

4.1.1 Reinforcement concepts

Extensive literature exists on the optimization of properties of sulfonated hydrocarbon ionomers. The often-mentioned freedom of design in creating new hydrocarbon PEM materials has led to a multiplicity of adjustment strategies. A significant portion of studies that look to

alter properties of existing hydrocarbon ionomers focuses on the improvement of transport properties (protons, water, gas). Studies that seek to alter viscoelastic properties of existing hydrocarbon ionomers – as is the goal in this work – typically include them in copolymerization approaches[18,21,23,82], cross-linking experiments[92,96–100], (nano)particle containing composite materials[12,101–104], or blending strategies[30,105–110].

Mechanical reinforcement of sPPS via copolymerization was investigated in 2012, where the unique transport and stability properties of sPPS could be retained while the introduction of a well phase-separating hydrophobic block lead to improved viscoelastic properties[82]. Water uptake in these block copolymers was successfully reduced; however, brittleness in the new materials was not fully resolved[82]. The complex synthetic pathway involved in the preparation of block copolymers further hindered the scalability of this approach.

Covalent cross-linking strategies are applied widely and have in the past been very successfully implemented in the suppression of excessive water uptake of hydrocarbon ionomers[111–114]. However, covalently cross-linked ionomers tend to exhibit enhanced brittleness and the process often offers little control over exact cross-linking degree. Still, such a cross-linking strategy could also be integrated and applied to membranes resulting from this work.

Heterogeneous composite materials making use of e.g. silica nanoparticles or chopped glass fibers are also widely and successfully implemented in reinforcement and improvement of hydrocarbon membranes[115–118]. However, particle-containing composites typically provide an increase in strength and stiffness, and do not resolve prior existing mechanical issues due to brittleness. While incorporation of rubbery particles is a common strategy to increase fracture toughness[119,120] in thermoplastics for technical applications, this cannot be translated straightforwardly into PEM materials.

Even though the binary mixture of two polymers is in most cases immiscible and cannot be utilized, blends are still an attractive reinforcement strategy for polymers: they can potentially make use of a wide array of materials that are commercially available and exhibit defined viscoelastic properties, ranging from elastomers (typically low strength, large reversible deformation) to thermoplastics (typically high strength, little reversible deformation). The blending approach also does not involve the alteration of the chemical structure of the base material (here: sPPS), which allows for the retention of desirable characteristic (transport and

stability) properties. The morphology of polymer blends can vary strongly and be characterized by mutual incompatibility, phase-separation on the micro scale, bi-continuity, fine dispersion of one phase in another, or homogeneous miscibility. Depending on the morphology, the properties of both components may be changed and combined in numerous ways[119,121]. Processing conditions play a crucial role in the determination of blend morphology, especially in phase-separating polymer blends[119,122]. To achieve a desired morphology (i.e., affect compatibility between blend components) the functionalization of existing, commercially available polymers is commonplace[123]. The functionalization of polymers can also enable a better understanding of blend component interaction and how their combined morphology gives rise to new properties. Therefore, in this work, polymer blends are chosen as a reinforcement approach to remedy brittleness in S360 and sPPS in general and eliminate their excessive swelling at high water activity.

4.1.2 Polymer blend thermodynamics

The reason as to why binary polymer blends typically are immiscible is explained by the thermodynamics that governs blend miscibility. The general requirement for miscibility in a polymer blend can be expressed in terms of the Gibbs free energy of mixing[121], ΔG_m according to

$$\Delta G_m = \Delta H_m - T\Delta S_m \tag{4.1}$$

with the enthalpy of mixing ΔH_m and the entropy involved in mixing ΔS_m.

A negative Gibbs free energy of mixing is the necessary requirement for two polymers to mix. To exclude unmixing into solid solution compositions the second derivation of ΔG_m with regards to concentration must be included. The requirement for full miscibility thus extends according to

$$\Delta G_m \leq 0 \,; \left(\frac{\partial^2 \Delta G_m}{\partial \phi_i^2}\right)_{T,p} > 0 \tag{4.2}$$

with the volume fraction of polymer i, ϕ_i, and pressure p.

The phase diagram of partially miscible blends is often marked by a lower critical solution temperature (LCST) or an upper critical solution temperature (UCST), as well as miscibility

gaps where the blend separates into two phases. These partially miscible blends are described by

$$\Delta G_m \leq 0 \; ; \left(\frac{\partial^2 \Delta G_m}{\partial \phi_i^2}\right)_{T,p} < 0 \tag{4.3}$$

The most prominently applied theory for the description of polymer blend thermodynamics is the statistical lattice theory developed by Huggins[124] and Flory[125] independently in 1941, and later extended by many authors[126,127]. In Flory-Huggins (FH) theory, the blend as a system is defined as a lattice consisting of N filled sites of equal volume. It is assumed that the polymer chains of polymer 1 and 2 with their respective volume fractions ϕ_i can be described as ideal semi-rigid chains with degree of polymerizations x_1 and x_2, respectively. The description of the entropy of mixing in an ideal binary polymer blend follows as

$$\Delta S_m = -R\left(\frac{\phi_1}{x_1} ln\phi_1 + \frac{\phi_2}{x_2}\ln \phi_2\right) \tag{4.4}$$

with the gas constant R.

Applying the concept of regular solutions and assuming all pair interactions in the framework of a mean-field theory leads to the description of the enthalpy of mixing ΔH_m as

$$\Delta H_m = RT\chi\phi_1\phi_2 \tag{4.5}$$

with the unitless Flory-Huggins interaction parameter χ.

For binary systems, the FH equation then reduces to

$$\Delta \mathrm{G_m} = RT\left(\frac{\phi_1}{x_1}\ln \phi_1 + \frac{\phi_2}{x_2}\ln \phi_2 + \chi\phi_1\phi_2\right) \tag{4.6}$$

It follows from the above description that the entropy of mixing in a binary polymer blend is insignificantly small due to the typically high degrees of polymerization and further decreases with increasing molecular weight. Specific attractive interaction between the two polymers is thus generally needed to induce miscibility. The specific interaction between the components also needs to be stronger than attractive interaction between two polymer chains of the same kind. Next to the Flory-Huggins theory, a number of theoretical approaches have been developed to describe polymer blends and to offer models that can empirically describe

miscibility in blends, ranging from further lattice theories, off-lattice theories, to a growing number of computational methods[119].

4.1.3 Compatibilization in polymer blends

Polymer blends for viscoelastic reinforcement of hydrocarbon ionomers have found considerable attention in the last two decades. The aforementioned required specific attractive interaction between a sulfonated ionomer and a desirable blend component often entails (a combination of) dipole-dipole interaction, hydrogen bonds, and/or electrostatic interaction (e.g. acid-base or ion-ion), to induce miscibility[99,108]. Due to the presence of a high concentration of sulfonic acid moieties (or salt forms thereof) in such a blend, miscible binary polymer blends often rely on attractive specific interaction between the blend component and the ionomer's functional groups[106,128]. Hydrogen bond induced miscibility is studied in-depth in nonionic blends[130] and was successfully applied to polymer blends with hydrocarbon ionomers in the past[109,131,132]. However, issues were reported pertaining to limited miscibility and loss of reinforcement effect at elevated temperature and water content[99,109]. Ion-ion interactions by means of the combination of a polyanionic material (i.e., a PEM) with a polycationic material (e.g., a quaternized nitrogen compound) are not studied, since their extremely strong interaction leads to immediate precipitation from their combined solution. In general, acid-base interactions are the prevalent type of interpolymer compatibilization in blends with hydrocarbon ionomers. It should be noted, that in literature acid-base interacting blends are often described as ionically cross-linked materials. Acid-base blends make use of polymeric bases among which poly(benzimidazole) (PBI) and its derivatives (PBIO, PBIOO) are the by far most prominent. An in-depth description of blends between sulfonated hydrocarbon ionomers and poly(benzimidazole) can be found below. PBI is also one of the few commercially available materials that fulfils the multifaceted requirements towards a blend component for use in PEMFCs and PEMWEs.

4.1.4 Blend component requirements

The requirements towards any polymeric component being considered for blending with sPPS originate from each respective target application. The most important requirement for use in sPPS-based blends is the ability of a blend component to enhance viscoelastic properties.

Further requirements entail the all-around stability of the blend component in terms of thermal, acid, hydrolytic, and general chemical robustness, as to not limit the applicability of sPPS-blends by the added blend component. Especially demands towards stability in the highly acidic environment within sPPS membranes (especially at low water contents) and stability towards hydrolysis (critical in PEMWE) are not met by many available materials. For practical reasons, commercial availability (to allow the desired scalability of the approach) as well as solubility in a common solvent with sPPS (DMAc, DMSO, NMP) are required within the scope of this work.

4.1.5 PBI blends in literature

The development of binary polymer blends comprising poly(benzimidazole)s and its closely related derivatives PBIO and PBIOO was initiated by with the discovery of miscibility between meta-PBI (m-PBI) and various poly(ether imide)s (PEI)[133,134]. The attractive interpolymer interactions, which often led to complete miscibility of PBI with PEI when co-casting (as is the process applied in this work), were identified to be hydrogen bonds[135,136]. Blends that utilized PBI were then studied extensively in context of high-performance textile fiber development and other fields, extending the scope of binary systems that form miscible blends with PBI drastically[135,137–139].

Within the field of PEM materials for low temperature fuel cells, research of PBI blends was pioneered by Kerres et al.[140,141], who first presented miscible blends of m-PBI and sulfonated poly(sulfone) (sPSU), as well as poly(ether ketone) (sPEK). To circumvent the instant precipitation from solution due to the strong acid-base interaction between the two components, shown in Figure 4.2, the acidic polymers were converted to a neutral salt form before casting.

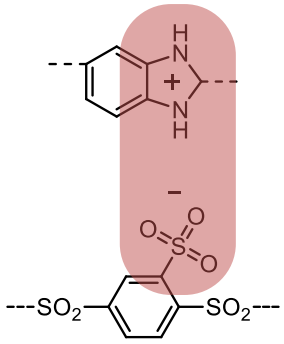

Figure 4.2 Schematic of an acid-base adduct in sPPS/PBI blends.

After film formation, the homogeneous blend membranes were conditioned in acidic solution to yield ionically interacting acid-base moieties. Since then, multiple studies as well as continued works by Kerres have led to a large number of sulfonated hydrocarbon ionomers that have been successfully included in homogeneous acid-base blends with PBI or its derivatives[106,142–162]. In these blends, PBI is utilized to provide increased mechanical and often thermochemical stability.

However, PBI blends do not come without drawbacks. This is because the acid-base interaction effectively consumes protonic charge carriers in the conditioned membrane. As a consequence, a blend membrane's IEC can be straightforwardly calculated by subtracting the added PBI's "IEC" from the amount of charge carriers provided by the sulfonated hydrocarbon ionomer. Additionally, IEC in blends is lowered by the volumetric addition of a non-conductive component. As a result, the amount of added PBI in blends of at least IEC of 1.3 meq g^{-1} is limited to typically around or below 10 wt% [141,143,146,153,160,162], limiting the reinforcing effect that PBI can exert on the material. High IEC water soluble hydrocarbon materials of 2.4-3.2 meq g^{-1} IEC were used in a study to produce blends with an overall IEC of 1.6 meq g^{-1} and included high PBI contents of up to 27 wt%[147] to mechanically reinforce them. The ionomer in the study utilized the same pure pol(phenylene sulfone) backbone that sPPS do, with exception of a fluorinated linker in the bi-sulfonated biphenolic monomer, yielding analogues of S360 and S220[108]. Even though a promising combination of conductivity and mechanical reinforcement seemed achievable, the necessity of an optimization of the polycondensation reaction to yield better intrinsic mechanical stability was concluded[147].

Molecular weights achieved in the above described study were limited to a number average molecular weight M_n of 10 kDa[108] for the S360 equivalent structure of two sulfonated and two non-sulfonated phenylene units in the (fluorine linker-containing) polysulfone backbone, and even lower for the S220 equivalent structure[108] of fully sulfonated phenylene rings. In stark contrast, this work makes use of S360 with M_n of 154 kDa (as reported in Chapter 3) and can build on the previously conducted optimized synthesis of S220 in 2012 which yielded high average molecular weights (M_W) of beyond 300 kDa[56]. This underlines the importance of taking a comprehensive approach to the viscoelastic reinforcement of promising highly sulfonated PEM materials, as is the strategy of this work.

4.1.6 Membrane formation and blend morphology

The membrane fabrication process is not only a crucial step in generating reproducible behavior from samples comprising of a single polymer[163–165] (see Chapter 3), but typically has significant impact on the formation of morphology in a binary polymer blend – especially in a mixture that tends to phase-separate[166], as mentioned above and studied extensively in literature[119]. A special situation arises when creating blends not from a polymer melt (as is more common[119]), but by solution co-casting the two components, as is the case in this work. This is in part because a full understanding of the process requires a precise description of the mixture thermodynamics for a specific composition (polymers and solvent), as well as its evolution during continuous solvent evaporation[167]. In addition, the kinetics with which the system goes from dilute solution to concentrated solution and finally to solid film can have a major impact[168]. An example in this work is the comparison of solution co-casting vs. the spray-coating[169] of a certain blend (seen Chapter 5): while during solution casting from high boiling point solvents such as DMAc polymers may stay mobilized for multiple hours, spray-coated membranes are formed (immobilized) within seconds (depending on the conditions). Consequently, significant effort is put into improving understanding of phase-separated morphologies in polymer blends and how a component's phase size, shape, and distribution can be affected as well as themselves affect blend material properties[119,120,170]. As mentioned in Chapter 1, and as will be highlighted by the findings in Chapter 5, versatility in the comprehensive approach to reinforcing sPPS membranes and to bringing this type of material

into application is a key aspect. Because of the uncertainty and unreliability that a phase-separating blend morphology implies, in combination with the extensive experience and success that was found by literature in generating homogeneously mixing PBI-containing acid-base blends, the process of film formation in phase-separating blends is not substance of this work. Instead, a homogeneously mixing blend (that is impervious to the membrane fabrication process) is desired. Therefore, experiments that investigate the effect of interpolymer interaction in blend solutions containing sPPS will focus exclusively on specific attractive interactions (their strength and concentration) and the resulting blends' cross-sectional morphology (via SEM following the solution co-casting as described in Chapter 2).

4.1.7 PBI blends with sPPS in literature

The second key aspect in choice of suitable polymer blend component – next to miscibility – is the capability to induce mechanical toughness. Thus, PBIO-containing acid-base blends present an attractive prospect for achieving the goal of this work, not only since they have been successfully employed for viscoelastic reinforcement of numerous other hydrocarbon ionomers, but also because they have already been tested in sPPS materials and proven to reinforce them in a similar manner: A study in our group prior to this work, published in 2014, applied PBIOO blending as a reinforcement concept to the multi-block copolymers comprising of pure sPPS blocks and alternating hydrophobic blocks[30]. Blend membranes with PBIOO exhibited expected behavior in terms of loss of IEC, and thus conductivity, but simultaneously dramatic improvement of tensile behavior[30]. Under highly humidified conditions of 80% RH at 80 °C, yield strength could be more than doubled and elongation at break increased more than eightfold[30]. Importantly, membranes created from PBIOO and the sPPS multi-block copolymer were homogeneously miscible in the tested compositions (2, 5, and 10 wt% PBIOO). Another key finding was the retention of sPPS-characteristic microstructure in PBIOO blends (via SAXS)[30]. This is important since it indicates that characteristic transport and stability properties of sPPS can be retained in PBI blends and that the concept can be transferred to pure sPPS (like S360 and S220).

4.2 TRADEOFF IN S360/PBI BLENDS

The tradeoff between retained high IEC (and thus high conductivity) and degree of viscoelastic reinforcement in homogeneous PBIO blends has no clear goal towards which the materials can be optimized in a straightforward manner. That is the result of the complex interrelationship between a number of components and parameters, that in combination describe a PEMFC of PEMWE system's performance and durability. Additionally, IEC in a PEM and thus water uptake under defined T/RH condition affects virtually all other properties of an ionomer membrane (see Chapter 3). Still, a reasonable choice can be made regarding minimum, "required" IEC in a hydrocarbon PEM as to stay an attractive competitor to state-of-the-art PFSAs. In the material class of sPPS, a reasonable IEC range for a membrane suited for PEMFC application is expected to be around 2 meq g^{-1} (previous estimation[30]: 1.8 meq g^{-1}). It should be noted that this number is different for different ionomer chemistries, as it is affected by e.g. the aggregation of sulfonic acid moieties on the polymer backbone. A lower specific conductivity than, for example, Nafion N211 can potentially be tolerated for hydrocarbon PEMs since they typically exhibit better gas separation properties (described in Chapter 1) allowing for the use of thinner membranes. Once again, the versatility of the approach in this work proves to be advantageous, as it allows the adjustment of the "required IEC" at a later technological stage. The development of expected IEC in a S360 blend with PBIO and in a hypothetical non-neutralizing blend as a function of composition is shown in Figure 4.3.

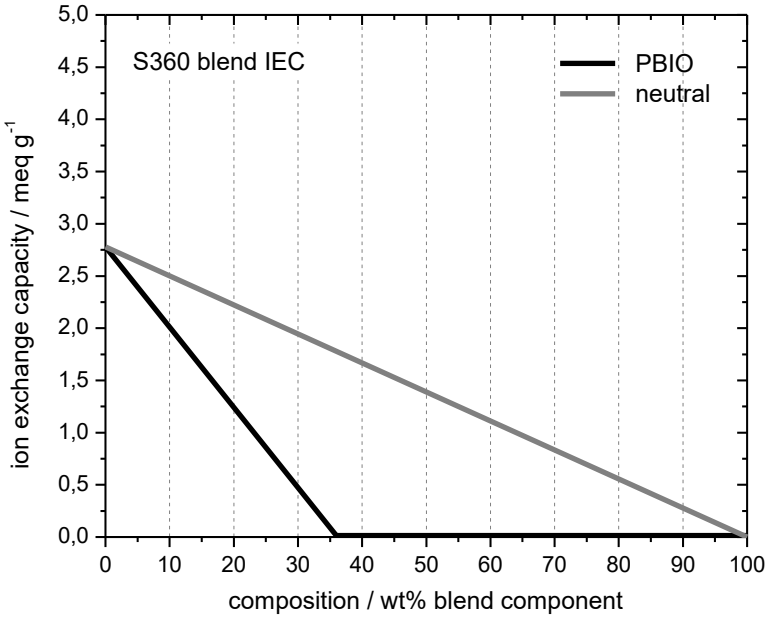

Figure 4.3 Evolution of theoretical IEC in S360 blends as a function of composition and blend component.

Starting with 2.78 meq g^{-1} at 100% S360, addition of PBIO (shown in Figure 4.4, with an equivalent weight referring to imidazole units of 200 meq g^{-1}) linearly reduces an S360 blend's theoretical IEC in a steep decline to 0 meq g^{-1} at a PBI content of around 36 wt%. An aforementioned "required" IEC of 2 meq g^{-1} is already met at a PBIO content of around 10 wt%.

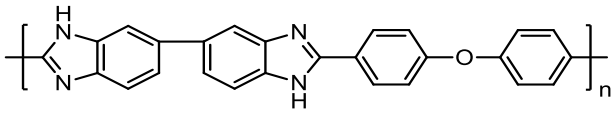

Figure 4.4 Chemical structure of PBIO.

In contrast to that, a hypothetical blend component that – under the assumption of identical miscibility and reinforcement effect in S360-based blends – does not make use of neutralizing acid-base interaction and merely reduces IEC in the blend by its volumetric compositional ratio could be added to S360 up to an amount of approx. 30 wt%. The potential of such hypothetical blend materials to combine highly desirable properties is the reason why the quest for such a

blend component is ongoing and could be valuable for the development of other hydrocarbon ionomers.

However, the advantages that PBIO offers, which have been described in the chapters above, as well as its proven miscibility and proven reinforcement effect with sPPS while retaining sPPS's characteristic morphology, transport, and stability properties, makes PBIO blends uniquely suited for further optimization of properties as will thus be the objective of Chapter 5.

To confirm the expected miscibility and continuously adjustable blend properties of S360/PBIO blends, both blend morphology and evolution of IEC are first probed. The cross-sectional morphologies of several S360-based PBIO containing blends as well as their titratable IEC are shown in Figure 4.5.

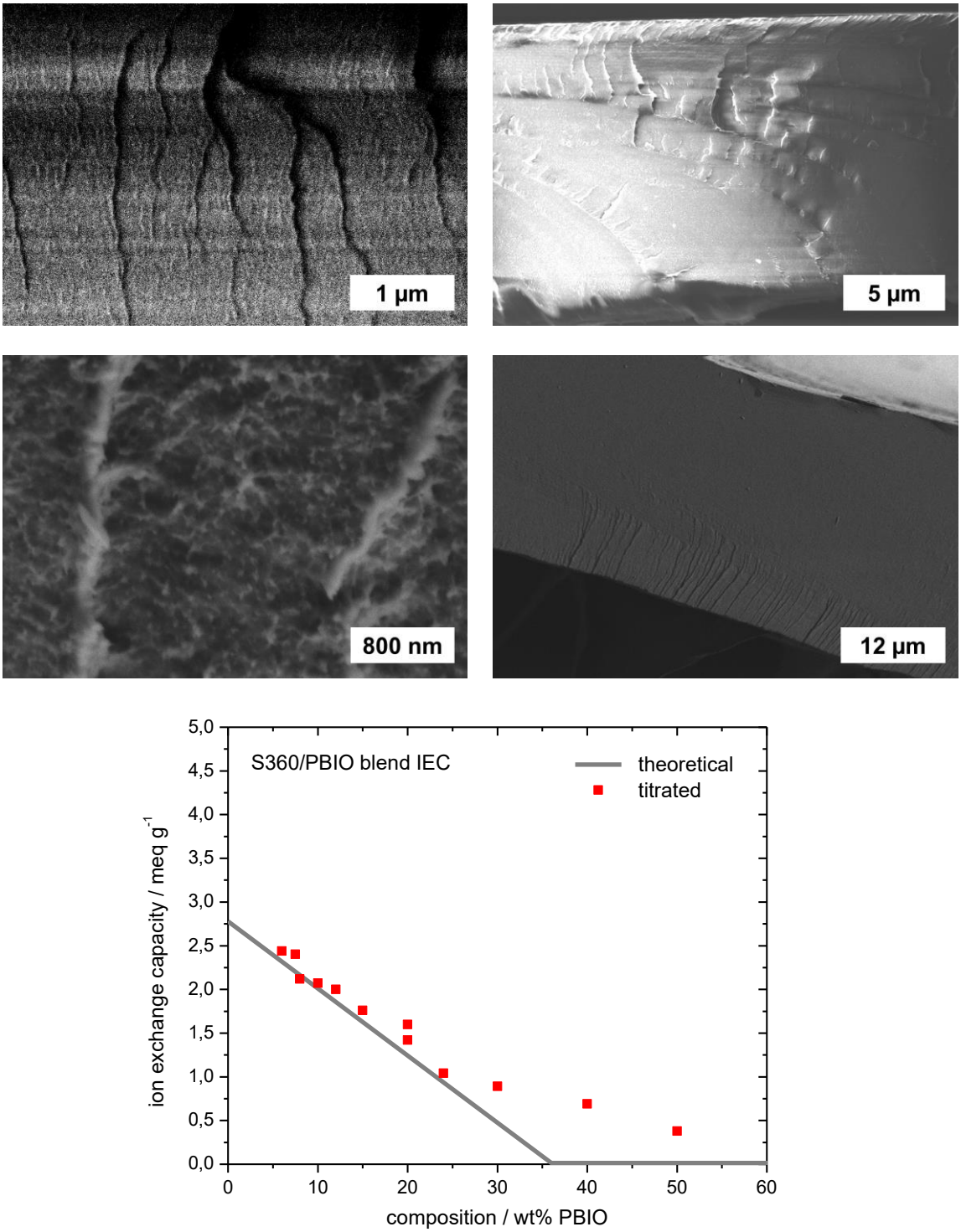

Figure 4.5 Cross-sectional SEM of S360/PBIO blends (from top left to right: 5 wt%, 7.5 wt%, 15 wt%, and 30 wt%) and evolution of experimental IEC in S360/PBIO blends.

All blends were prepared according to the procedure described in the literature[140,161] and above in Chapter 2.5.2. The procedure entails first the dissolution of S360 in DMAc, which is subsequently neutralized with tripropylamine (TPA) or ion exchanged to yield the Li-ion salt form, followed by the addition of dried PBIO, which is dissolved at elevated temperature overnight (depending on the composition) while stirring. The filtered mixture is solution cast in vacuum at elevated temperature to yield a clear membrane, which is conditioned and subsequently analyzed in SEM. All PBIO blend membranes exhibit a fully homogeneous blend morphology and no phase-pure polymeric regimes can be detected via SEM, even at high magnification and by enhanced contrasting. Dark regions visible in some images above correspond to the cross-sections' topographies and are not compositional inhomogeneities. No adverse effects on miscibility based on the employed counterion for S360 was observed. The blends' titratable IECs further match very well to the theoretically expected values. This is in accordance with most literature reports[30,141,160,162] and further underlines the mutual compatibility in sPPS/PBIO blends, as does the progression of conductivity reduction with increasing PBIO content, which will be described in Chapter 5. At high PBIO contents, which are not relevant for application due to exceedingly low IEC, deviation from theoretically expected IECs is found. This can be explained by incomplete neutralization of residual few sulfonic acid sites due to conformational restrictions and is expected to occur.

4.3 MODEL ACID-BASE POLYMER BLEND

Seeing both the complex thermodynamics (and kinetics) involved in creating not only a partially but fully miscible polymer blend and the ease with which PBI (and its derivatives) can be homogeneously mixed with numerous sulfonated hydrocarbons in solution co-casting processes, makes studies to better understand this blend system and acid-base interactions in these processes worthwhile. Additionally, the above-mentioned quest for non-neutralizing (but mixing) materials is still ongoing and starts with a better description of the miscible system at hand.

An aspect that further is glanced over in most studies utilizing PBI blends, is the inconsistency in the description of the blend mixture. As is extensively studied in literature and described above, miscibility in a binary polymer blend typically requires attractive interpolymer

interaction. PBI-containing blends are described as acid-base blends which is often implicitly concluded to mean that miscibility in those homogeneous mixtures arises from said interaction. However, even though the relevant properties of such blends after conditioning (re-acidification of the membrane after casting) are characterized by the presence of strong acid-base interactions, these interactions are not available in solution and during the membrane formation process as a consequence of the aforementioned neutralization, as is depicted in Figure 4.6. A complex acid-base equilibrium with the added organic base can further be excluded since ion exchange to Li-salt form can be applied interchangeably for sPPS and further Na-salt form for most studied blends. An empirical study to investigate acid-base interactions in sPPS-based polymer blends and how they can affect miscibility was thus designed.

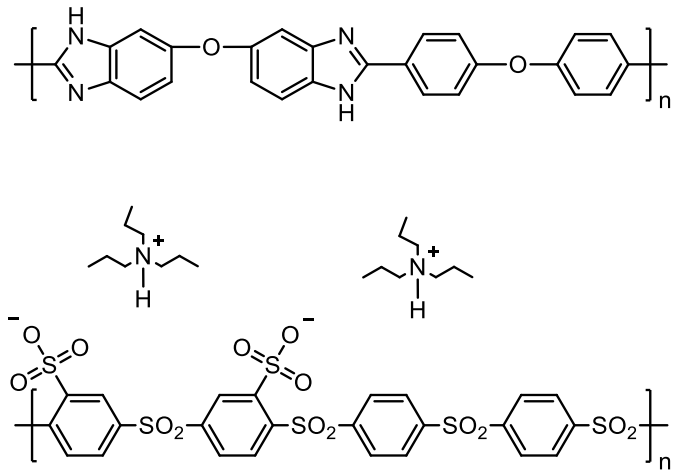

Figure 4.6 Chemical structure of neutralized S360 in the presence of PBIO.

A commercially available polymer suitable as a blend component in such a model system with sPPS that at the same time is well soluble in DMAc, can be readily and reliably modified[123,171] with basic groups of varying basicity[97,172] and is structurally related to sPPS (as to avoid overbearing issues from dissimilar chain aggregation tendencies) is polysulfone (PSU), shown in Figure 4.7.

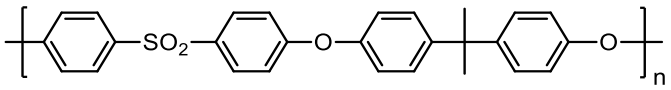

Figure 4.7 Chemical structure of PSU.

PSU has in the past been studied due to its potential as a sulfonated ionomer (see Chapter 1) and is a well-established high-performance thermoplastic with good membrane forming properties[173]. The statistical electrophilic modification of PSU to yield pyridine-functionalized polymers of varying basicity strength in a broad concentration range (i.e., modification degree in % of monomer units) follows previously established routes[97] and was performed prior to this work (see Chapter 2).

pK_b = 8.4

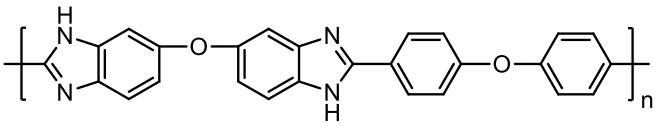

pK_b = 8.8

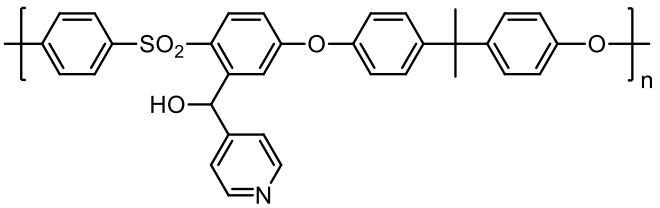

PSU-Py(Me)

pK_b = 10.9

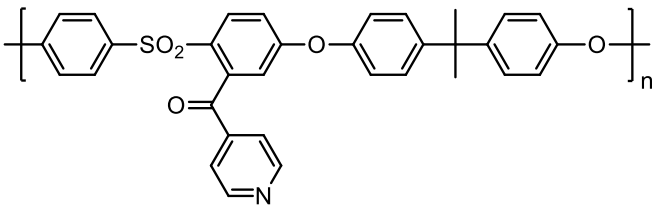

PSU-Py(Keto)

Figure 4.8 Chemical structures and pK_b values of PBIO, PSU-Py(Me), and PSU-Py(Keto).

The modification degrees of PSU-Py(Me) and PSU-Py(Keto) used in the following study of the effect that acid-base interaction strength and concentration in S360 blends have, are listed with their respective equivalent weights in Table 3.

Table 3 Modification degrees (in % of monomer units) of PSU-Py(Me) and PSU-Py(Keto) and their respective equivalent weights in g mol^{-1}.

PSU-Py(Me)-X%		***60%*** *(EW 844)*	***35%*** *(EW 1371)*	***5%*** *(EW 8958)*
PSU-Py(Keto)-X%	***90%*** *(EW 597)*	***60%*** *(EW 843)*	***23%*** *(EW 2029)*	***7%*** *(EW 6427)*

Names for the two kinds of modified PSU are chosen in a way to signify the chemical nature of the tether by which pyridine moieties are attached to the PSU backbone. As a result of the chemical nature of that tether, a base of similar strength as that of benzimidazole (pK_B of 8.4), PSU-Py(Me) (pK_B of approx. 8.8) and an orders of magnitude weaker base, PSU-Py(keto) (pK_B of approx. 10.9) were created and studied in S360-based blends (for comparability, each containing 20 wt% of the respective PSU and all membranes fabricated as described in Chapter 2.5.2).

4.4 MORPHOLOGY DEVELOPMENT IN S360/PSU-PY BLENDS

S360 is not miscible with pristine PSU. A dilute blend solution composed of 80wt% H-S360 and 20wt% PSU in DMAc remains clear with a sPPS-typical slight yellow-golden color to it but turns turbid during solvent evaporation (in vacuum at 60°C) prior to film formation. This is a clear indication that the two components are incompatible and phase-separate on a macroscopic scale. Cross-sectional SEM of an 80/20 (wt%) H-S360/PSU blend membrane is shown in Figure 4.9 below.

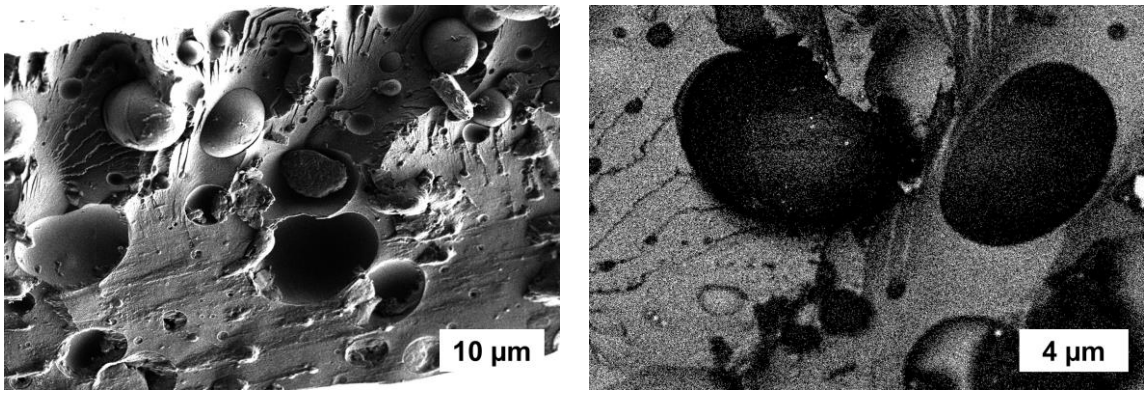

Figure 4.9 Cross-sectional SEM of an 80/20 H-S360/PSU blend.

In the cross-section, large round particles of less electron dense pure PSU (revealed via a backscattered electron detector, BSD, Figure 4.9 right) are seen to be loosely embedded in an S360 matrix. PSU particles of up to around 10 µm size are scattered throughout the entire membrane with a tendency to accumulate near the membrane's top surface, presumably due to their lower density compared to S360. Even though the polymeric backbones are similar, this phase-separation behavior is not surprising, since no specific attractive interaction between pristine PSU and S360 exists in solution.

Strongly basic PSU-Py(Me) with a modification degree of 60% (corresponding to ratio of monomeric units bearing a pyridine moiety, EW for PSU-Py(Me)-60% is 844 g meq^{-1}, roughly a fourth of functional groups compared to PBIO with EW = 200 g meq^{-1}) precipitates from solution when added to H-S360 (in an 80/20 blend mixture) in a similar manner that PBIO does. Visually, this is accompanied by first turbidity of the blend solution followed by precipitation of white polymer aggregates. Analogous to PBIO-comprising blends, the blend mixture was then neutralized which led to immediate dissolution of the prior insoluble acid-base aggregates. Cross-sectional SEM images of the resulting blend membrane were recorded and are shown in Figure 4.10.

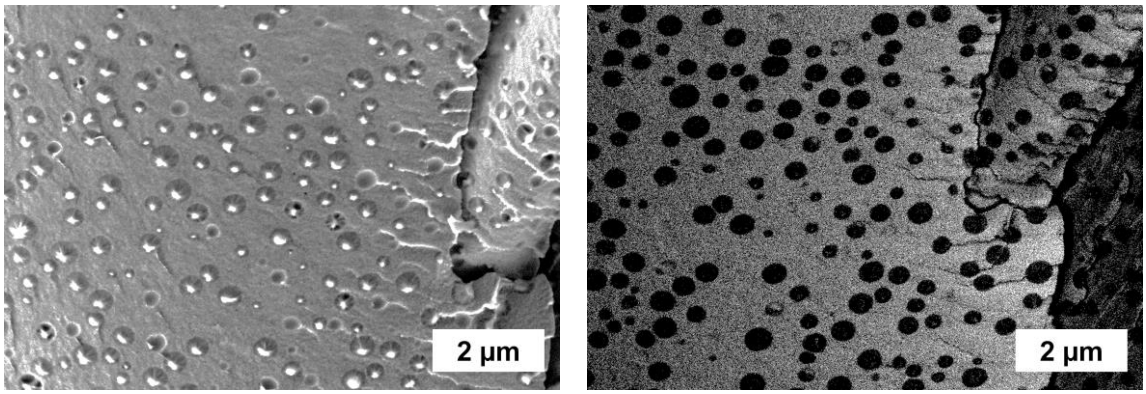

Figure 4.10 Cross-sectional SEM of an 80/20 TPA-S360/PSU-Py(Me)-60% blend.

A significant difference in phase-separation behavior is found compared to pristine PSU, even though specific attractive interactions are inhibited during membrane formation. While this is likely due to several parameters, a contribution could stem from the impaired tendency of S360 to self-aggregate when neutralized. Still, a clear phase-separation between the TPA-S360 matrix and round PSU-Py(Me)-60% particles can be identified and is on the scale of 0.7-0.4 µm. Dispersion of PSU-rich phases on a smaller scale was not observed.

With decreasing modification degree of PSU-Py(Me) to 35%, the blend solution with S360 which is prepared in the same manner as above does not require neutralization and no significant turbidity of the blend solution during membrane formation is observed. As a consequence, and different to blends prepared from PBIO, uninhibited acid-base interaction is actually available during the membrane formation process. Cross-sectional SEM of a 80/20 blend of H-S360/PSU-Py(Me)-35% (EW = 1371 g meq^{-1}) are depicted in Figure 4.11.

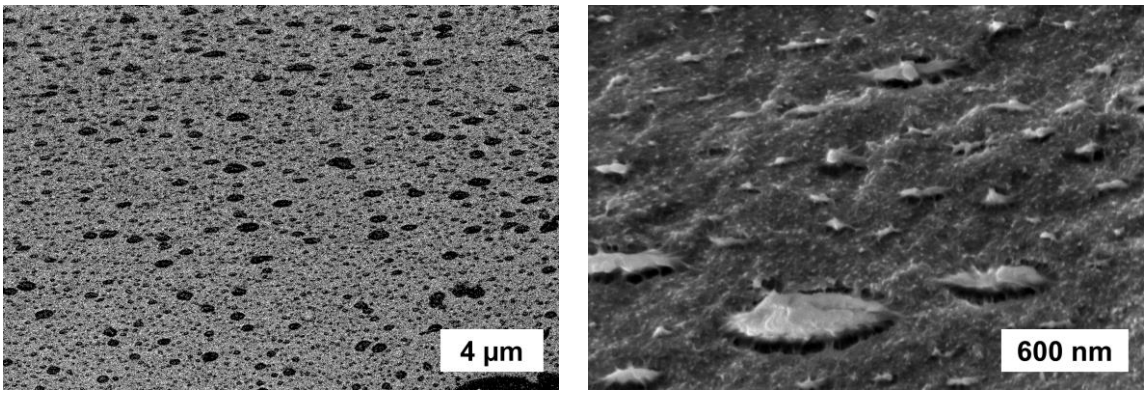

Figure 4.11 Cross-sectional SEM of an 80/20 H-S360/PSU-Py(Me)-35% blend.

Again, phase-separated particles formed by PSU-rich phase in the blend's cross-section can be observed, which strongly vary in size from 30 nm to 1.5 µm. Especially the strongly dispersed small regions of PSU-rich phase are well embedded in the S360 matrix. The observed phenomena are interpreted as such, that the strong acid-base interaction between S360 and PSU-Py(Me) inevitably leads to the formation of badly soluble acid-base aggregates (as was seen for PSU-Py(Me)-60%), but due to the reduced concentration in PSU-Py(Me)-35% can be utilized in solution to compatibilize S360 with PSU. As a result, well-embedded PSU-rich phases of < 50 nm are formed. At the same time, the observed tendency for aggregation on a larger scale may be overly sensitive towards processing conditions and could also originate from inhomogeneous distribution of the statistically attached pyridine moieties (yielding behavior closer to the one observed for unmodified PSU). This interpretation is supported by the morphology found in a blend cast from a non-neutralized 80/20 mixture of H-S360/PSU-Py(Me)-5% (EW = 8958 g meq^{-1}), that was analyzed in SEM and which is shown in Figure 4.12.

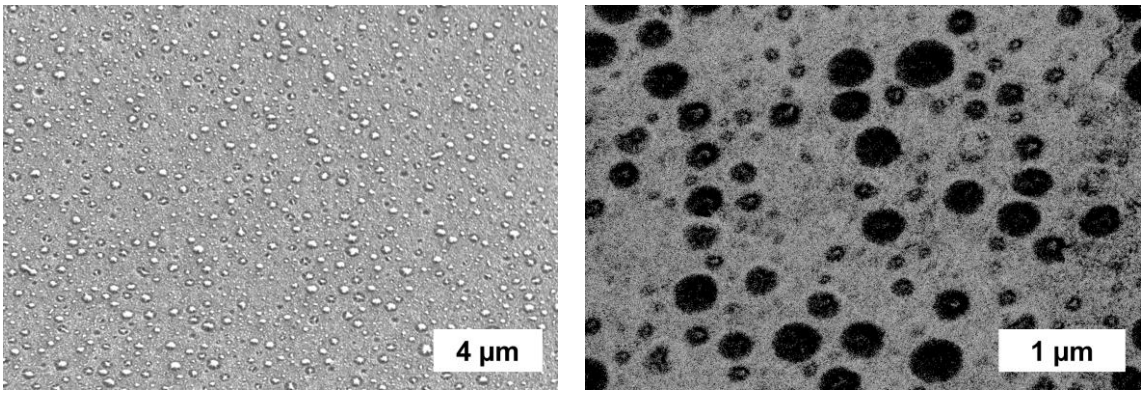

Figure 4.12 Cross-sectional SEM of an 80/20 H-S360/PSU-Py(Me)-5% blend.

Here, the majority of PSU is part of strongly phase-separated particles of approx. 0.4 µm diameter, while a smaller portion (compared to PSU-Py(Me)-35%) is finely dispersed in particles of around 100 nm. This fits to the above formed assumptions of the effect of inhomogeneous statistical modification of PSU which leads to a larger ratio (compared to PSU-Py(Me)-35%) of insufficiently modified polymeric chains.

In summary, it is remarkable how the mutual compatibility between S360 and PSU is enhanced by utilizing non-neutralized strongly interacting sites, even at low concentration. However, the precise control over optimal interaction concentration as to not require neutralization (as for PSU-Py(Me)-60%), but to induce compatibilized distribution of all PSU chains (avoiding inhomogeneities as for PSU-Py(Me)-35%) appears complex. Since the neutralized blend containing PSU-Py(Me)-60% exhibited the least pronounced compatibilization with S360, significant contribution of acid-base interactions in neutralized PBIO blend solutions towards miscibility should not be assumed.

In the next step, interpolymer interaction which is expected to be qualitatively weaker is studied by utilizing the less basic PSU, PSU-Py(Keto), shown in Figure 4.8 above, with similar modification degrees (as listed in Table 3) and under identical conditions. The reduction in basicity and hence reduction in interaction strength is confirmed by the absence of turbidity of the blend solutions even for high modification degrees of PSU (PSU-Py(Keto)-90% and during solvent evaporation, as described below. Consequently, no neutralization is needed.

An 80/20 blend comprising of H-S360 and PSU-Py(Keto)-7% (EW = 6427 g mol^{-1}) was prepared in the same manner as above and the membrane's cross-section analyzed via SEM, as shown in Figure 4.13.

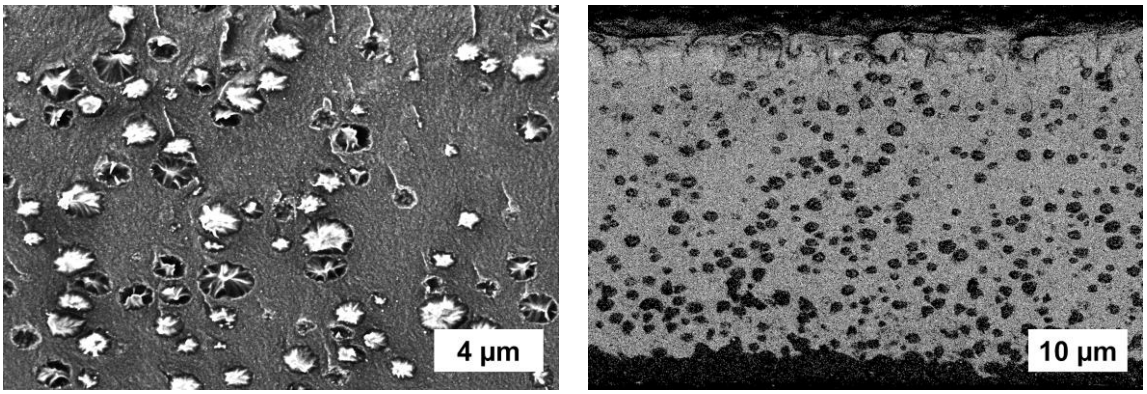

Figure 4.13 Cross-sectional SEM of an 80/20 H-S360/PSU-Py(Keto)-7% blend.

PSU-Py(Keto)-7% phase-separates from the S360 matrix and forms particles of 0.7 - 1.8 µm size which are embedded throughout the entire cross-section. The change in blend morphology compared to pristine PSU is significant, but compatibility is less enhanced compared to PSU-Py(Me)-5% shown in Figure 4.12 above. This is expected to be the direct result of reduced interaction strength in the less basic pyridine functionalized PSU.

With increasing modification degree of PSU-Py(Keto) the particle size and distribution of phase separated PSU in blends comprising 80 wt% H-S360 indicate an improved mutual compatibility: PSU-Py(Keto)-23% (EW = 2029 g mol^{-1}) can be cast from clear non-neutralized solution and the formed membrane's cross-section was analyzed via SEM as is shown in Figure 4.14.

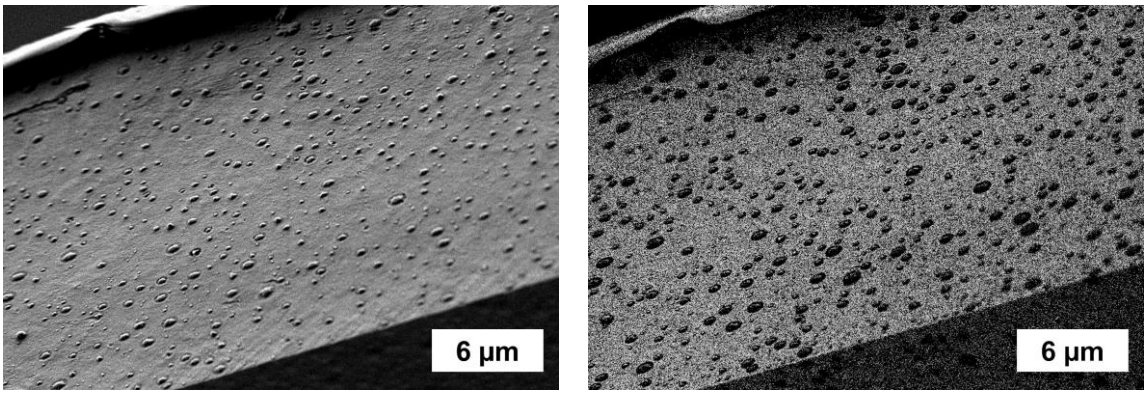

Figure 4.14 Cross-sectional SEM of an 80/20 H-S360/PSU-Py(Keto)-23% blend.

While the finely dispersed PSU phase (of < 50 nm) which was found for more basic pyridine-functionalized PSU above is not observed here, the blend morphology shows an increase in compatibilization (by means of reduced PSU-particle diameter) between S360 and PSU-Py(Keto)-23% compared to lower concentrations. Well-embedded PSU particle diameters are roughly 150 - 800 nm in size and evenly distributed throughout the membrane. At 60% modification degree of PSU-Py(Keto) (EW = 843 g mol^{-1}), PSU appears to be finely dispersed in the S360 matrix, but remains phase-separated, as is shown in cross-sectional SEM in Figure 4.15.

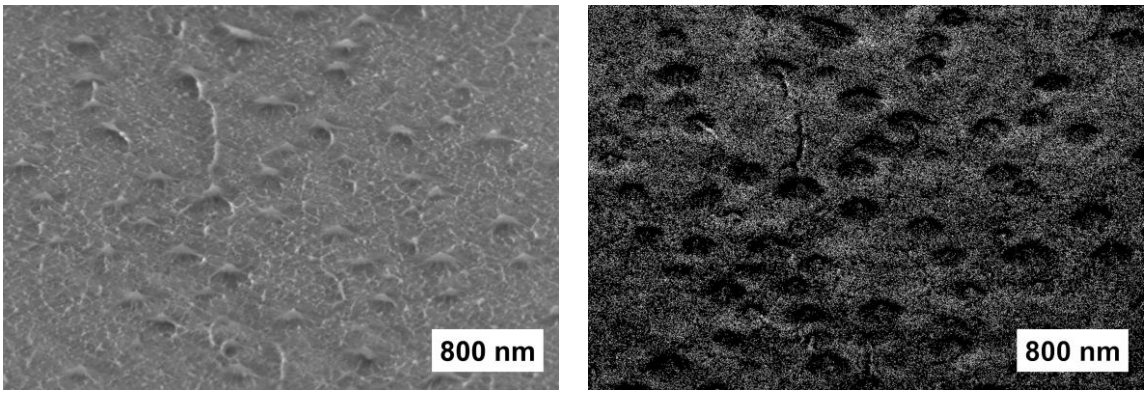

Figure 4.15 Cross-sectional SEM of an 80/20 H-S360/PSU-Py(Keto)-60% blend.

The PSU-rich phases are very even in size and approx. 200 nm in diameter. The narrow phase size distribution supports the assumptions made from the experiments above, where unevenly

distributed but strong interaction led to considerable variation in aggregation size. Instead, weak acid-base interaction between H-S360 and PSU-Py(Keto) appears to almost linearly increase mutual compatibility with increasing modification degree. Further increase in interaction concentration is achieved by casting a blend solution comprising H-S360 and close to fully functionalized PSU-Py(Keto)-90% (EW = 597 g mol^{-1}). As with all blend solutions containing PSU-Py(Keto) there is no need for neutralization. The formed clear blend membrane of 80/20 H-S360/PSU-Py(Keto)-90% is subsequently analyzed via SEM, as depicted in Figure 4.16.

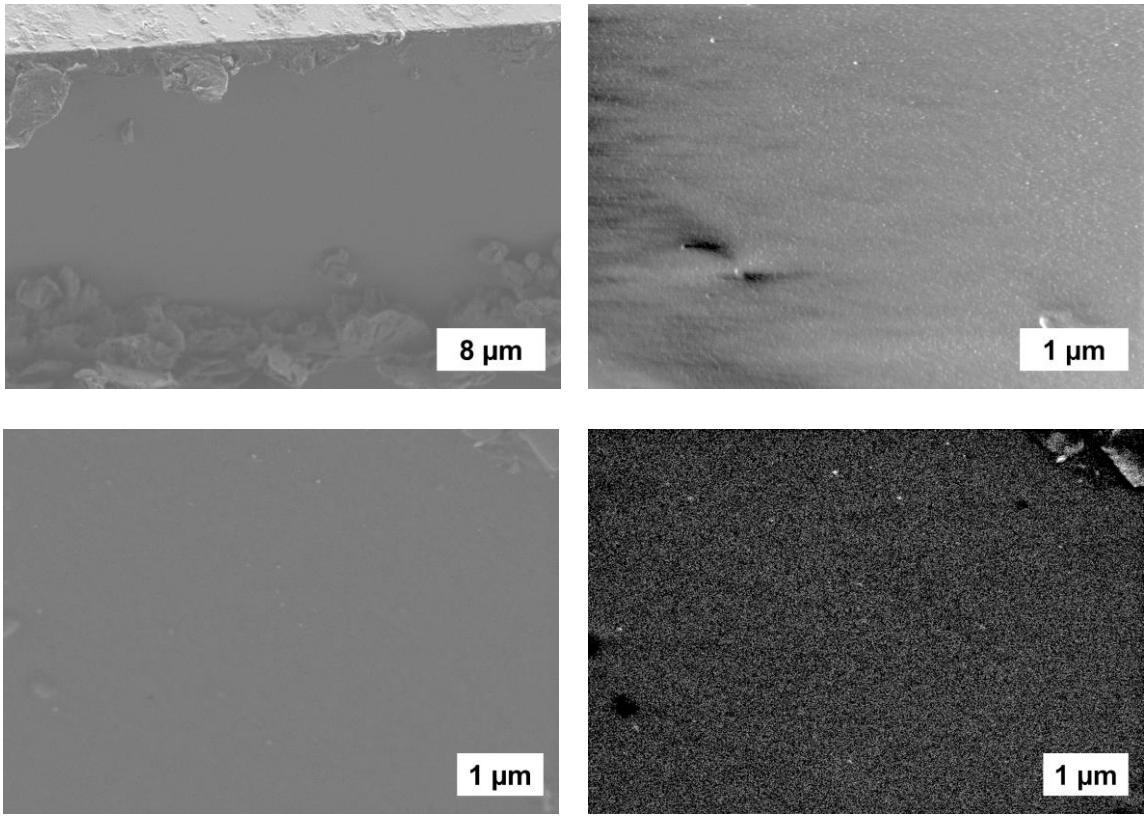

Figure 4.16 Cross-sectional SEM of an 80/20 H-S360/PSU-Py(Keto)-90% blend.

The blend membrane appears homogeneous, and no phase-separation is detectable. At very high magnification, indications of structures in the range of up to 10 nm can be found, but this information cannot be reliably interpreted. Irrespective of the ultimate existence of such small PSU-rich phases, this 80/20 blend of H-S360 and PSU-Py(Keto)-90% exhibits the highest compatibility – if not miscibility – out of all studied PSU blends of various interaction strengths and concentrations.

In line with assumptions made earlier these results indicate that in blends with S360 interaction between sulfonic acid moieties and weak bases such as PSU-Py(Keto) can be used to induce compatibility in a blend system that phase-separates on a large scale in its unaltered state. On the other hand, strong interaction between sulfonic acid moieties and strong bases such as PSU-Py(Me) seems significantly harder to appropriately tune. As a result, compatibility close to miscibility could not be reached for S360/PSU-Py(Me) blends this work. Together with the

conclusions drawn above, that acid-base interaction cannot play a relevant role in the formation of a miscible morphology in PBIO-containing neutralized blend solutions, the presence of a high concentration of much weaker interacting moieties in those solutions is likely. A possible specific interaction that could fulfil this role are hydrogen bonds, originating from the non-basic imidazole nitrogen, towards either the sulfone linkages in the polymer backbone, or – as is a unifying characteristic of all studied hydrocarbon ionomers – towards the dissociated sulfonic acid salt moieties, as is shown in Figure 4.17.

4.5 SPECIFIC INTERACTIONS IN S360/PBI BLENDS

The ascription of miscibility in acid-base blends with PBI (and its derivatives) to hydrogen bond formation (as is schematically shown for a blend solution and a membrane after conditioning in Figure 4.17) is neither new nor far-fetched.

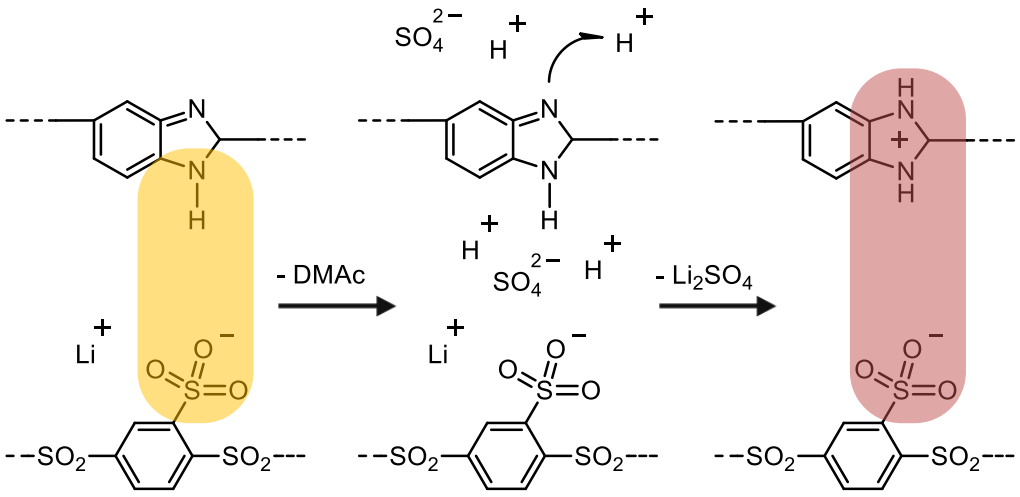

Figure 4.17 Schematic of the evolution of interpolymer interaction in a non-acidic Li-S360/PBIO blend solution (left), its acidification during membrane conditioning (middle), and in the final (acid-base) membrane (right).

In fact, PBI's ability to form hydrogen bonds with itself and numerous other materials is the origin of many of PBI's attractive properties and reason for its widespread application, as is described in detail above. The ascription is also not new, since a membrane study by Deimede et al. in 2000[158] was able to prove in a series of sulfonated PSUs (sPSU) blended with PBI in various compositions from their Na-ion form via Raman- and IR spectroscopical

analyses the existence of hydrogen bonds between PBI's "N-H" group and the sulfonate groups (at high sulfonation degrees also of the backbone's sulfone unit) of sPSU[158] in the membranes. An unambiguous analysis of the bands was only possible due to the rigorous drying – at 200 °C in vacuum for 3 days[158] – of the freshly cast membranes. The rising degree of miscibility (non-miscible in case of un-sulfonated PSU) with increasing IEC of sPSU correlated with expected and systematic change in the blend membranes spectra, allowing for the identification of the involved groups. Other studies only reflect briefly on the contribution that hydrogen bonds may play for miscibility[106,146,153] and rarely discuss the process of membrane formation directly[141]. However, the above cited study as well as most other investigations of interactions in PBI blends characterize the resulting membrane instead of the solution from which the membrane is slowly formed. Therefore, it is still not clear whether hydrogen bonds between PBI and the sulfonated ionomer contribute to even distribution of both polymers in solution and are the cause for a common membrane formation process that ultimately ends in a homogeneous morphology. Another possible explanation could be related to what is well described for the sol-gel process in the formation of orthophosphoric acid (PA) doped PBI membranes[174]: here, PBI is first polymerized and then cast from solution in pyrophosphoric acid, which during immobilization of polymer chains and membrane formation is consciously hydrolyzed (typically with atmospheric water[175]) to yield orthophosphoric acid. Since PA is a non-solvent for PBI, the polymer quickly transitions from solution state to gel state[176] to yield a robust membrane with high PA doping level. The reason as to why such membranes can be used and exhibit sufficient mechanical properties is that PBI forms a hydrogen-bonded network with itself already in solution[177], which is "frozen" by the sudden change in solubility. A schematic of such a network of interacting PBI moieties is shown in Figure 4.18.

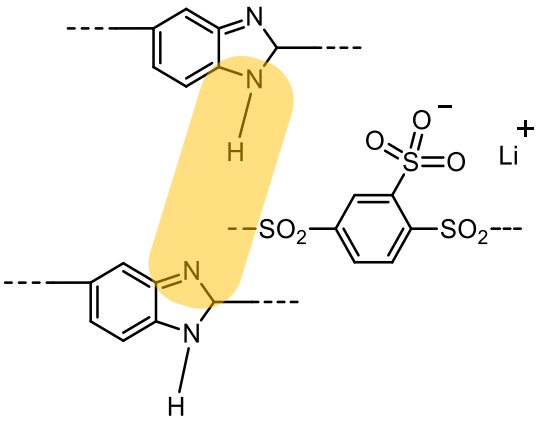

Figure 4.18 Schematic of a hydrogen-bonded PBI unit in blend solution in which non-acidic sPPS is embedded, .

Such a PBI network could potentially be imbibed with solvated non-acidic sPPS ionomer strains in a semi-dilute solution. This would mean, that no specific attractive interaction between blend components induces the observed miscibility, but that it is a consequence of the blend's ability to be simultaneously "co-cast" as a uniform membrane in which a prior formed, and well distributed PBI network is retained. A precise understanding of this mechanism in future studies could provide valuable insights for polymer blends in general and for understanding the unique character of poly(benzimidazole) in these systems.

Regardless of the precise mechanism, it is important to note, that while acid-base interactions are key contributors to attractive properties in conditioned PBIO blend membranes with hydrocarbon ionomers and sPPS, they play an insignificant role in creating their homogeneously mixed morphologies. In future works, the insight that attractive interpolymer interaction in the studied blend solutions need not be the same type or even part of the interpolymer interactions in the final membrane could lead to successful design of non-neutralizing blend components for use in hydrocarbon ionomer PEMs.

4.6 HYDROGEN BONDS IN S360 BLENDS

A potential route towards non-neutralizing blend components for use in sPPS blends is briefly explored in the following and based on the assumed significant contribution of hydrogen bonds to miscibility. Poly(ether imide) (PEI) has in the past been studied as both, a sulfonated ionomer

(see Chapter 1) and a constituent in blend membranes for viscoelastic reinforcement. However, compatibility of a sulfonated ionomer with PEI is typically limited[140]. The same proves to be true for S360, as casting an 80/20 membrane of Li-S360/PEI yields a macro-phase separated morphology (similar to what was found in S360 blends with pristine PSU) as is shown in its cross-sectional SEM in Figure 4.19.

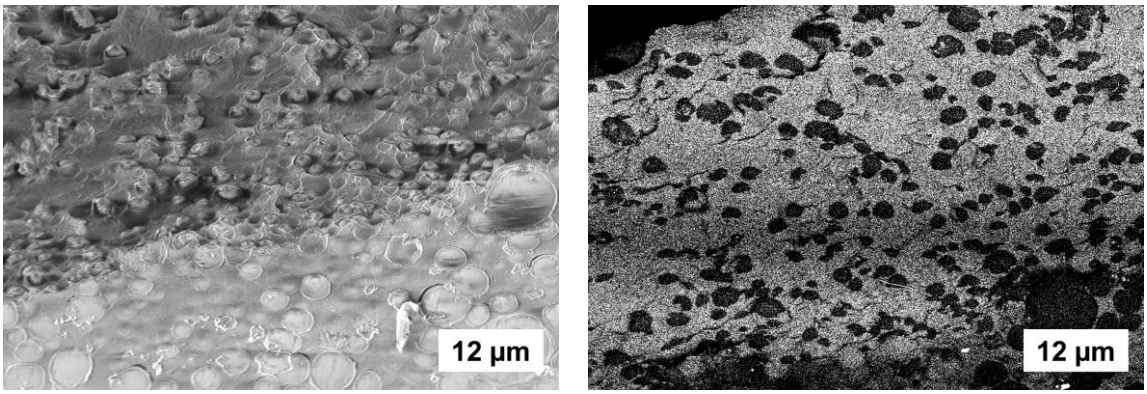

Figure 4.19 Cross-sectional SEM of an 80/20 Li-S360/PEI blend.

However, PEI can also be processed from its poly(amic acid) (PAA) precursor which typically is later condensed upon thermal treatment to yield PEI. The general structure evolution during the condensation reaction and imide formation is shown in Figure 4.20.

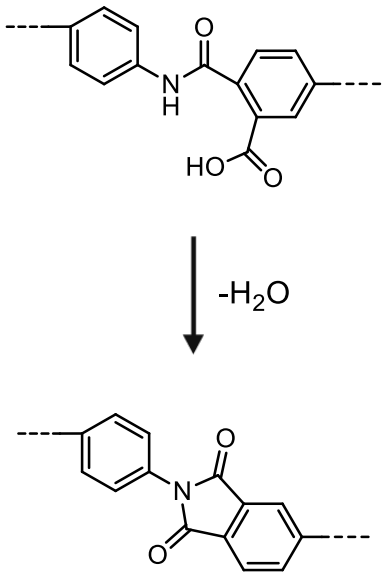

Figure 4.20 Schematic of the condensation reaction of an amic acid moiety to yield an imide moiety.

The advantage of such a PAA "precursor" is therefore its capability to form hydrogen bonds originating from the amidic "N-H" (and carboxylic "COOH") groups. To test this, a blend solution containing 20 wt% commercial PAA-type precursor was prepared. A theoretical evolution of blend component interaction is shown in Figure 4.21.

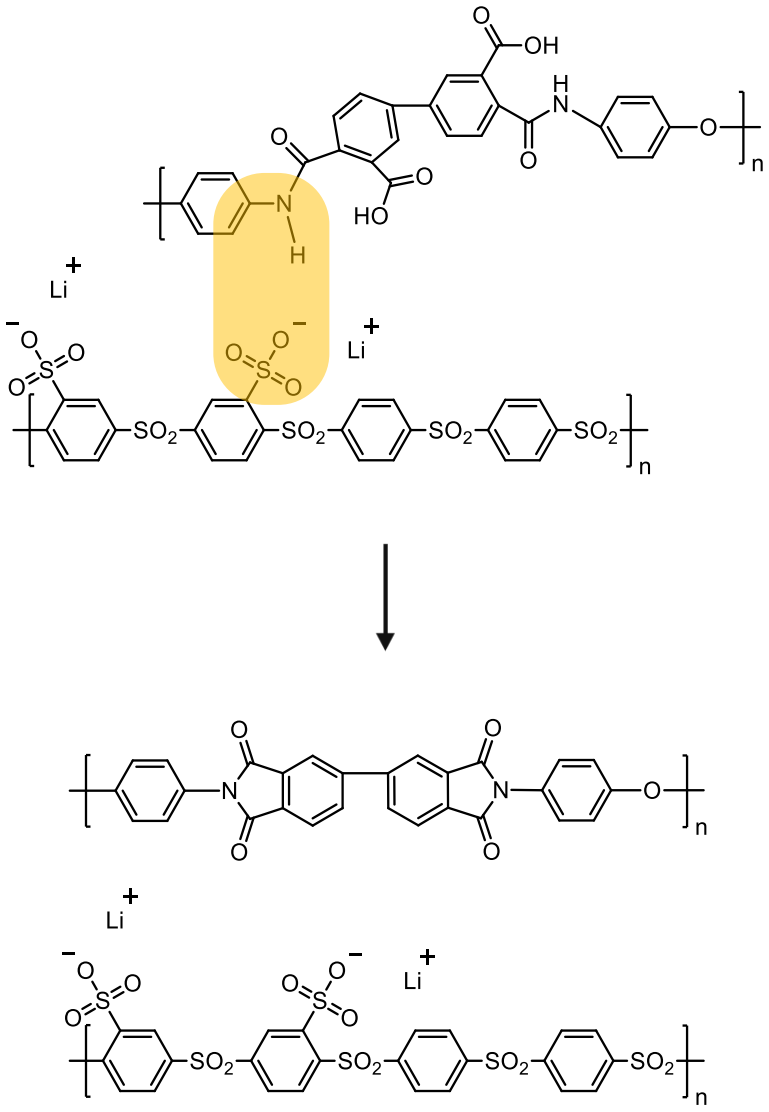

Figure 4.21 Schematic of potential blend interaction evolution during condensation of PAA to PEI.

The resulting clear but brittle membrane's morphology was analyzed via SEM and is depicted in Figure 4.22.

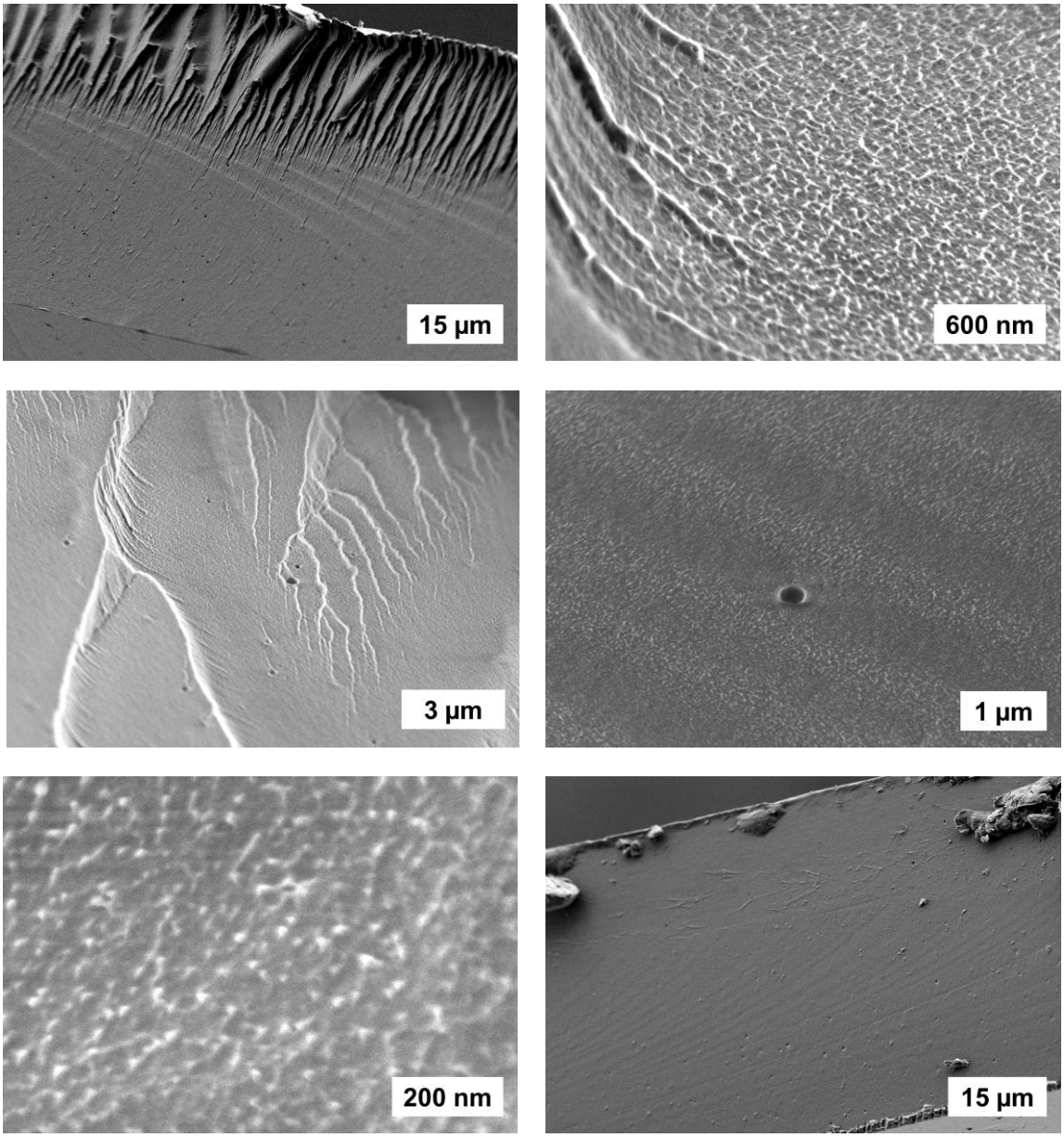

Figure 4.22 Cross-sectional SEM of an 80/20 Li-S360/precursor PAA blend.

The difference in compatibility between PEI and its precursor PAA with Li-S360 is tremendous and may be the effect of the accessible hydrogen bond interactions between S360 and PAA in its non-condensed form. While the blend remains brittle under dry conditions, this could be a promising path towards the design of new non-neutralizing blend components in further studies.

4.7 CHAPTER SUMMARY

In this chapter, acid-base polymer blends as reinforcement strategy for sPPS were explored and blends of sPPS and PBIO were chosen for further optimization. A model acid-base polymer blend system was studied regarding the effect that interpolymer interaction strength and concentration have on morphology in S360 blends.

- Literature supports the choice of PBI-containing acid-base blends for the viscoelastic reinforcement of sPPS, due to its unique miscibility with ionomers and properties. In contrast to literature, the comprehensive approach followed in this work allows for the use of high molecular weight ionomers (see Chapter 3 and our previous work[56]) to form and optimize acid-base blends comprising PBIO (see Chapter 5).
- Strong acid-base interaction (as is the case in PBIO and PSU-Py(Me)) in sPPS blend solutions without neutralization are difficult to tune as to contribute to mutual polymer compatibility, but avoid precipitation.
- In contrast, weak acid-base interaction (as is the case in PSU-Py(keto)) offers a seemingly linear increase of mutual compatibility in sPPS-blends with continuous increase of interaction concentration, similar to what is observed in miscible blends with PBIO.
- From literature and empirical evidence, it is concluded that the miscibility inducing interaction in PBI-containing blends is not acid-base interaction but could be hydrogen bonding instead. Alternatively, the formation of a PBI network in semi-dilute solution could lead to the same behavior.
- It may be concluded that interaction in the final membrane need not be the same as the miscibility inducing interaction in solution. The investigation of a model system containing pol(amic acid) and sPPS support this described concept.

The findings in this chapter may help open paths towards new blend concepts for hydrocarbon ionomers, which should focus on the choice of miscibility inducing interpolymer interactions in solution. The deeper understanding of the blending behavior of PBIO in sPPS blends enables the conscious optimization of their properties in the following chapter.

5 DEVELOPMENT OF SPPS/PBI BLENDS FOR FUEL CELLS AND ELECTROLYZERS

In this chapter (see Figure 5.1), acid-base polymer blends comprising PBIO and sPPS are characterized and optimized with regard to high conductivity and high mechanical robustness. Thin blend membranes for PEMFC application are created in different processes and evaluated in fuel cells for the first time.

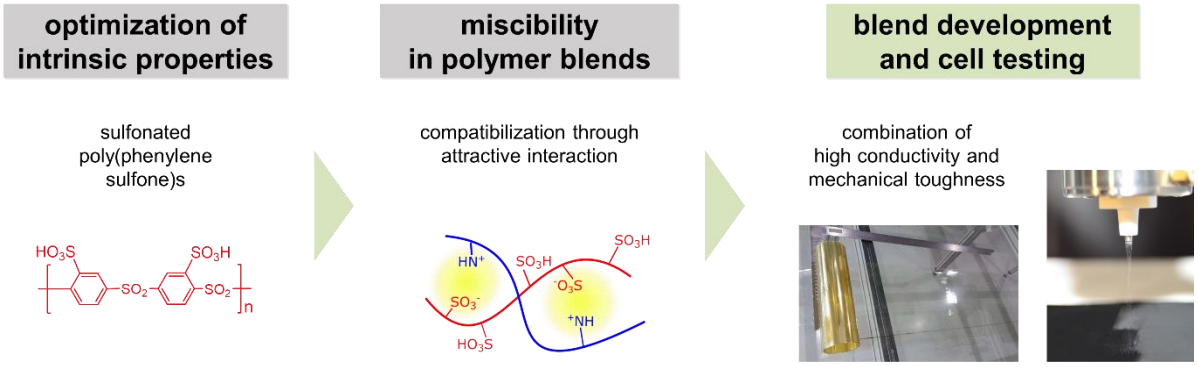

Figure 5.1 Thesis structure, third chapter.

As described in Chapter 2, measurement of FC-performance and durability in this chapter was performed by Dr. Carolin Klose (HS-IMTEK).

5.1 BACKGROUND

5.1.1 PEMFC cell assembly and design

Different methods exist to produce and assemble the symmetrically layered structure of a PEM fuel cell, comprising of gas diffusion layers (GDL, e.g., carbon paper), catalyst layers (CL, e.g.,

platinum on carbon) and a membrane at the heart of it. The development of such methods is typically driven by the goal of enhanced performance and durability of the total membrane electrode assembly (MEA), e.g., by enhancing the membrane-electrode interface, or by increasing control over the uniformity of each layer and their combination. As a result, a number of strategies that make use of e.g. compositional gradients in the electrode[178,179], geometrically patterned electrodes[180], patterned membranes[181–183], additional interface layers[184,185], ionomer-impregnated electrodes[186], or the direct membrane depositioning (DMD) atop the catalyst layer via ink-screen printing or spray-coating, have been explored in recent years[187]. DMD was first introduced by Klingele et al.[188] and has since gained interest due to its significant effect on power density as a result of an improved membrane-electrode interface[189,190] and the potential application of ultra-thin membranes (supported by the GDE on which the membrane is deposited). Variations in cell design originating from the different MEA fabrication processes also affect the mechanical burden that the membrane is subjected to – by using a combination of a soft GDL and a sub-gasket in their cell design, Ishikawa et al. achieved an increase in wet-dry cycle durability of their hydrocarbon-based MEA by more than two orders of magnitude[84]. The pros and cons of different processes that result in different membrane requirements should thus be explored when a cell is developed and optimized for new PEMs.

5.1.2 Accelerated stress tests (AST) of membranes in PEMFCs

The target lives for fuel cell systems of beyond 5000 h for automotive applications[191] requires the ability to rapidly evaluate new materials and their durability in accelerated stress tests (AST). Data from ASTs also allows to quantitatively evaluate the tradeoff in cost, lifetime, and performance in PEMs[192]. A variety of AST protocols are established that offer a range of membrane testing conditions, which can be used to support development of a PEM alongside its progression through different technological readiness levels. Among them, evaluation of mechanical durability (typically via RH-cycling) and evaluation of chemical durability (in terms of susceptibility towards radical attack as a consequence of hydrogen gas permeability, typically via potential hold at open-circuit voltage (OCV) at high T, low RH) are the most relevant for early stages in a PEM's development[16]. It should be noted, that mitigation

strategies (e.g., the incorporation of radical scavengers such as Ce^{3+} and Mn^{2+} in PFSA membranes[193]) can not be directly transferred to hydrocarbon PEMS (e.g., due to significantly shorter lifetimes of highly reactive radicals in proximity to aromatic structures[16,194]). Additionally, the often significantly higher IEC of hydrocarbon PEMs compared to that of PFSAs (as described in Chapter 1) and similar water uptake (in terms of λ, as shown in Chapter 3.2) over a wide range of relative humidity result in significantly higher water volume content at high RH and makes recording gas permeability (or OCV-hold AST) as a function of RH more urgent for hydrocarbon ionomers than for PFSAs, and should thus be included in their extended evaluation.

5.2 PROPERTIES OF S360/PBI BLENDS

Membrane requirements in a hypothetical future PEMFC stack that can be designed and operated with the viscoelastic shortcomings of sPPS membranes in mind, can neither be clearly defined at this stage nor straightforwardly translated to ex situ measured tensile properties. However, a very blatant requirement is that of non-brittleness under typical storage, handling, and processing conditions, as well as in operando in typical cell designs and under typical AST (accelerated stress test) conditions (e.g., mechanical durability testing via humidity cycling).
Similar to what reproducible high quality of pure S360 enables in this work with regard to the systematic study and optimization of blends for viscoelastic reinforcement of sPPS materials, a robust, non-brittle sPPS-blend PEM of high conductivity would allow reliable material testing in operando and enable the deliberate design of an optimal PEMFC MEA for sPPS membranes.
As was already alluded to in the previous chapters, S360 and PBIO are homogeneously miscible in the entire relevant compositional range of 0-50 wt% PBI content (when prepared as described in Chapter 2.5.2). The evolution of titratable IEC in S360/PBI blends following closely the theoretically expected, as shown in Figure 4.5 above and Figure 5.2 below, further suggests that blend properties in sPPS/PBI blends may be changed in a continuous way with increasing PBIO content.

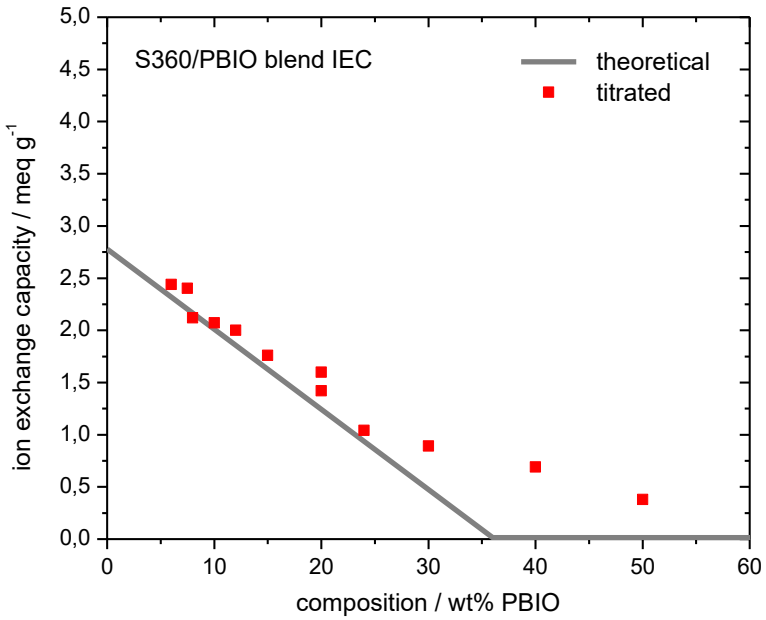

Figure 5.2 Evolution of theoretical and experimental IEC in S360/PBIO blends as a function of composition.

As was mentioned above, this behavior allows for the straightforward adjustment of the simultaneously affected parameters proton conductivity and viscoelastic reinforcement, which facilitates the optimization of binary sPPS/PBIO blends based on data from cell measurements. However, the detrimental effect an increasing PBIO content has on conductivity in homogeneous PBI blends is the reason why studies in literature typically are restricted to low PBI contents of around 10 wt%. The specific proton conductivity of various S360/PBIO blends measured in a wide range of relative humidity, shown in Figure 5.3, portrays this exact issue and supports the choice of the previously defined "required" IEC of sPPS/PBIO blends of around 2 meq g^{-1} for PEMFC application.

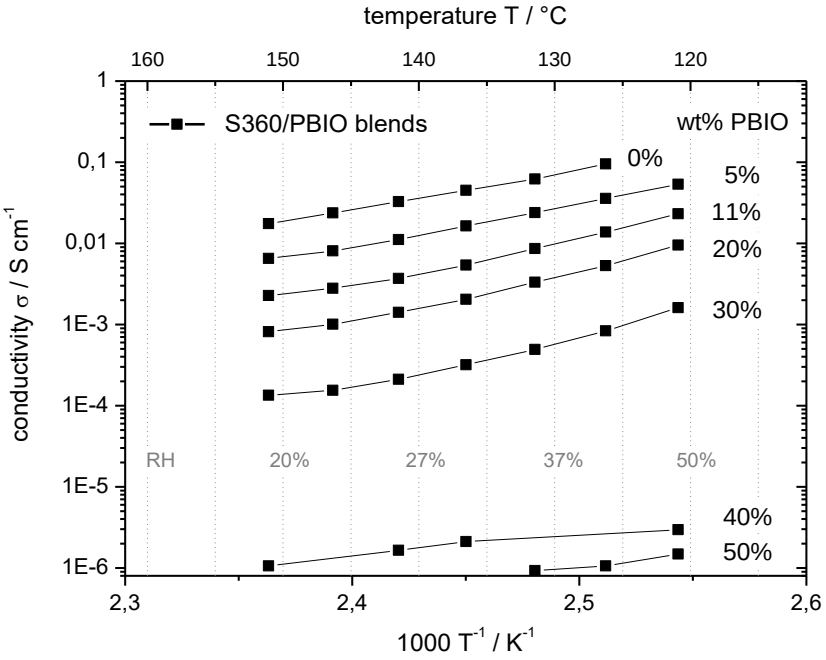

Figure 5.3 Proton conductivity of several S360/PBIO blends at $p(H_2O)=10^5$ Pa as a function of temperature.

The materials exhibit an almost parallel downward shift of conductivity with increasing PBIO content with no adverse effects on percolation (for PBIO contents < 40 wt%). However, at a PBIO content of around 15 wt% (IEC of 1.61 meq g^{-1}) in the blend, conductivity is reduced compared to that of pure S360 by a factor of 10. Within the scope of this work the conductivity of a blend comprising a PBIO content of 7.5 wt% (IEC of 2.19 meq g^{-1}, EW of 456 g mol^{-1}) was consequently chosen as target for required performance for initial studies in PEMFCs.

Importantly, brittleness in the studied blends was qualitatively assessed next and as described previously. The test was conducted by repeatedly bending membranes, which were vacuum dried (at 90 °C) for multiple days. Dried membranes with PBIO contents of 0-20 wt% readily fractured into multiple pieces in this test. S360 blends containing 30 wt% and above (all of which exhibit insufficient conductivity) on the other hand were very robust and withstood rigorous bending, even if repeated multiple times over the course of several days and repeated drying of the samples. Therefore, the mechanical robustness that a 70/30 blend of S360/PBIO exhibits was defined as a target for non-brittle, tough behavior of sPPS-materials.

A representative comparison of tensile properties of pure S360 and blends containing 7.5 wt% PBIO (compromise for retained high conductivity) and 30 wt% PBIO (compromise for non-brittleness) is depicted in their elongation-to-break measurements at 30% RH, shown in Figure 5.4.

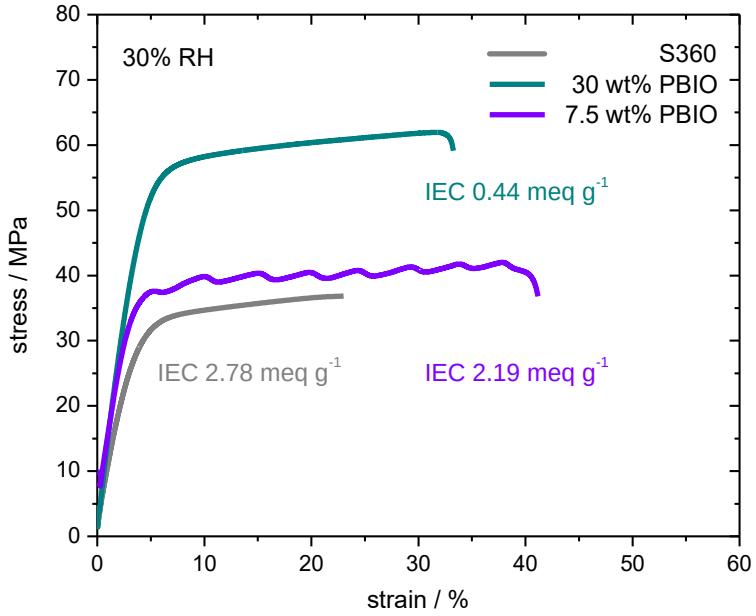

Figure 5.4 Tensile tests of S360 and S360/PBIO blends containing 7.5 wt% and 30 wt% PBIO at 30% RH (90 °C).

The IECs of the tested samples are 2.78 meq g-1 (0 wt% PBIO), 2.19 meq g-1 (7.5 wt% PBIO), and 0.44 meq g-1 (30wt % PBIO), respectively. Under the assumption of similar λ-values for non-interacting sulfonic acid moieties of S360 in all membranes under the tested conditions (which are within the regime of exothermal Langmuir adsorption, described in Chapter 3.2), this corresponds to approximate water volume fractions of 22 vol% (0 wt% PBIO), 18 vol% (7.5 wt% PBIO), and 4 vol% (30wt % PBIO), respectively. The most significant difference in tensile behavior of the tested membranes lies in the dramatic increase in yield strength with increasing PBIO content, from roughly 25 MPa to approx. 47 MPa (7.5 wt% PBIO) and 58 MPa (30 wt%PBIO). Especially for the blend with 30 wt% PBIO this is mostly due to the reduction of IEC (to around 0.4 meq g^{-1}). Otherwise, tensile behavior is expected to result from the combined contributions of the materials' water contents, the expected similarity in local hydration of S360 polymer strains and the overall PBIO content which is embedded in the

blends' miscible morphologies. Not only may the blend morphology's characteristics change as a function of composition, but single parameters may dominate tensile behavior under certain T/RH conditions, therefore, a description of this complex behavior is offered at the end of this chapter.

5.3 PROPERTIES OF S220/PBI BLENDS

The findings from above shown experiments make it apparent that the combination of the desired high conductivity and the desired high mechanical robustness is not attainable in a single acid-base blend membrane comprised of S360 and PBIO. However, the versatility of the blending approach chosen in this work allows not only for the variation of composition, but also for the variation of the employed sPPS. Sulfonated poly(phenylene sulfone) with an IEC of 4.55 meq g-1, termed sPPS-220 or S220 is shown in Figure 5.5 and was described above.

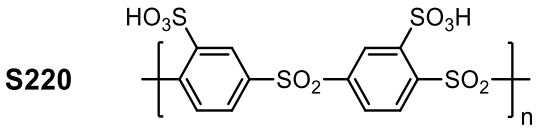

Figure 5.5 Chemical structure of S220.

S220 as a pure material is well characterized[43] and its synthesis has already been optimized in 2012, yielding extremely high molecular weights of up to M_W = 330 kDa[56]. Segments of S220 were also employed in the preparation of multi block copolymers[82] and their subsequent blending with PBI[30]. Due to its intrinsic water solubility and bad membrane forming properties by itself it could not be employed in the assessment of a suitable reinforcement approach for sPPS up until this point. The homogeneous blend morphology in a 75/25 mixture of S220 and PBIO and the evolution of IEC in S220/PBIO blends is shown in Figure 5.6.

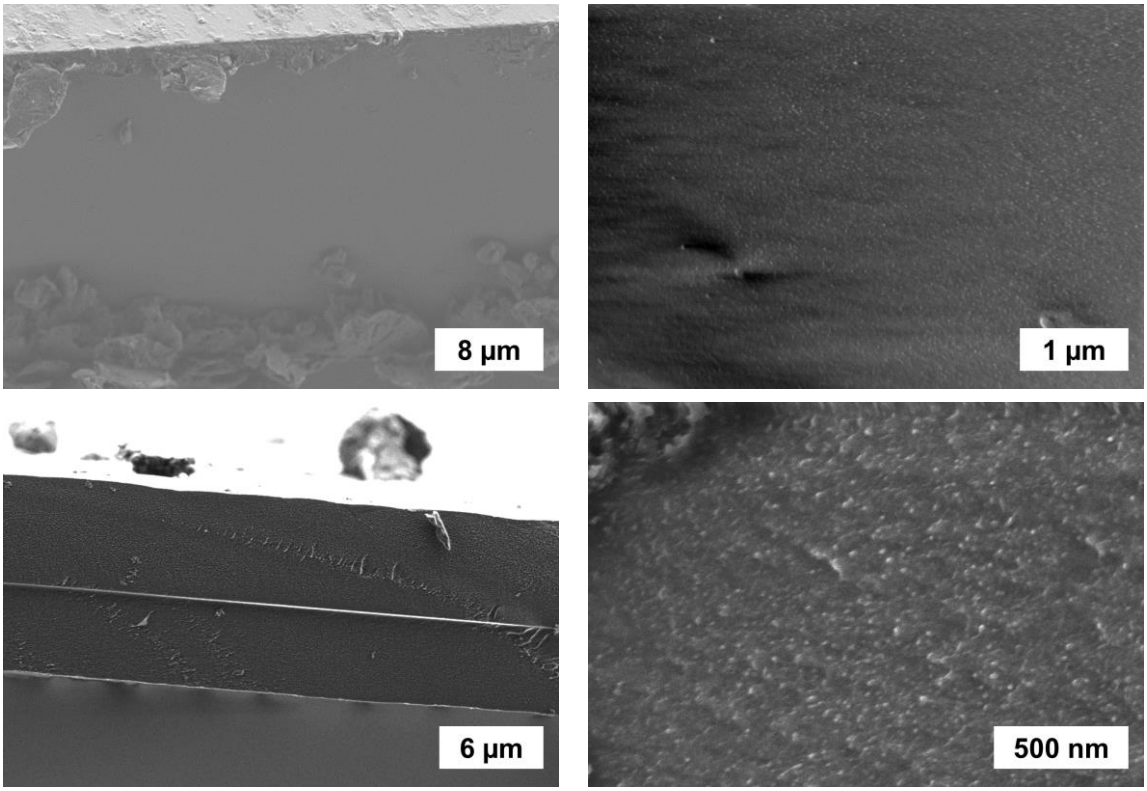

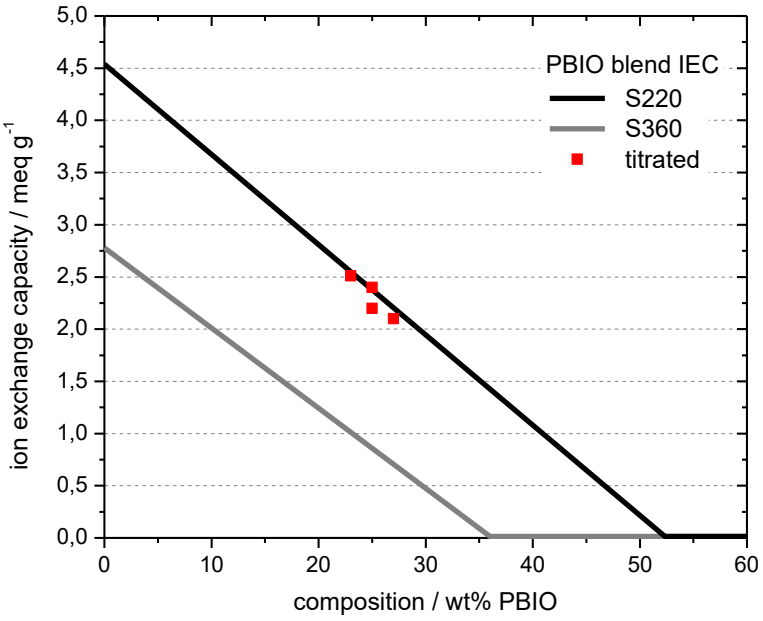

Figure 5.6 Cross-sectional SEM of several S220/PBIO blends (from top left to right 23 wt%, 25 wt%, 25 wt%, and 27 wt% PBIO) and evolution of IEC in S220/PBIO blends.

The chemical structure of pure S220 containing only sulfonated phenylene units leads to the material's high IEC. The miscibility found for all sPPS materials studied so far also translates to homogeneous mixtures formed from S220 and PBIO, fabricated in the same manner as blends of S360 and PBIO, as seen in the cross-sectional morphologies. Most interestingly, the evolution of S220/PBIO blend IEC as a function of composition shows the potential of this new binary mixture: a similar IEC as that of 7.5 wt% PBIO containing S360 blends is reached at remarkably high PBI contents of around 25 wt% (IEC of 2.16 meq g^{-1}), with experimentally titrated IEC matching the theoretically expected one, as expected. The specific proton conductivity of such a blend comprised of 75 wt% S220 and 25 wt% was subsequently measured and is shown in Figure 5.7.

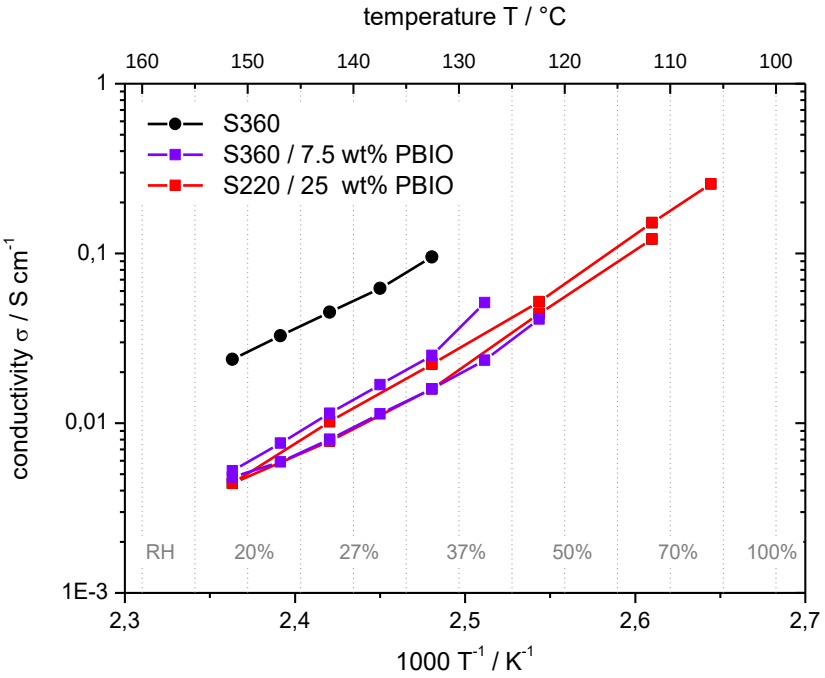

Figure 5.7 Proton conductivity of S360, a 75/25 S220/PBIO blend, and a 92.5/7.5 S360/PBIO blend at $p(H_2O)=10^5$ Pa as a function of temperature.

The conductivity of the studied S220/PBIO blend with IEC 2.16 meq g^{-1} closely matches that of previously studied S360/PBIO blend with IEC 2.19 meq g^{-1}. Combined with the results from conductivity in S360-based PBIO blends this leads to the assumption that the IEC of sPPS/PBI blends allows for a straightforward prediction of their respective conductivity, disregarding the

choice of sPPS. Tensile tests of the highly conductive S220 blend containing 25 wt% PBIO at 90% RH and 30% RH were subsequently performed, and their results are shown in Figure 5.8 and Figure 5.9. Tensile test results of S360/PBIO blends with significantly reduced IEC (and conductivity) are included for comparability.

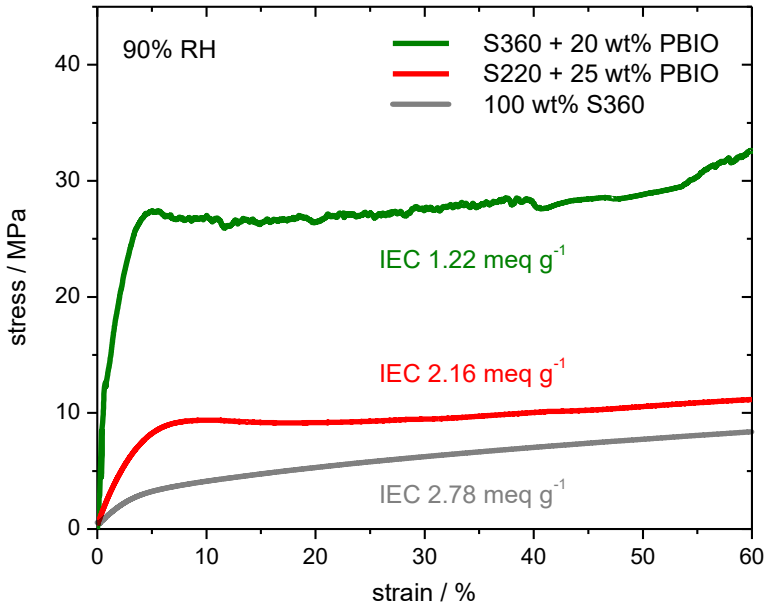

Figure 5.8 Tensile tests of S360 and blends of 80/20 S360/PBIO as well as 75/25 S220/PBIO at 90% RH (50 °C).

At high humidity of 90% RH, Young's modulus and Yield strength reflect the considerable high IEC that is retained in the S220 blend, while the observed strengthening effect in the 80/20 blend of S360/PBIO should be mostly ascribed to the significant reduction of water volume content in the material due to the strongly reduced IEC. Still, the yielding behavior of the S220 blend which is not observed in pure S360 could indicate that the high concentration of acid-base interacting sites in the material thwart the plastic deformation of the material to a certain degree, even in highly humidified conditions.

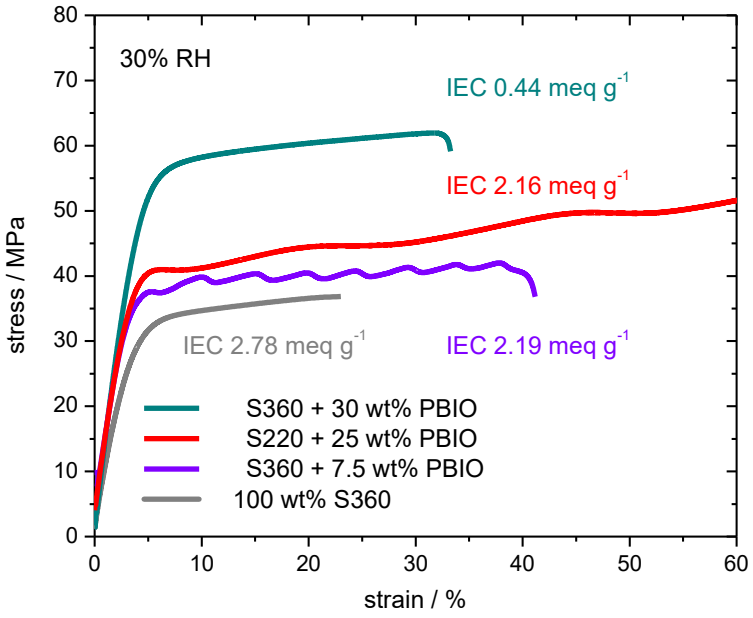

Figure 5.9 Tensile tests of S360 and S360/PBIO blends containing 7.5 wt% and 30wt%, as well as an S220/PBIO blend containing 25 wt% PBIO at 30% RH (90°C).

At 30% RH, typically the onset (in terms of further reduction of RH) of brittle behavior in pure S360, Young's modulus and Yield strength of the S220 blend are almost identical to the one found in the S360 blend comprising 7.5 wt% PBIO which has the same IEC. It can thus be concluded that, water content as the result of retained high IEC in the S220 blend dominates the tensile behavior of the material. The considerable elongation at break > 60% which is not found in the S360 blend of identical IEC, may be the indication of a strongly interacting acid-base adduct network that may stabilize the material during plastic deformation and thus allow for significant elongation prior to breaking. Young's modulus, yield strength and elongation at break of the studied 75/25 S220/PBIO blend at 90% RH (50 °C) and 30% RH (90 °C) are listed in Table 4.

Table 4 Tensile test results for a 75/25 S220/PBIO blend at 90% RH (50 °C) and 30% RH (90 °C).

75/25 S220/PBIO	**90% RH *(50 °C)***	**30% RH *(90 °C)***
Water content (vol%)	41	18
Young's modulus (MPa)	196	968
Yield strength (MPa)	8	40
Elongation at break (%)	>60	>60

When qualitatively assessing the brittleness of a blend comprising 75 wt% S220 and 25wt% PBIO (under identical conditions as was done prior), the clear and stiff membrane remains unaffected by the severe drying (≥3 d at 90 °C in vacuum) and rigorous bending and twisting which it is subjected to, indicating the achievement of target non-brittleness and mechanical toughness. To quantify this implied mechanical toughness, which was derived from the properties of a 70/30 blend of S360/PBIO, the S220 blend's tensile behavior was evaluated under severely dry conditions of 10% RH at 90 °C, the exciting results of which are shown in Figure 5.10. For comparability, tensile test data measured on a fully robust pure PBIO membrane (cast in the same manner) is included as well as that of a (non-conductive) S360 blend comprising 30 wt% PBIO (IEC of 0.44 meq g^{-1}).

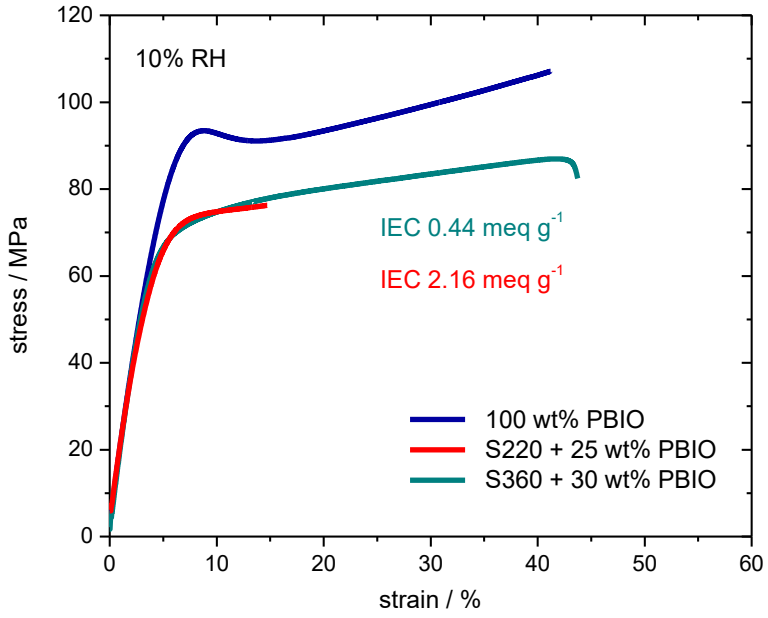

Figure 5.10 Tensile tests of pure PBIO, a 70/30 S360/PBIO, and a 75/25 S220/PBIO blend at 10% RH (90°C).

Young's modulus, yield strength and elongation at break of pure, solution cast PBIO, the 70/30 S360/PBIO blend, and the 75/25 S220/PBIO blend are listed in Table 5.

Table 5 Tensile test results for solution cast PBIO and a 75/25 S220/PBIO blend at 10% RH (90 °C).

	PBIO	**70/30 S360/PBIO**	**75/25 S220/PBIO**
Water content (vol%)	-	4	18
Young's modulus (MPa)	1730	1800	1520
Yield strength (MPa)	93	67	71
Elongation at break (%)	-	43	15

Elongation at break could not be recorded for pure PBIO, since the tensile test machine reached its maximum force prior to breaking of the sample. Interestingly, a pure PBI-O membrane shows a similar stiffness compared to the studied S360 blend by means of Young's modulus of around roughly 1700 MPa, with the high IEC S220 blend remaining slightly softer. This is

expected to be due to the remaining water in the S220 blend which still accounts for roughly 18 vol% (λ of 3.5 at 10% RH, as shown in Figure 5.11).

Excitingly, the yield strength of the S220 blend and the S360 blend of comparable (25 vs 30 wt%) PBIO content are almost the same in dry conditions (10% RH). This is in strong contrast to previous measurements at 30% RH and 90% RH, where yield strength and overall tensile behavior was dominated by the residual blend IEC. In dry conditions however, the S360 blend with IEC 0.44 meq g^{-1} and the S220 blend with IEC 2.16 meq g^{-1} exhibit the same strength. Plastic deformability of the S360 blend is considerably more pronounced (43 vs. 15% elongation at break) than that of the S220 blend but that does not take away from the overall mechanical toughness of the highly conductive membrane.

These observations lead to the hypothesis that under humidified conditions of $\geq$ 30% RH, when λ reaches a value of 4-5, and non-interacting sulfonic acid moieties are well hydrated, tensile behavior and (yield) strength of sPPS/PBIO blends is determined primarily by the blend IEC. Only a further reduction in relative humidity, to a point where λ reaches a value of 2-3, and the aqueous-ionic domain in sPPS nano-morphology becomes "salt-like", does the considerably high PBI content in the S220/PBIO blend dominate the materials tensile behavior and as a consequence negate the brittleness that pure sPPS exhibits under similar conditions (see Chapter 3). This particularly robust and conductive 75/25 S220/PBIO blend membrane is expected to be well suited for production on a larger scale and integration into existing processing and cell assembly protocols to be compared with state-of-the-art PFSA PEMs.

In the exciting and accelerating development of sPPS-based blends for application, it is important to reevaluate the characteristic stability properties of pure sPPS and, if they are retained in the more complex binary blends with PBIO. As was mentioned before, the stability of the blend component should not be limiting but can be critical e.g., due to insufficient hydrolytic stability (e.g., PEI, see Chapter 4.6). To probe this, the reversibility of water uptake behavior at high temperature and high water activity are typically chosen[43], with intermittent drying. Both, a hydration isotherm and a reversible water uptake measurement at $p(H_2O) = 10^5$ Pa (while cycling between 110 °C and 180 °C) was conducted for a 75/25 blend of S220/PBIO via TGA, under the same conditions as those used in the initial characterization of S220[43], and is shown in Figure 5.11.

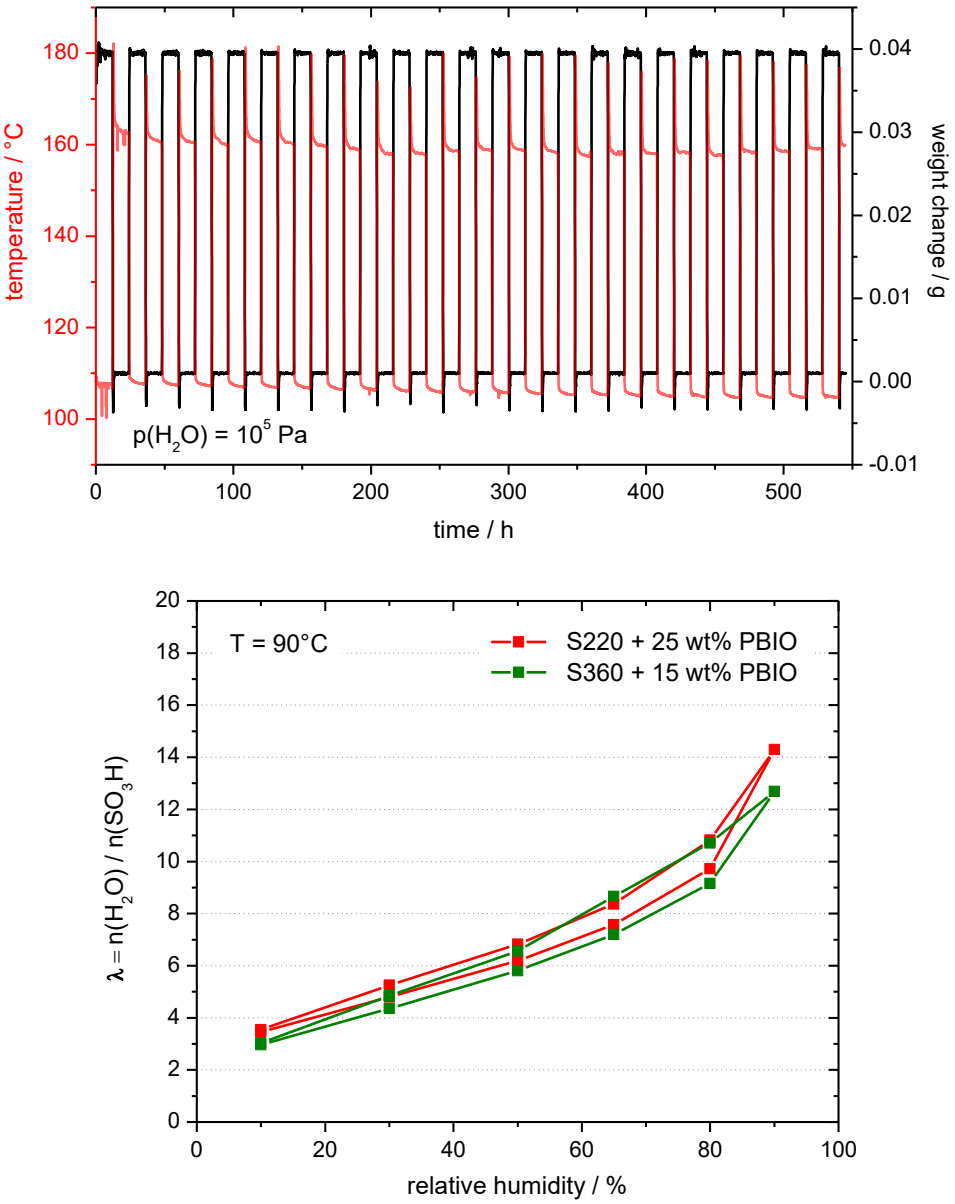

Figure 5.11 Reversible water uptake at $p(H_2O)=10^5$ Pa as a function of temperature and time and hydration isotherm for a 75/25 S220/PBIO and a 85/15 S360/PBIO blend at 90 °C.

The preserved extreme stability towards hydrolysis (as per the full reversibility of water uptake in the conducted test under conditions that typically favor de-sulfonation reactions, which is described in detail in literature[43]) is highly encouraging and underlines the tremendous potential of sPPS-based PBIO blends.

However, the limitations of this extraordinary blend composition, that combines high conductivity and mechanical toughness in a unique way, must be considered as well. Due to the intrinsic water solubility of pure S220, the risk of "leeching" out S220 from the ionically interacting blend morphology must be assessed. While any loss of IEC in the blend due to loss of S220 from the material is detrimental to its use in PEMWEs, the same behavior is not expected to be significant or of lifetime-limiting nature in PEMFCs, but surely must be monitored there as well. The results of a leeching test conducted by submerging membranes cast from a 75/25 blend of S220/PBIO into pure water at 25 °C and at PEMWE-typical 80 °C are shown in Figure 5.12.

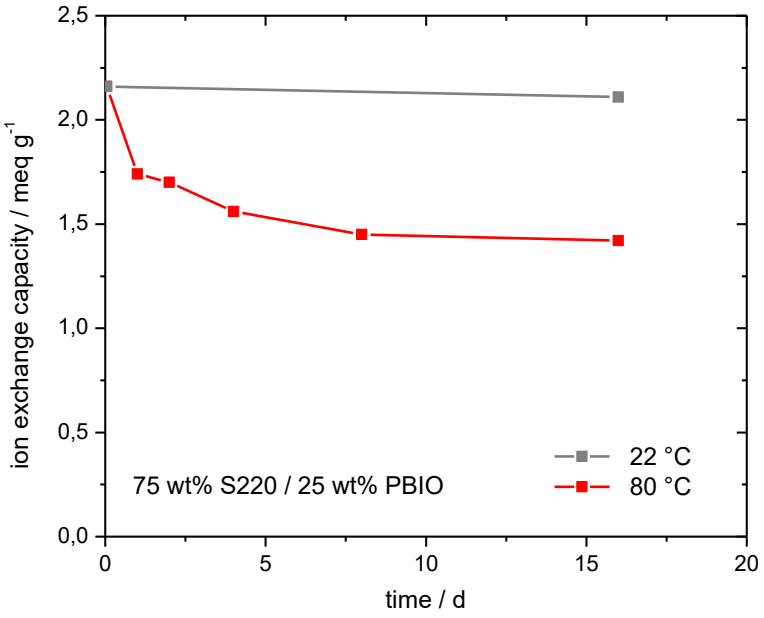

Figure 5.12 Evolution of experimental IEC in 75/25 S220/PBIO blends in deionized water at 80 °C and 22 °C over time.

The evolution of IEC was determined by titration of residual IEC in the membranes which were kept in (heated) water for different amounts of time. The intrinsically water soluble S220 may be removed from the ionically interacting blend morphology, in a process that is strongly accelerated with increasing temperature. This may be due to the fact that the exothermal acid-base interaction between PBIO and S220 is weakened with increasing temperature. Other explanations may be rooted in the excessively large water uptake of such blends at high

temperature, which may be a prerequisite for enabling mobilization of S220 polymer strains from the blend morphology in the first place. A cross-linking strategy that could be implemented in the large-scale fabrication of S220-based blends would potentially remedy this issue. Also, a further fine-tuning of the sPPS/PBIO blend system by means of adjusting IEC of sPPS as to arrive at materials that are intrinsically non-water soluble but have significantly higher IEC than S360 (i.e., "S340"-"S240") is currently underway and the subject of future studies.

5.4 S360/PBI BLENDS FOR PEMWE APPLICATION

In the meantime, the tailoring of sPPS/PBIO blends for PEMWE application can be oriented on the specific requirements of excellent gas-separation properties in operando when fully hydrated, while compromises can be made on the mechanical toughness under severely dry conditions. As was described in Chapter 3, as a consequence the thickness of PFSA membranes in state-of-the-art PEMWE systems is approximately around 100 µm.

It should also be considered that proton conductivity under PEMWE conditions, i.e., in water, is not affected in the same manner by blending as in the PEMFC-relevant range of 0 - 100% RH. To illustrate this, a similar evolution of conductivity in S360/PBIO blends as was shown in Figure 5.3 above is recorded for several blends submerged in water. The evolution of S360/PBIO blend conductivity in water as a function of PBIO content and normalized against that of S360 at 50% RH and in water at 60 °Cis shown in Figure 5.13.

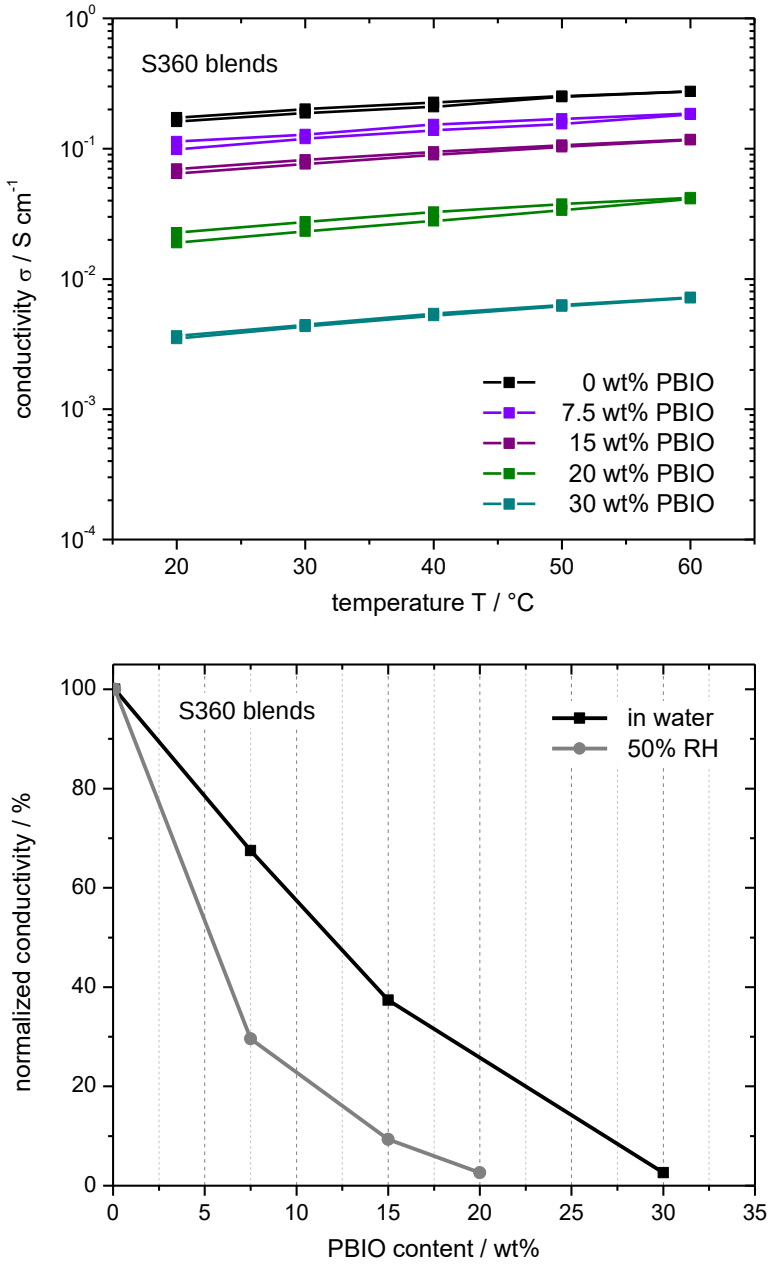

Figure 5.13 Proton conductivity of several S360/PBIO blends in water as a function of temperature and evolution of conductivity in S360/PBIO blends as a function of PBIO content for 50% RH and in water at 60 °C.

As is shown, the conductivity of a blend containing 15 wt% PBIO at 50% RH is reduced compared to pure S360 by an order of magnitude. However, when submerged in water, conductivity is only reduced by approx. 60 %, which is roughly the same as the reduction of

conductivity in 7.5 wt% PBIO containing blends under FC-typical conditions (compared to pure S360). With water uptake of $\lambda = 21$ at room temperature, an S360 blend with 15 wt% PBIO exhibits a considerable reduction of water volume content compared to pure S360 which is expected to lead to reduced gas permeability in operando. As a consequence, such a blend could potentially be employed as a thin membrane (< 50 µm) in a PEMWE cell. Thus, a blend of S360 containing 15 wt% PBIO was chosen to be fabricated on a pilot line by FUMATECH BWT within the scope of PSUMEA-3 (see Chapter 2) and will be utilized in future PEMWE studies. The IEC of an 85/15 S360/PBIO blend is 1.61 meq g^{-1} and represents a first approximation of the "required" IEC in sPPS membranes for PEMWE application but is not optimized here.

5.5 PEMFC CELLS BASED ON SPPS/PBI BLEND

As mentioned in Chapter 5.1, requirements towards the mechanical durability of a PEM arise not only from the operational window of a fuel cell system, but also the employed cell design and processing by which the MEA is assembled. With the progression of sPPS-based MEAs on the technology readiness level in mind and to enable accessible widespread testing, it is critical to include PFSA-typical processing and testing in the demonstration of this class of PEMs. At the same time, the advantages that emerging technologies – such as spray-coated ultra-thin DMD membranes – could offer for sPPS-MEAs should be explored and their potential evaluated.

Therefore, spray-coating of thin membranes was performed with sPPS/PBIO blends for the first time within the scope of this work. In DMD cells the thin membrane is supported by the gas diffusion electrode (GDE) on which it is coated, which allows for the application of blends that lack mechanical toughness, such as the previously characterized mixture of 92.5 wt% S360 and 7.5 wt% PBIO. As was described above, a number of parameters can be varied in order to affect membrane formation and its thickness and to adjust the membrane-electrode interface (i.e., avoid impregnation of the porous layer by the ionomer) during spray-coating. The cross-section of a 92.5/7.5 S360/PBIO blend sprayed onto a GDE (Freudenberg H23C8, Pt-loading: 0.5 mg cm^{-2}) was recorded via SEM and is depicted in Figure 5.14, showing how DMD processing can make ultra-thin sPPS-based membranes available for PEMFCs. In a feasibility

study, such a DMD-cell's polarization curve was recorded in ideal conditions (4 cm^2 cell area, H_2/O_2, 2.5 bar back pressure, over-stoichiometric flow rate).

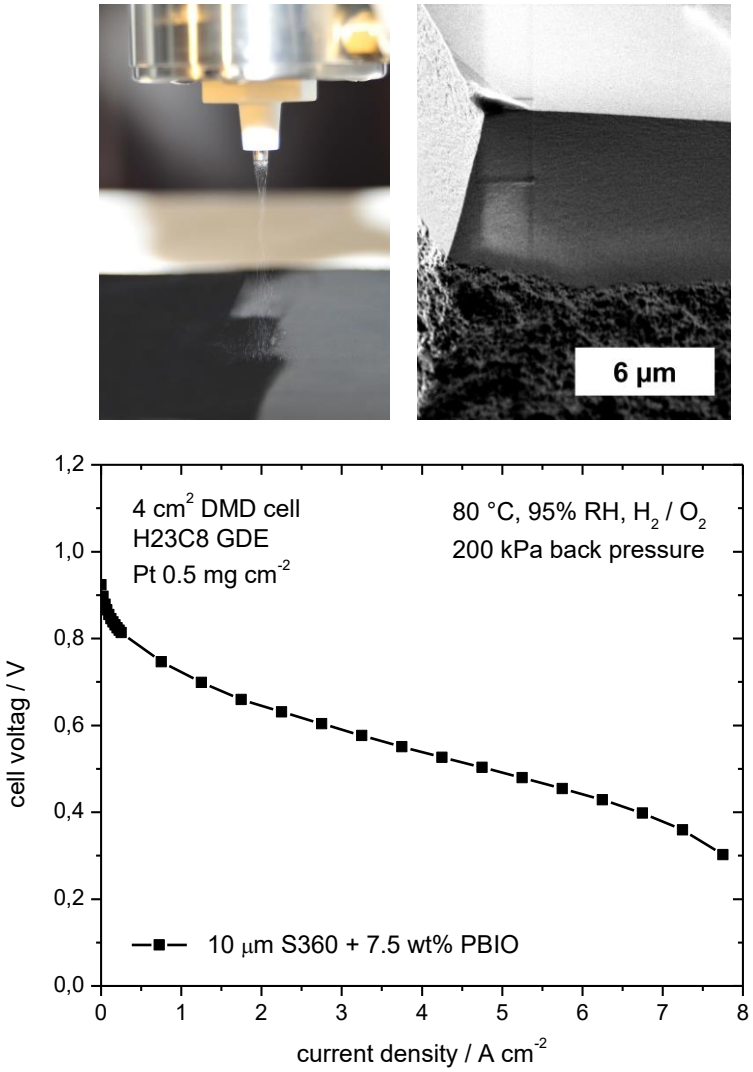

Figure 5.14 Image of membrane spray coating, resulting cross-sectional SEM of a DMD half cell,and polarization curve of a 10 µm membrane in a 4 cm2 DMD cell with 0.5 mg cm^{-2} in H2/O2 with 200 kPa back pressure at 80 °C and 95% RH.

Albeit not related to application-relevant conditions, the results highlight the extremely high power density that can be accessed in DMD cells based on sPPS/PBIO blends and will be explored with robust sPPS blends in the future.

The high mechanical toughness achieved in S220 blends with 25 wt% PBIO also makes the established fabrication process of PEMFC MEAs – via preparation of CCMs, typically in a

decal process – accessible for sPPS and can facilitate widespread testing of the material. With that, the scale at which membrane material is required also extends significantly. Thus, several blends of different thickness comprising of 75 wt% S220 and 25 wt% PBIO were fabricated on a pilot line by FUMATECH BWT, as is shown in Figure 5.15, within the scope of PSUMEA-3 (as described in Chapter 2) and will be utilized to deliberately design sPPS-MEAs and optimize their operation towards the strengths of sPPS in future works.

Figure 5.15 Image of a 75/25 S220/PBIO blend fabricated on a commercial pilot line by FUMATECH BWT.

Once again, important first steps in the development of sPPS-based PEMFCs include the confirmation of ex-situ found properties for sPPS with regard to transport (proton, water, gas) and stability (chemical, thermal, mechanical). Since they are fundamentally different to those of PFSAs, established protocols for e.g., durability testing membranes in accelerated stress tests (AST) may not be directly applicable to this new type of MEAs. For example, the common AST for chemical durability of a membrane is conducted at 90 °C 30% RH. In the test, permeation of hydrogen gas through the membrane leads to the formation of highly reactive radicals that contribute to chemical degradation of the ionomer. However, since gas permeability is strongly affected by water content, and high IEC hydrocarbon membranes show significantly higher water volume content at high RH compared to PFSAs, AST protocols should be adjusted or extended accordingly. Still, in the established AST protocol to determine chemical durability (at 90 °C and 30% RH under open circuit voltage), shown in Figure 5.16, an sPPS blend showed significantly slower deterioration of cell voltage during 100 h compared

to a N112 membrane of twice the thickness, while at the same time providing significantly higher initial cell voltage.

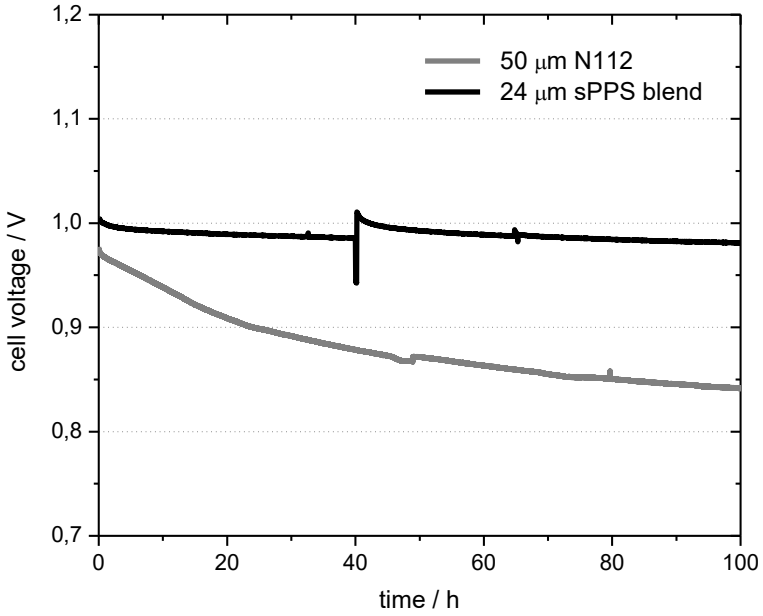

Figure 5.16 Voltage evolution of a blend membrane during an OCV hold test at 30% RH and 90 °C compared to N112.

This observation is expected to be the direct consequence of the initially described highly attractive chemothermal stability and transport behavior of sPPS, which include good gas separation properties – thus showing the transferability of ex situ properties of sPPS to in operando shown behavior.

Ultimately, there is a vast number of fundamental and technical aspects yet to be explored, but with access to thin, mechanically tough blend membranes at a large scale that combine high conductivity and high stability in a unique way, an important step is taken towards sPPS-based membranes for PEMFC application.

5.6 CHAPTER SUMMARY

In this chapter acid-base polymer blends comprising PBIO and sPPS were optimized with regards to high conductivity and mechanical robustness. Thin blend membranes for PEMFC application were created via spray-coating and on a technical scale and the unique properties of sPPS evaluated in fuel cell durability tests for the first time.

- Acid-base PBIO blends with sPPS allow for deliberate and continuous tuning of blend properties, where conductivity is compromised for viscoelastic reinforcement. The significant loss of charge carriers in blends of S360 and PBIO excluded the use of more than 7.5 wt% PBIO in S360 blends for fuel cell application.
- For application in PEMWE, 15wt% PBIO in S360 offers a suitable combination of robustness combined with sufficient conductivity, further underlining the versatility of sPPS/PBIO blends.
- PBIO blends comprising S220 allow for significant increase in its compositional content while maintaining high conductivity. PBIO content of 25wt% in S220 blends leads to sPPS membranes that, for the first time, are simultaneously highly conductive and mechanically tough under dry conditions. The strongly interacting but water soluble S220 can be leeched out when submerged in 80 °C water making it stable enough for PEMFC but not suitable for PEMWE application.
- Thin sPPS/PBIO blends were prepared on a large scale and for the first time used in durability tests in fuel cells, showing significantly reduced loss of cell voltage compared to an almost twice as thick PFSA membrane over 100 h.

The results in this chapter allow for the production and rigorous testing of robust sPPS/PBIO blend membranes for further development for PEMFC application and offer a platform that can enable the targeted design of this new class of PEMs.

6 CONCLUSION & OUTLOOK

Fuel cells (FC) and water electrolyzers (WE) are key technologies for enabling hydrogen as an energy vector for the successful decarbonization of energy systems worldwide. Proton exchange membranes (PEM) that can be used as polymeric electrolytes in both applications play an important role in system cost, performance, and adaptability.

Current membranes are derived from perfluorosulfonic acid functionalized fluorinated polymers (PFSAs) which were first described in the 1960s. Their unique molecular structure provides PFSAs with a special set of properties around which modern PEMFC and PEMWE systems are designed. As a result, their drawbacks, which are intrinsic to their chemistry and entail high cost, severe ecological impact (duo to the employed fluorine chemistry), softening at elevated temperature, and considerable gas permeability (crucial in WE) are currently mitigated by the use of expensive reinforcement strategies. From a technological perspective, an upstream solution would be the use of alternative membrane materials that can be much more versatile, thermally stable, cheaper, and ecologically safe while possessing better gas-separation properties. However, of the vast number of alternate materials studied so far, few possessed an attractive balance of properties that is required for a successful technology integration and includes high stability, high conductivity, and mechanical durability.

This work described the comprehensive approach (shown in Figure 6.1) to the viscoelastic reinforcement of sulfonated poly(phenylene sulfone)s (sPPS), which offer highly attractive proton-, gas-, and water transport properties for application, as well as excellent chemothermal and hydrolytic stability. However, their extreme polarity and molecular structure give rise to typical viscoelastic shortcomings in form of excessive swelling in water and brittleness under dry conditions. The comprehensive approach to the viscoelastic reinforcement of sPPS in this work comprised the optimization of intrinsic properties of S360, the identification and better understanding of a suitable and versatile polymer blending strategy with poly(benzimidazole) (PBIO), and the optimization and balancing of properties in sPPS/PBIO blends.

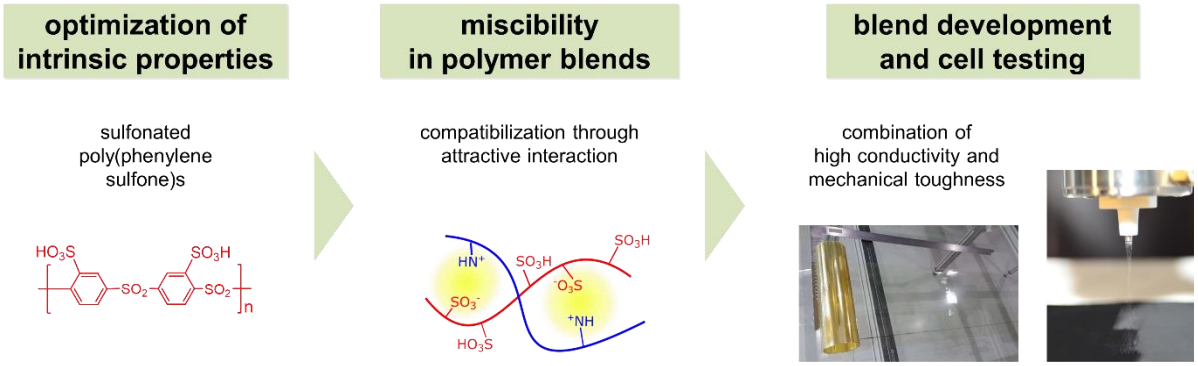

Figure 6.1 Thesis structure, conclusion.

In the first part of this work, the exceptional good performance of pure S360 (sPPS with 360 g meq^{-1}) was shown for the first time in a fluorine-free, S360-based PEMWE cell, which was enabled by the prior optimized step-growth polymerization of the ionomer. Record performance (of 3.48 A cm^{-2} at 1.8 V, at 80 °C with a 100 µm thick membrane) among comparable fluorine-free PEMWE studies was achieved, which underlined the potential of sPPS for application.

To overcome the mechanical shortcomings that pure sPPS and S360 face, homogeneously mixing polymer blends with commercial PBIO were adopted for blends with pure sPPS. In a model blend system of S360 with pyridine-functionalized poly(sulfone) (PSU) attractive acid-base interpolymer interaction was systematically varied (with regards to strength and concentration) to grant better understanding thereof. In the model blend system, weak interpolymer interaction was found to significantly enhance miscibility at high interaction concentration. As a result, the contribution that interpolymer hydrogen bonds may have on miscibility between PBIO and sulfonated ionomers was explored, and a new blend concept derived from it.

Finally, the blend system of sPPS/PBIO was optimized to meet criteria regarding mechanical robustness and transport properties of PEMFC and PEMWE applications. The integration of S220 (sPPS with 220 g meq^{-1}) allowed for considerable increase of PBIO contents in the blends and led to a unique combination of high conductivity and mechanical toughness, finally eliminating brittleness in sPPS-based membranes. Fuel cell tests with sPPS/PBI blends that

were fabricated via spray coating as well as in a commercial membrane casting process showed the scalability of the approach and the large degree of freedom in the design of sPPS-based cells for PEMFC application.

This work is the foundation for ongoing and future work that focuses on exploring the variation in IEC and synthetic approach to yield high IEC sPPS (close to S220) that are resistant to leeching from robust PBIO blend membranes under PEMWE conditions. Another focus of future studies can be the optimization of sPPS membranes for PEMWE application by reducing water uptake in water significantly, e.g. by covalent cross-linking, or the exploration of further blend components, or the embedment of sPPS blends into a strong, porous matrix that can withstand the strong swelling pressure. A natural step towards the development of sPPS-based MEAs can further be the explicit study of sPPS as the sole proton conducting ionomer in the catalyst layers of FC and WE cells, as was done for the first time in the feasibility study in this work. However, the complexity of the processes that take place at the electrodes requires a step-wise and systematic study of fundamental properties of such new catalyst layers. The findings in this work regarding the varying contributions that e.g., PBIO content, blend IEC, and water volume content have on viscoelastic properties of an sPPS/PBIO blend at different conditions merits further in-depth studies to better understand the interplay of these parameters. Finally, long-term durability study of robust and conductive sPPS/PBIO blend membranes in fuel cells should be conducted and the operation window of sPPS-based MEAs be explored as to clarify the strengths and weaknesses of sPPS-PEMs in application.

7 REFERENCES

1. IEA. Key World Energy Statistics 2020. https://www.iea.org/reports/key-world-energy-statistics-2020 (2020).
2. Orecchini, F. & Santiangeli, A. Beyond smart grids - The need of intelligent energy networks for a higher global efficiency through energy vectors integration. *Int. J. Hydrogen Energy* **36**, 8126–8133 (2011).
3. Orecchini, F., D'Orazio, A., Valitutti, V. & Fiori, C. Renewability of energy resources, energy vectors, and energy technologies for mobility. in *Handbook of Sustainable Engineering* 1043–1064 (Springer Netherlands, 2013). doi:10.1007/978-1-4020-8939-8_116.
4. Pivovar, B., Rustagi, N. & Satyapal, S. Hydrogen at Scale (H2@Scale) key to a clean, economic, and sustainable energy system. *Electrochem. Soc. Interface* **27**, 47–52 (2018).
5. Dell, R. M., Moseley, P. T. & Rand, D. A. J. Hydrogen, Fuel Cells and Fuel Cell Vehicles. in *Towards Sustainable Road Transport* 260–295 (Elsevier, 2014). doi:10.1016/b978-0-12-404616-0.00008-6.
6. Fonseca, J. D., Camargo, M., Commenge, J. M., Falk, L. & Gil, I. D. Trends in design of distributed energy systems using hydrogen as energy vector: A systematic literature review. *Int. J. Hydrogen Energy* **44**, 9486–9504 (2019).
7. Carmo, M., Fritz, D. L., Mergel, J. & Stolten, D. A comprehensive review on PEM water electrolysis. *Int. J. Hydrogen Energy* **38**, 4901–4934 (2013).
8. Ajanovic, A. & Haas, R. Economic and Environmental Prospects for Battery Electric- and Fuel Cell Vehicles: A Review. *Fuel Cells* vol. 19 515–529 (2019).
9. Olabi, A. G., Wilberforce, T. & Abdelkareem, M. A. Fuel cell application in the automotive industry and future perspective. *Energy* **214**, 118955 (2021).
10. Hess, M. *et al.* Terminology of polymers containing ionizable or ionic groups and of polymers containing ions (IUPAC Recommendations 2006). *Pure Appl. Chem.* **78**, 2067–2074 (2006).
11. Grot, W. *Fluorinated Ionomers*. *Fluorinated Ionomers* (Elsevier Inc., 2011). doi:10.1016/C2010-0-65926-8.

12. Kusoglu, A. & Weber, A. Z. New Insights into Perfluorinated Sulfonic-Acid Ionomers. *Chem. Rev.* **117**, 987–1104 (2017).
13. Kreuer, K.-D. Ion conducting membranes for fuel cells and other electrochemical devices. *Chem. Mater.* **26**, 361–380 (2014).
14. Kreuer, K. D. & Portale, G. A critical revision of the nano-morphology of proton conducting ionomers and polyelectrolytes for fuel cell applications. *Adv. Funct. Mater.* **23**, 5390–5397 (2013).
15. Miyake, J. & Miyatake, K. Fluorine-free sulfonated aromatic polymers as proton exchange membranes. *Polym. J.* **49**, 487–495 (2017).
16. Gubler, L., Nauser, T., Coms, F. D., Lai, Y.-H. & Gittleman, C. S. Prospects for Durable Hydrocarbon-Based Fuel Cell Membranes. *J. Electrochem. Soc.* **165**, 3100–3103 (2018).
17. Skalski, T. J. G. *et al.* Sulfophenylated Terphenylene Copolymer Membranes and Ionomers. *ChemSusChem* **11**, 4033–4043 (2018).
18. Peckham, T. J. & Holdcroft, S. Structure-morphology-property relationships of non-perfluorinated proton-conducting membranes. *Adv. Mater.* **22**, 4667–4690 (2010).
19. Raja Rafidah, R. S., Rashmi, W., Khalid, M., Wong, W. Y. & Priyanka, J. Recent progress in the development of aromatic polymer-based proton exchange membranes for fuel cell applications. *Polymers (Basel).* **12**, 1061 (2020).
20. Li, N. *et al.* Enhancement of proton transport by nanochannels in comb-shaped copoly(arylene ether sulfone)s. *Angew. Chemie - Int. Ed.* **50**, 9158–9161 (2011).
21. Miyahara, T., Hayano, T., Matsuno, S., Watanabe, M. & Miyatake, K. Sulfonated polybenzophenone/poly(arylene ether) block copolymer membranes for fuel cell applications. *ACS Appl. Mater. Interfaces* **4**, 2881–2884 (2012).
22. Lee, H. F. *et al.* Synthesis and proton conductivity of sulfonated, multi-phenylated poly(arylene ether)s. *J. Polym. Sci. Part A Polym. Chem.* **52**, 2579–2587 (2014).
23. Tian, S., Meng, Y. & Hay, A. S. Membranes from poly(aryl ether)-based ionomers containing randomly distributed nanoclusters of 6 or 12 sulfonic acid groups. *Macromolecules* **42**, 1153–1160 (2009).
24. Miyatake, K., Chikashige, Y., Higuchi, E. & Watanabe, M. Tuned polymer electrolyte

membranes based on aromatic polyethers for fuel cell applications. *J. Am. Chem. Soc.* **129**, 3879–3887 (2007).

25. Asano, N. *et al.* Aliphatic/aromatic polyimide ionomers as a proton conductive membrane for fuel cell applications. *J. Am. Chem. Soc.* **128**, 1762–1769 (2006).
26. Yin, Y. *et al.* Water stability of sulfonated polyimide membranes. *Macromolecules* **39**, 1189–1198 (2006).
27. Lee, H.-S., Badami, A. S., Roy, A. & McGrath, J. E. Segmented sulfonated poly(arylene ether sulfone)- *b* -polyimide copolymers for proton exchange membrane fuel cells. I. Copolymer synthesis and fundamental properties. *J. Polym. Sci. Part A Polym. Chem.* **45**, 4879–4890 (2007).
28. Yamazaki, K. & Kawakami, H. High proton conductive and low gas permeable sulfonated graft copolyimide membrane. *Macromolecules* **43**, 7185–7191 (2010).
29. Wang, F. *et al.* Synthesis of highly sulfonated poly(arylene ether sulfone) random(statistical) copolymers via direct polymerization. *Macromol. Symp.* **175**, 387–396 (2001).
30. Titvinidze, G., Wohlfarth, A., Kreuer, K. D., Schuster, M. & Meyer, W. H. Reinforcement of highly proton conducting multi-block copolymers by online crosslinking. *Fuel Cells* **14**, 325–331 (2014).
31. Lee, H. F. *et al.* Effect of ketone versus sulfone groups on the properties of poly(arylene ether)-based proton exchange membranes. *J. Mater. Sci.* **51**, 9805–9821 (2016).
32. Schuster, M., Kreuer, K. D., Andersen, H. T. & Maier, J. Sulfonated poly(phenylene sulfone) polymers as hydrolytically and thermooxidatively stable proton conducting ionomers. *Macromolecules* **40**, 598–607 (2007).
33. Skalski, T. J. G., Britton, B., Peckham, T. J. & Holdcroft, S. Structurally-Defined, Sulfo-Phenylated, Oligophenylenes and Polyphenylenes. *J. Am. Chem. Soc.* **137**, 12223–12226 (2015).
34. Fujimoto, C. H., Hickner, M. A., Cornelius, C. J. & Loy, D. A. Ionomeric poly(phenylene) prepared by Diels-Alder polymerization: Synthesis and physical properties of a novel polyelectrolyte. *Macromolecules* **38**, 5010–5016 (2005).
35. Si, K., Dong, D., Wycisk, R. & Litt, M. Synthesis and characterization of poly(para-

phenylene disulfonic acid), its copolymers and their n-alkylbenzene grafts as proton exchange membranes: High conductivity at low relative humidity. *J. Mater. Chem.* **22**, 20907–20917 (2012).

36. Goto, K., Rozhansk, I., Yamakawa, Y., Otsuki, T. & Naito, Y. Development of aromatic polymer electrolyte membrane with high conductivity and durability for fuel cell. *Polym. J.* **41**, 95–104 (2009).
37. Miyake, J. *et al.* Design of flexible polyphenylene proton-conducting membrane for next-generation fuel cells. *Sci. Adv.* **3**, (2017).
38. Long, Z. & Miyatake, K. High-Performance Fuel Cell Operable at 120 °C Using Polyphenlyene Ionomer Membranes with Improved Interfacial Compatibility. *ACS Appl. Mater. Interfaces* **13**, 15366–15372 (2021).
39. Kreuer, K.-D. On the development of proton conducting polymer membranes for hydrogen and methanol fuel cells. *J. Memb. Sci.* **185**, 29–39 (2001).
40. Kreuer, K.-D. On the development of proton conducting materials for technological applications. *Solid State Ionics* **97**, 1–15 (1997).
41. Ise, M. Polymer-Elektrolyt-Membranen: Untersuchungen zur Mikrostruktur und zu den Transporteigenschaften für Protonen und Wasser. (Max Planck Institute for Solid State Research, 2000).
42. De Araujo, C. C. *et al.* Poly(p-phenylene sulfone)s with high ion exchange capacity: ionomers with unique microstructural and transport features. *Phys. Chem. Chem. Phys.* **11**, 3010 (2009).
43. Schuster, M. *et al.* Highly sulfonated poly(phenylene sulfone): Preparation and stability issues. *Macromolecules* **42**, 3129–3137 (2009).
44. Kim, Y. S. Polymer Electrolytes with High Ionic Concentration for Fuel Cells and Electrolyzers. *ACS Applied Polymer Materials* vol. 3 1250–1270 (2021).
45. Sata, T. *Ion Exchange Membranes: Preparation, Characterization, Modification and Application*. (Royal Society of Chemistry, 2004). doi:10.1007/BF02190013.
46. Katcharava, Z. *et al.* in preparation. (2021).
47. Klose, C. *et al.* All-Hydrocarbon MEA for PEM Water Electrolysis Combining Low Hydrogen Crossover and High Efficiency. *Adv. Energy Mater.* **10**, (2020).

48. Port, A. B. & Still, R. H. Synthesis and characterisation of poly(arylene sulphides)-Part II. Thermal analysis studies on poly(phenylene sulphide), poly(2-methyl phenylene sulphide), and poly(2,6-dimethyl phenylene sulphide) and related systems. *Polym. Degrad. Stab.* **1**, 193–204 (1979).
49. Colquhoun, H. M. Crystal and molecular simulation of poly(1,4-phenylenesulfone). *Polymer (Guildf).* **38**, 991–994 (1997).
50. Colquhoun, H. M. & Williams, D. J. Crystal and molecular simulation of high-performance polymers. *Acc. Chem. Res.* **33**, 189–198 (2000).
51. Colquhoun, H. M. *et al.* Crystal and molecular structures of poly(1,4-phenylenesulfone) and its trisulfone and tetrasulfone oligomers. *Macromolecules* **35**, 1685–1690 (2002).
52. Robello, D. R., Ulman, A. & Urankar, E. J. Poly(p-phenylene sulfone). *Macromolecules* **26**, 6718–6721 (1993).
53. Rikukawa, M. & Sanui, K. Proton-conducting polymer electrolyte membranes based on hydrocarbon polymers. *Progress in Polymer Science (Oxford)* vol. 25 1463–1502 (2000).
54. Hickner, M. A., Ghassemi, H., Kim, Y. S., Einsla, B. R. & McGrath, J. E. Alternative polymer systems for proton exchange membranes (PEMs). *Chem. Rev.* **104**, 4587–4611 (2004).
55. Titvinidze, G., Kaltbeitzel, A., Manhart, A. & Meyer, W. H. Synthesis and characterisation of sulphonated poly(arylene sulphone) terpolymers with triphenylphosphine oxide moieties for proton exchange membrane fuel cells. *Fuel Cells* **10**, 390–400 (2010).
56. Atanasov, V. *et al.* Highly sulfonated poly(phenylene sulfones): Optimization of the polymerization conditions. *Polym. Bull.* **68**, 317–326 (2012).
57. Kim, Y. S. & Pivovar, B. S. Moving Beyond Mass-Based Parameters for Conductivity Analysis of Sulfonated Polymers. *Annu. Rev. Chem. Biomol. Eng.* **1**, 123–148 (2010).
58. Alberti, G., Narducci, R. & Sganappa, M. Effects of hydrothermal/thermal treatments on the water-uptake of Nafion membranes and relations with changes of conformation, counter-elastic force and tensile modulus of the matrix. *J. Power Sources* **178**, 575–583 (2008).

59. Reucroft, P. J., Rivin, D. & Schneider, N. S. Thermodynamics of Nafion-vapor interactions. I. Water vapor. *Polymer (Guildf).* **43**, 5157–5161 (2002).
60. Vallieres, C. *et al.* On Schroeder's paradox. *J. Memb. Sci.* **278**, 357–364 (2006).
61. Kreuer, K.-D. The role of internal pressure for the hydration and transport properties of ionomers and polyelectrolytes. *Solid State Ionics* **252**, 93–101 (2013).
62. Kreuer, K.-D. Corrigendum to "The role of internal pressure for the hydration and transport properties of ionomers and polyelectrolytes". *Solid State Ionics* **328**, 35–36 (2018).
63. Shin, D. W., Guiver, M. D. & Lee, Y. M. Hydrocarbon-Based Polymer Electrolyte Membranes: Importance of Morphology on Ion Transport and Membrane Stability. *Chemical Reviews* vol. 117 4759–4805 (2017).
64. Gross, M., Maier, G., Fuller, T., MacKinnon, S. & Gittleman, C. Design rules for the improvement of the performance of hydrocarbon-based membranes for proton exchange membrane fuel cells (PEMFC). in *Handbook of Fuel Cells* (John Wiley & Sons, Ltd, 2010). doi:10.1002/9780470974001.f500018.
65. Kreuer, K. D. Hydrocarbon membranes. in *Handbook of Fuel Cells* (2010). doi:10.1002/9780470974001.f303037.
66. Esmaeili, N., Gray, E. M. A. & Webb, C. J. Non-Fluorinated Polymer Composite Proton Exchange Membranes for Fuel Cell Applications – A Review. *ChemPhysChem* vol. 20 2016–2053 (2019).
67. Carothers, W. H. Studies on polymerization and ring formation. I. An introduction to the general theory of condensation polymers. *J. Am. Chem. Soc.* **51**, 2548–2559 (1929).
68. Rudin, A. & Choi, P. *The Elements of Polymer Science and Engineering*. (2013). doi:10.1016/C2009-1-64286-6.
69. Odian, G. *Principles of Polymerization*. (John Wiley & Sons, Inc., 2004). doi:10.1002/047147875x.
70. Stanford, J. L. & Stepto, R. F. T. Rate theory of irreversible linear random polymerisation. Part 1. - Basic theory. *J. Chem. Soc. Faraday Trans. 1 Phys. Chem. Condens. Phases* **71**, 1292–1307 (1975).
71. Stepto, R. F. T. & Waywell, D. R. A study of intramolecular reaction during linear

polyurethane formation. *Die Makromol. Chemie* **152**, 263–275 (1972).

72. Su, W.-F. Principles of Polymer Design and Synthesis. *Extracts* 19 (2013).
73. Aricò, A. S. *et al.* Polymer electrolyte membranes for water photo-electrolysis. *Membranes (Basel).* **7**, (2017).
74. Ayers, K. E. *et al.* Research Advances towards Low Cost, High Efficiency PEM Electrolysis. *ECS Trans.* **33**, 3–15 (2019).
75. Albert, A., Lochner, T., Schmidt, T. J. & Gubler, L. Stability and Degradation Mechanisms of Radiation-Grafted Polymer Electrolyte Membranes for Water Electrolysis. *ACS Appl. Mater. Interfaces* **8**, 15297–15306 (2016).
76. Grigoriev, S. A., Porembsky, V. I. & Fateev, V. N. Pure hydrogen production by PEM electrolysis for hydrogen energy. in *International Journal of Hydrogen Energy* vol. 31 171–175 (Pergamon, 2006).
77. Chandesris, M. *et al.* Numerical modelling of membrane degradation in PEM water electrolyzer: Influence of the temperature and current density. in *International Conference on Fundamentals and Development of Fuel Cells, FDFC2015* vol. 40 1353–1366 (2015).
78. Frensch, S. H. *et al.* Impact of iron and hydrogen peroxide on membrane degradation for polymer electrolyte membrane water electrolysis: Computational and experimental investigation on fluoride emission. *J. Power Sources* **420**, 54–62 (2019).
79. Liu, H., Coms, F. D., Zhang, J., Gasteiger, H. A. & Laconti, A. B. Chemical degradation: Correlations between electrolyzer and fuel cell findings. in *Polymer Electrolyte Fuel Cell Durability* 71–118 (Springer New York, 2009). doi:10.1007/978-0-387-85536-3_5.
80. Park, J. E. *et al.* High-performance proton-exchange membrane water electrolysis using a sulfonated poly(arylene ether sulfone) membrane and ionomer. *J. Memb. Sci.* **620**, (2021).
81. Wei, G., Xu, L., Huang, C. & Wang, Y. SPE water electrolysis with SPEEK/PES blend membrane. *Int. J. Hydrogen Energy* **35**, 7778–7783 (2010).
82. Titvinidze, G. *et al.* Proton conducting phase-separated multiblock copolymers with sulfonated poly(phenylene sulfone) blocks for electrochemical applications: Preparation, morphology, hydration behavior, and transport. *Adv. Funct. Mater.* **22**,

4456–4470 (2012).

83. Mittelsteadt, C. K. & Liu, H. Conductivity, permeability, and ohmic shorting of ionomeric membranes. in *Handbook of Fuel Cells* 1–14 (2010). doi:10.1002/9780470974001.f500025.

84. Ishikawa, H. *et al.* Use of a sub-gasket and soft gas diffusion layer to mitigate mechanical degradation of a hydrocarbon membrane for polymer electrolyte fuel cells in wet-dry cycling. *J. Power Sources* **325**, 35–41 (2016).

85. Lai, Y. H., Mittelsteadt, C. K., Gittleman, C. S. & Dillard, D. A. Viscoelastic stress analysis of constrained proton exchange membranes under humidity cycling. *J. Fuel Cell Sci. Technol.* **6**, 0210021–02100213 (2009).

86. Yoshida-Hirahara, M., Takahashi, S., Yoshizawa-Fujita, M., Takeoka, Y. & Rikukawa, M. Synthesis and investigation of sulfonated poly(p-phenylene)-based ionomers with precisely controlled ion exchange capacity for use as polymer electrolyte membranes. *RSC Adv.* **10**, 12810–12822 (2020).

87. Kreuer, K.-D., Weppner, W. & Rabenau, A. Investigation of proton-conducting solids. *Solid State Ionics* **3**–**4**, 353–358 (1981).

88. Harrison, W., Wang, F., Kim, Y. S., Hickner, M. & McGrath, J. E. Synthesis, characterization and morphologial influence of bisphenol structure on the direct synthesis of sulfonated poly(arylene ether sulfone) copolymers. *Am. Chem. Soc. Polym. Prepr. Div. Polym. Chem.* **43**, 700–701 (2002).

89. Yoon, S. J., Choi, J. H., Hong, Y. T. & Lee, S. Y. Synthesis and characterization of sulfonated poly(arylene ether sulfone) ionomers incorporating perfluorohexylene units for DMFC membranes. *Macromol. Res.* **18**, 352–357 (2010).

90. Bai, Z. & Dang, T. D. Direct Synthesis of Fully Sulfonated Polyarylenethioether Sulfones as Proton-Conducting Polymers for Fuel Cells. *Macromol. Rapid Commun.* **27**, 1271–1277 (2006).

91. Bae, B., Miyatake, K. & Watanabe, M. Effect of the hydrophobic component on the properties of sulfonated poly(arylene ether sulfone)s. *Macromolecules* **42**, 1873–1880 (2009).

92. Zhang, Y., Kim, J.-D. D. & Miyatake, K. Effect of thermal crosslinking on the properties

of sulfonated poly(phenylene sulfone)s as proton conductive membranes. *J. Appl. Polym. Sci.* **133**, 1–8 (2016).

93. Skulimowska, A. *et al.* Proton exchange membrane water electrolysis with short-side-chain Aquivion® membrane and IrO2 anode catalyst. *Int. J. Hydrogen Energy* **39**, 6307–6316 (2014).
94. Siracusano, S., Baglio, V., Lufrano, F., Staiti, P. & Aricò, A. S. Electrochemical characterization of a PEM water electrolyzer based on a sulfonated polysulfone membrane. *J. Memb. Sci.* **448**, 209–214 (2013).
95. Badwal, S. P. S., Giddey, S. & Ciacchi, F. T. Hydrogen and oxygen generation with polymer electrolyte membrane (PEM)-based electrolytic technology. *Ionics (Kiel).* **12**, 7–14 (2006).
96. Mabrouk, W. *et al.* Synthesis and characterization of new proton exchange membrane deriving from sulfonated polyether sulfone using ionic crosslinking for electrodialysis applications. *Polym. Eng. Sci.* **60**, 3149–3158 (2020).
97. Kerres, J., Ullrich, A. & Hein, M. Preparation and characterization of novel basic polysulfone polymers. *J. Polym. Sci. Part A Polym. Chem.* **39**, 2874–2888 (2001).
98. Asadi Tashvigh, A., Luo, L., Chung, T. S., Weber, M. & Maletzko, C. A novel ionically cross-linked sulfonated polyphenylsulfone (sPPSU) membrane for organic solvent nanofiltration (OSN). *J. Memb. Sci.* **545**, 221–228 (2018).
99. Kerres, J. A. Blended and cross-linked ionomer membranes for application in membrane fuel cells. *Fuel Cells* **5**, 230–247 (2005).
100. Ito, H., Maeda, T., Nakano, A. & Takenaka, H. Properties of Nafion membranes under PEM water electrolysis conditions. *Int. J. Hydrogen Energy* **36**, 10527–10540 (2011).
101. Zaidi, S. M. J., Mikhailenko, S. D., Robertson, G. P., Guiver, M. D. & Kaliaguine, S. Proton conducting composite membranes from polyether ether ketone and heteropolyacids for fuel cell applications. *J. Memb. Sci.* **173**, 17–34 (2000).
102. Kesava, M. & Dinakaran, K. SnO2 nanoparticles dispersed carboxylated Poly(arylene ether sulfones) nanocomposites for proton exchange membrane fuel cell (PEMFC) applications. *Int. J. Hydrogen Energy* **46**, 1121–1132 (2021).
103. Sun, C. *et al.* Hybrid inorganic-organic proton-conducting membranes based on SPEEK

doped with WO3 nanoparticles for application in vanadium redox flow batteries. *Electrochim. Acta* **309**, 311–325 (2019).

104. Hosseinabadi, P., Hooshyari, K., Javanbakht, M. & Enhessari, M. Synthesis and optimization of nanocomposite membranes based on SPEEK and perovskite nanoparticles for polymer electrolyte membrane fuel cells. *New J. Chem.* **43**, 16232–16245 (2019).
105. Luo, L., Chung, T. S., Weber, M., Staudt, C. & Maletzko, C. Molecular interaction between acidic sPPSU and basic HPEI polymers and its effects on membrane formation for ultrafiltration. *J. Memb. Sci.* **524**, 33–42 (2017).
106. Won, M., Kwon, S. & Kim, T. H. High performance blend membranes based on sulfonated poly(arylene ether sulfone) and poly(p-benzimidazole) for PEMFC applications. *J. Ind. Eng. Chem.* **29**, 104–111 (2015).
107. Zuo, Z., Fu, Y. & Manthiram, A. Novel Blend Membranes Based on Acid-Base Interactions for Fuel Cells. **4**, 1627–1644 (2012).
108. Kerres, J. A. Design concepts for aromatic ionomers and ionomer membranes to be applied to fuel cells and electrolysis. *Polym. Rev.* **55**, 273–306 (2015).
109. Cui, W., Kerres, J. & Eigenberger, G. Development and characterization of ion-exchange polymer blend membranes. *Sep. Purif. Technol.* **14**, 145–154 (1998).
110. Kerres, J. Blend concepts for fuel cell membranes. in *Polymer Membranes for Fuel Cells* vol. 5 185–221 (Springer US, 2009).
111. Kim, K., Heo, P., Han, J., Kim, J. & Lee, J. C. End-group cross-linked sulfonated poly(arylene ether sulfone) via thiol-ene click reaction for high-performance proton exchange membrane. *J. Power Sources* **401**, 20–28 (2018).
112. Lee, H. *et al.* Simple and effective cross-linking technology for the preparation of cross-linked membranes composed of highly sulfonated poly(ether ether ketone) and poly(arylene ether sulfone) for fuel cell applications. *ACS Appl. Energy Mater.* **3**, 10495–10505 (2020).
113. Subramanian, C., Giotto, M., Weiss, R. A. & Shaw, M. T. Chemical cross-linking of highly sulfonated polystyrene electrospun fibers. *Macromolecules* **45**, 3104–3111 (2012).

114. Zhu, Y., Zieren, S. & Manthiram, A. Novel crosslinked membranes based on sulfonated poly(ether ether ketone) for direct methanol fuel cells. *Chem. Commun.* **47**, 7410–7412 (2011).
115. Li, Z. *et al.* Enhanced proton conductivity of proton exchange membranes by incorporating sulfonated metal-organic frameworks. *J. Power Sources* **262**, 372–379 (2014).
116. Zhang, Z. *et al.* Enhanced proton conductivity of sulfonated poly(arylene ether ketone sulfone) polymers by incorporating phosphotungstic acid-ionic-liquid-functionalized metal-organic framework. *J. Memb. Sci.* **630**, 119304 (2021).
117. Hou, H. *et al.* Thermal crosslinked and nanodiamond reinforced SPEEK composite membrane for PEMFC. *Int. J. Hydrogen Energy* **38**, 3346–3351 (2013).
118. Nor, N. A. M. *et al.* A novel imogolite-reinforced sulfonated polyphenylsulfone as proton exchange membrane in fuel cell applications. *J. Environ. Chem. Eng.* **9**, 105641 (2021).
119. Utracki, L. A. & Wilkie, C. A. *Polymer blends handbook*. (Springer Netherlands, 2014). doi:10.1007/978-94-007-6064-6.
120. Manson, J. A. & Sperling, L. H. *Polymer Blends and Composites*. (Springer US, 1976). doi:10.1007/978-1-4615-1761-0.
121. Robeson, L. M. *Polymer Blends, A Comprehensive Review.* (Carl Hanser Verlag, 2007).
122. Pracella, M. Micro- and nanostructured multiphase polymer blend systems: Phase morphology and interfaces. in 1–443 (CRC Press, 2005). doi:10.1002/macp.200600584.
123. Guiver, M. D., Black, P., Tam, C. M. & Deslandes, Y. Functionalized polysulfone membranes by heterogeneous lithiation. *J. Appl. Polym. Sci.* **48**, 1597–1606 (1993).
124. Huggins, M. L. Solutions of long chain compounds. *The Journal of Chemical Physics* vol. 9 440 (1941).
125. Flory, P. J. Thermodynamics of high polymer solutions. *The Journal of Chemical Physics* vol. 9 660–661 (1941).
126. Koningsveld, R. Partial miscibility of multicomponent polymer solutions. *Adv. Colloid Interface Sci.* **2**, 151–215 (1968).
127. Utracki, L. Investigations of the phenomena of coacervation. Part III. Phase equilibrium

in the three-component system toluene–ethanol–polystyrene. *J. Appl. Polym. Sci.* **6**, 399–403 (1962).

128. Eisenberg, A., Kim, J. & Ratner, M. Introduction to Ionomers. *Phys. Today* **52**, 68–68 (1999).
129. Zhang, W., Tang, C. M. & Kerres, J. Development and characterization of sulfonated-unmodified and sulfonated-aminated PSU Udel® blend membranes. *Sep. Purif. Technol.* **22**–**23**, 209–221 (2001).
130. Coleman, M. M. & Painter, P. C. Hydrogen bonded polymer blends. *Progress in Polymer Science* vol. 20 1–59 (1995).
131. Tucker, R. T., Han, C. C., Dobrynin, A. V. & Weiss, R. A. Small-angle neutron scattering analysis of blends with very strong intermolecular interactions: Polyamide/ionomer blends. *Macromolecules* **36**, 4404–4410 (2003).
132. Bodart, P. *et al.* 7Li static and MAS n.m.r. studies on blends of polyamide-6 and lithium sulfonated polystyrene ionomers. *Polymer (Guildf).* **40**, 569–576 (1999).
133. Leung, L., Williams, D. J., Karasz, F. E. & MacKnight, W. J. Miscible blends of aromatic polybenzimidazoles and aromatic polyimides. *Polym. Bull.* **16**, 457–464 (1986).
134. Guerra, G., Choe, S., Williams, D. J., Karasz, F. E. & Macknight, W. J. Fourier Transform Infrared Spectroscopy of Some Miscible Polybenzimidazole/Polyimide Blends. *Macromolecules* **21**, 231–234 (1988).
135. Karasz, F. E., MacKnight, W. J. & Musto, P. Hydrogen Bonding in Polybenzimidazole/ Poly (ether imide) Blends: A Spectroscopic Study. *Macromolecules* **24**, 4762–4769 (1991).
136. Ahn, T. K., Kim, M. & Choe, S. Hydrogen-bonding strength in the blends of polybenzimidazole with BTDA- and DSDA-based polyimides. *Macromolecules* **30**, 3369–3374 (1997).
137. Arunbabu, D., Sannigrahi, A. & Jana, T. Blends of polybenzimidazole and poly(vinylidene fluoride) for use in a fuel cell. *J. Phys. Chem. B* **112**, 5305–5310 (2008).
138. Chen, F. *et al.* Polybenzimidazole and Polyvinylpyrrolidone Blend Membranes for Vanadium Flow Battery. *J. Electrochem. Soc.* **167**, 060511 (2020).

139. Wang, Y., Goh, S. H. & Chung, T. S. Miscibility study of Torlon® polyamide-imide with Matrimid® 5218 polyimide and polybenzimidazole. *Polymer (Guildf).* **48**, 2901–2909 (2007).

140. Kerres, J., Ullrich, A., Meier, F. & Häring, T. Synthesis and characterization of novel acid-base polymer blends for application in membrane fuel cells. *Solid State Ionics* **125**, 243–249 (1999).

141. Kerres, J. *et al.* Preparation, characterization and fuel cell application of new acid-base blend membranes. *J. New Mater. Electrochem. Syst.* **3**, 229–239 (2000).

142. Mack, F., Aniol, K., Ellwein, C., Kerres, J. & Zeis, R. Novel phosphoric acid-doped PBI-blends as membranes for high-temperature PEM fuel cells. *J. Mater. Chem. A* **3**, 10864–10874 (2015).

143. Schönberger, F., Hein, M. & Kerres, J. Preparation and characterisation of sulfonated partially fluorinated statistical poly(arylene ether sulfone)s and their blends with PBI. *Solid State Ionics* **178**, 547–554 (2007).

144. Zhang, H. *et al.* Composite membranes based on highly sulfonated PEEK and PBI: Morphology characteristics and performance. *J. Memb. Sci.* **308**, 66–74 (2008).

145. Li, Q. F. *et al.* Properties, degradation and high temperature fuel cell test of different types of PBI and PBI blend membranes. *J. Memb. Sci.* **347**, 260–270 (2010).

146. Feng, S. *et al.* Novel method for the preparation of ionically crosslinked sulfonated poly(arylene ether sulfone)/polybenzimidazole composite membranes via in situ polymerization. *J. Memb. Sci.* **346**, 105–112 (2010).

147. Katzfuß, A., Krajinovic, K., Chromik, A. & Kerres, J. Partially fluorinated sulfonated poly(arylene sulfone)s blended with polybenzimidazole. *J. Polym. Sci. Part A Polym. Chem.* **49**, 1919–1927 (2011).

148. Wang, J. *et al.* Highly compatible acid-base blend membranes based on sulfonated poly(ether ether ketone) and poly(ether ether ketone-alt-benzimidazole) for fuel cells application. *J. Memb. Sci.* **415**–**416**, 644–653 (2012).

149. Kerres, J. A., Katzfuß, A., Chromik, A. & Atanasov, V. Sulfonated poly(styrene)s-PBIOO® blend membranes: Thermo-oxidative stability and conductivity. *J. Appl. Polym. Sci.* **131**, (2014).

150. Chromik, A. *et al.* Stability of acid-excess acid-base blend membranes in all-vanadium redox-flow batteries. *J. Memb. Sci.* **476**, 148–155 (2015).
151. Cichon, P. J. *et al.* Sulfonated poly(arylene thioether phosphine oxide)s and poly(arylene ether phosphine oxide)s PBI-blend membranes and their performance in SO2 electrolysis. *Int. J. Hydrogen Energy* **41**, 4521–4537 (2016).
152. Quartarone, E., Angioni, S. & Mustarelli, P. Polymer and composite membranes for proton-conducting, high-temperature fuel cells: A critical review. *Materials* vol. 10 687 (2017).
153. Lee, J. K. & Kerres, J. Synthesis and characterization of sulfonated poly(arylene thioether)s and their blends with polybenzimidazole for proton exchange membranes. *J. Memb. Sci.* **294**, 75–83 (2007).
154. Katzfuß, A., Krajinovic, K., Chromik, A. & Kerres, J. A. Preparation and Characterization of New Sulfonated Partially Fluorinated Polyarylenesulfones and Their Blends with Polybenzimidazole. *ECS Trans.* **33**, 719–733 (2019).
155. Peach, R., Krieg, H. M., Krüger, A. J., Bessarabov, D. & Kerres, J. Stability of ionic-covalently cross-linked PBI-blended membranes for SO2 electrolysis at elevated temperatures. *Int. J. Hydrogen Energy* **45**, 2447–2459 (2020).
156. Kerres, J. *et al.* Partially fluoridated arylene polyethers and their ternary blend membranes with PBI and H3PO4. Part I. Synthesis and characterisation of polymers and binary blend membranes. in *Fuel Cells* vol. 8 175–187 (John Wiley & Sons, Ltd, 2008).
157. Seyb, C. & Kerres, J. Novel partially fluorinated sulfonated poly(arylenethioether)s and poly(aryleneether)s prepared from octafluorotoluene and pentafluoropyridine, and their blends with PBI-Celazol. *Eur. Polym. J.* **49**, 518–531 (2013).
158. Deimede, V., Voyiatzis, G. A., Kallitsis, J. K., Qingfeng, L. & Bjerrum, N. J. Miscibility behavior of polybenzimidazole/sulfonated polysulfone blends for use in fuel cell applications. *Macromolecules* **33**, 7609–7617 (2000).
159. Kerres, J. A. Development of ionomer membranes for fuel cells. *J. Memb. Sci.* **185**, 3–27 (2001).
160. Kerres, J., Tang, C. M. & Graf, C. Improvement of properties of poly(ether ketone) ionomer membranes by blending and cross-linking. *Ind. Eng. Chem. Res.* **43**, 4571–4579

(2004).

161. Kerres, J. *et al.* Cross-linked polyaryl blend membranes for polymer electrolyte fuel cells. *Fuel Cells* **4**, 105–112 (2004).
162. Kerres, J. A., Xing, D. & Schönberger, F. Comparative investigation of novel PBI blend ionomer membranes from nonfluorinated and partially fluorinated poly arylene ethers. *J. Polym. Sci. Part B Polym. Phys.* **44**, 2311–2326 (2006).
163. Robertson, G. P. *et al.* Casting solvent interactions with sulfonated poly(ether ether ketone) during proton exchange membrane fabrication. *J. Memb. Sci.* **219**, 113–121 (2003).
164. Lee, M. *et al.* Effects of block length and solution-casting conditions on the final morphology and properties of disulfonated poly(arylene ether sulfone) multiblock copolymer films for proton exchange membranes. *Polymer (Guildf).* **50**, 6129–6138 (2009).
165. Gutoff, E. B., Cohen, E. D. & Kheboian, G. I. *Coating and Drying Defects*. (John Wiley & Sons, Inc., 2006). doi:10.1080/07373939508917085.
166. Yamamura, M., Horiuchi, K., Kajiwara, T. & Adachi, K. Decrease in solvent evaporation rate due to phase separation in polymer films. *AIChE J.* **48**, 2711–2714 (2002).
167. Viviani, M., Lova, P. & Portale, G. Structural Transitions During Formation and Rehydration of Proton Conducting Polymeric Membranes. *Macromol. Rapid Commun.* (2021) doi:10.1002/marc.202000717.
168. Shams Es-haghi, S. & Cakmak, M. Drying of Polymer Solutions: Modeling and Real-Time Tracking of the Process. in *Roll-to-Roll Manufacturing: Process Elements and Recent Advances* 65–110 (Wiley-VCH Verlag, 2018). doi:10.1002/9781119163824.ch3.
169. Kajiya, T. & Doi, M. Dynamics of drying process of polymer solution droplets: Analysis of polymer transport and control of film profiles. *Nihon Reoroji Gakkaishi* **39**, 17–28 (2011).
170. Bussink, J., van de Grampel, H. T. & Weber, M. Polymer Blends. in *Ullmann's Encyclopedia of Industrial Chemistry* 1–39 (Wiley-VCH Verlag GmbH & Co. KGaA,

2017). doi:10.1002/14356007.a21_273.pub2.

171. Nagase, Y., Naruse, A. & Matsui, K. Chemical modification of polysulphone: 1. Synthesis of polysulphone/polydimethylsiloxane graft copolymer. *Polymer (Guildf).* **30**, 1931–1937 (1989).
172. Takamuku, S. Poly(arylene ether sulfone)s with different positions of pyridyl groups: Synthesis of the basic diphenyl sulfone dihalide monomers in lithiation and the optimal polymerization in condensation. *Polymer (Guildf).* **131**, 73–83 (2017).
173. R. J. Cotter. *Engineering plastics. A handbook of polyarylethers*. vol. 39 (Gordon and Breach Science Publishers, 1996).
174. Xiao, L. *et al.* High-temperature polybenzimidazole fuel cell membranes via a sol-gel process. *Chem. Mater.* **17**, 5328–5333 (2005).
175. Chen, J. C., Hsiao, Y. R., Liu, Y. C., Chen, P. Y. & Chen, K. H. Polybenzimidazoles containing heterocyclic benzocinnoline structure prepared by sol-gel process and acid doping level adjustment for high temperature PEMFC application. *Polymer (Guildf).* **182**, 121814 (2019).
176. Ross-Murphy, S. B. Rheological characterization of polymer gels and networks. *Polym. Gels Networks* **2**, 229–237 (1994).
177. Perry, K. A. *et al.* A comparative study of phosphoric acid-doped m-PBI membranes. *J. Polym. Sci. Part B Polym. Phys.* **52**, 26–35 (2014).
178. Lefebvre, M. C., Martin, R. B. & Pickup, P. G. Characterization of ionic conductivity profiles within proton exchange membrane fuel cell gas diffusion electrodes by impedance spectroscopy. *Electrochem. Solid-State Lett.* **2**, 259–261 (1999).
179. Wang, Q. *et al.* Functionally Graded Cathode Catalyst Layers for Polymer Electrolyte Fuel Cells. *J. Electrochem. Soc.* **151**, A950 (2004).
180. Towne, S., Viswanathan, V., Holbery, J. & Rieke, P. Fabrication of polymer electrolyte membrane fuel cell MEAs utilizing inkjet print technology. *J. Power Sources* **171**, 575–584 (2007).
181. Kim, S. M. *et al.* High-performance fuel cell with stretched catalyst-coated membrane: One-step formation of cracked electrode. *Sci. Rep.* **6**, 1–7 (2016).
182. Aizawa, M. & Gyoten, H. Effect of Micro-Patterned Membranes on the Cathode

Performances for PEM Fuel Cells under Low Humidity. *J. Electrochem. Soc.* **160**, F417–F428 (2013).

183. Bae, J. W., Cho, Y. H., Sung, Y. E., Shin, K. & Jho, J. Y. Performance enhancement of polymer electrolyte membrane fuel cell by employing line-patterned Nafion membrane. *J. Ind. Eng. Chem.* **18**, 876–879 (2012).
184. Oh, K. H. *et al.* Interlocking membrane/catalyst layer interface for high mechanical robustness of hydrocarbon-membrane-based polymer electrolyte membrane fuel cells. *Adv. Mater.* **27**, 2974–2980 (2015).
185. Wang, L., Advani, S. G. & Prasad, A. K. Membrane electrode assembly with enhanced membrane/electrode interface for proton exchange membrane fuel cells. *J. Phys. Chem. C* **117**, 945–948 (2013).
186. Wang, Z. & Nagao, Y. Effects of Nafion impregnation using inkjet printing for membrane electrode assemblies in polymer electrolyte membrane fuel cells. *Electrochim. Acta* **129**, 343–347 (2014).
187. Breitwieser, M., Klingele, M., Vierrath, S., Zengerle, R. & Thiele, S. Tailoring the Membrane-Electrode Interface in PEM Fuel Cells: A Review and Perspective on Novel Engineering Approaches. *Advanced Energy Materials* vol. 8 1701257 (2018).
188. Klingele, M., Breitwieser, M., Zengerle, R. & Thiele, S. Direct deposition of proton exchange membranes enabling high performance hydrogen fuel cells. *J. Mater. Chem. A* **3**, 11239–11245 (2015).
189. Vierrath, S. *et al.* The reasons for the high power density of fuel cells fabricated with directly deposited membranes. *J. Power Sources* **326**, 170–175 (2016).
190. Breitwieser, M. *et al.* Water management in novel direct membrane deposition fuel cells under low humidification. *Int. J. Hydrogen Energy* **41**, 11412–11417 (2016).
191. DOE. *Fuel cell technologies office multiyear research, development and demonstration plan*. www.energy.gov/sites/prod/files/2016/06/f32/fcto_myrdd_fuel_cells_0.pdf (2015).
192. Mukundan, R. *et al.* Membrane Accelerated Stress Test Development for Polymer Electrolyte Fuel Cell Durability Validated Using Field and Drive Cycle Testing. *J. Electrochem. Soc.* **165**, F3085–F3093 (2018).

193. Coms, F. D., Liu, H. & Owejan, J. E. Mitigation of Perfluorosulfonic Acid Membrane Chemical Degradation Using Cerium and Manganese Ions. *ECS Trans.* **16**, 1735–1747 (2008).

194. Buxton, G. V., Greenstock, C. L., Helman, W. P. & Ross, A. B. Critical Review of rate constants for reactions of hydrated electrons, hydrogen atoms and hydroxyl radicals in Aqueous Solution. *J. Phys. Chem. Ref. Data* **17**, 513–886 (1988).